



# Optimization of an in-vivo verification system using TLD dosimetry – metrological validation using the ISO 28057:2014 standard

Andreia Cristina Maia Oliveira

Mestrado em Física Médica

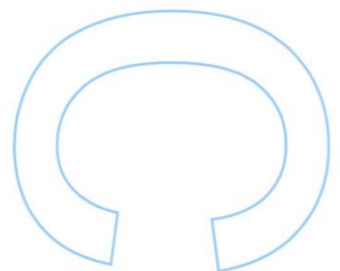
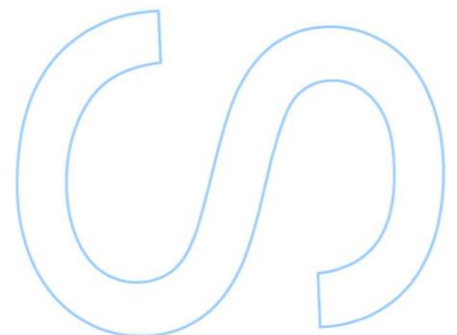
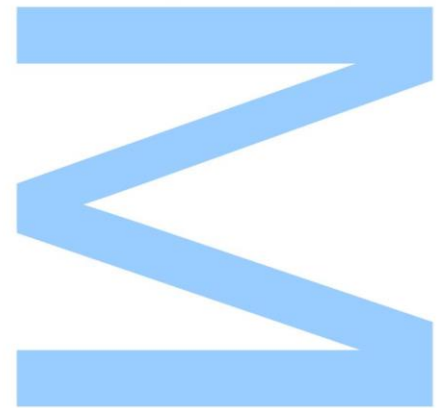
Departamento de Física e Astronomia  
2017

## Orientador

João António Miranda dos Santos, PhD, Assessor de Saúde (Física Médica), Instituto Português de Oncologia Francisco Gentil, EPE; Professor Afiliado da Universidade do Porto (ICBAS)

## Coorientadora

Anabela Gregório Dias, PhD, Assistente de Saúde (Física Médica), Instituto Português de Oncologia Francisco Gentil, EPE

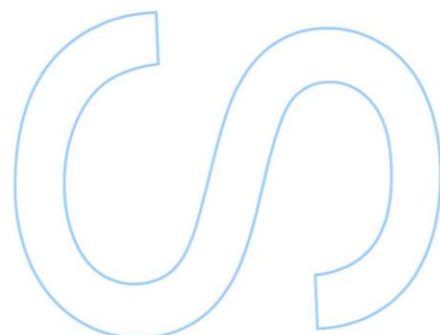
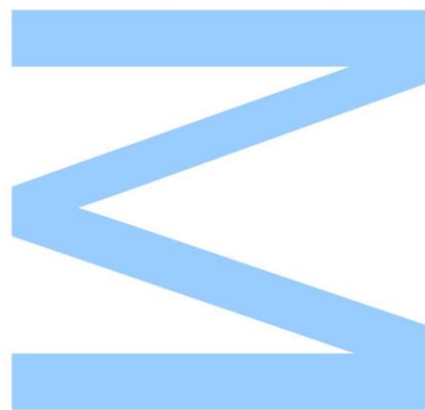




Todas as correções determinadas pelo júri, e só essas, foram efetuadas.

O Presidente do Júri,

Porto, \_\_\_\_ / \_\_\_\_ / \_\_\_\_







# Acknowledgments

This page is a truly expression of my gratitude to all the people who collaborated with me to create this dissertation. My sincere thanks to all those people who contribute for my personal and academic journey that, at the moment, culminates in the delivery of this document.

Specially, to Dr. João Santos who always encouraged me and unlocked the doors, literally, to the world of medical physics. He allowed me the realization of an internship program in IPO-Porto and then proposed the continuation of the project of internship on thermoluminescence to a highest level: this present dissertation. In addition, I cannot forget to thank all the knowledge and experience that he shared with me. It is also necessary to emphasize all the availability to teach, provide bibliographic material like articles and his sympathy. And the latest thanks to my supervisor is for his patient to review this extensive document.

To Dr. Anabela Dias, my co-supervisor, who always expedited the process of irradiation, so it was a big help in experimental part. Thanks for the total contribution during this dissertation, including the review of the thesis.

To all the professionals of IPO-Porto which in one way or another supported me, in particular to Dr. Joana Lencart for is availability to help me, to Filipe Dias for his willingness to introduce me initially to the experimental part and to Vera because she's the one who listens to me at the IPO when things do not go the way they should.

To all DIRE collaborators, particularly Miguel and Joana, who welcomed me for a week and showed me what their lab work is all about. A special "thank you" to Dr. João Alves who allowed my integration in DIRE and kindly provided me access to his PhD thesis, which proved to be a valuable bibliographic support in this scientific area.

To all my professors, from my primary teacher, through the mathematics teacher to the quantum mechanics teacher, each of you contributes to the student I am today.

To my parents, because without them I would not literally be here. I wanted to accentuate my mother for never letting me give up and always support and believe in me and my father for all the times he transported me. Thank you for all the sacrifices you made to allow me to study until to this point! Thank you mama and dad! To my little sister for being my room mate and tolerate my paranoia. To my big family, my grandparents, my godfather, my uncles, my cousins and to Martim for the moments we had together. To my grandfather Beto, who would be super proud at this time, because from my tender age he believed that little girl would go far.

To my college colleagues, specially Miguel and João, who made the academic course less tortuous and more enjoyable. To my friends, specifically to Sara and David for being as crazy as me and so understanding me so well. To my neighbours and my friends of Resende who proportionate me good moments which allowed me to recover and gain strength to continue.

To the man of my life for supporting me in the most difficult times, for believing in me when I could not do it myself and for being my boyfriend and my best friend. In particular, for your help in the computational part adjacent to writing this thesis. Thank you for being by my side!

Thanks! Muito obrigada! Andreia Maia Oliveira



*"The pursuit of truth and beauty is a sphere of activity in which we are permitted to remain children all our lives."*

Attributed to Albert Einstein





# Abstract

One of the major objectives of dosimetry in Radiotherapy is to ensure that the prescribed dose is actually deposited in the planning target volume (PTV) in the patient. Therefore, it is necessary to use several methodologies that can test beam parameters and deposited dose. Usually, the *in vivo* dosimetry (IVD) can be achieved by thermoluminescent dosimetry (TLD) or diodes. Recently, other methods are also being implemented, such as portal dosimetry or radiochromic films. Nevertheless, TLD still is the most reliable method and the most versatile for the majority of clinical situations. However, this methodology requires specific training, careful metrological considerations and a certain amount of investment in special equipments. The purpose of this work is to apply the ISO 28057:2014 standard in order to guarantee the reliability and accuracy indispensable in clinical IVD with thermoluminescence dosimeters (TLD's) when applied on or in the patient or phantoms.

In this project, two batches from different manufacturers were compared, relating its physical characteristics. Each batch was composed by one hundred dosimeters (LiF: Mg, Ti), produced by Radcard (MTS-100) and by Thermo Scientific™ (TLD-100). For an initial calibration, the glow curves of all TLD's irradiated by a *Varian™ TrueBeam™* linear accelerator (LINAC) were obtained and analyzed. The first applied correction summand was the background subtraction of each detector. Then, it was necessary to proceed with the reader response characterization and geometric corrections due to beam heterogeneity in the case of simultaneous irradiation of more than one detector (25 TLD's were irradiated simultaneously). For the last one it was applied a novel method: the dose values obtained by the ionization chamber matrix (OCTAVIUS Detector 1500) placed across the beam during the irradiation in the TLD's distribution area. To accomplish the calibration of the TLD's, the efficiency of each detector, the Element Correction Coefficient (ECC) was determined for each dosimeter.

Following the ISO 28057:2014 recommendations, each batch was characterized by establishing its homogeneity, repeatability, linearity, energy dependence and, most importantly, the uncertainty budget associated to the dose measurement.

In the last stage of this work, the work compares dose measurements made *in vivo* in a Rando anthropomorphic phantom with the dose calculated by the treatment planning system (TPS). The measurements made during a simulated plan and correspondent irradiation using a clinical set-up, resulted in an identification of a positioning error of the phantom, which supports the use of this IVD methodology in the clinical practice. The use of this dosimeters have the advantage of not give additional irradiation to the patient.

Finally, taking into account the results obtained it is demonstrable that, at present, there is still room for optimization of the performance of the radiotherapy treatments, which will in the future allow the patient to receive a treatment of considerably higher quality.

Key-words: External Radiotherapy; Metrological Characterization; *In Vivo* Dosimetry; TLD.



# Resumo

Na área da Radioterapia, um dos principais objetivos da dosimetria passa por garantir que a dose prescrita seja realmente a dose depositada no volume alvo no paciente, daí se revelar necessário utilizar diversas metodologias por forma a testar os parâmetros do feixe e a dose depositada por este. Habitualmente, a dosimetria *in vivo* recorre aos TLD's ou aos díodos. Porém, recentemente, outros métodos, como a dosimetria portal ou o uso de filmes radiocrômicos, têm também sido implementados. No entanto, a TLD ainda é o método mais confiável e o mais versátil para a generalidade das situações clínicas. Apesar das vantagens inerentes a esta metodologia, apresenta como inconveniente o fator de requerer um treino técnico específico, bem como a exigência de considerações metrológicas particulares e um investimento em materiais e equipamentos exclusivamente destinados a este fim. O objetivo primordial deste trabalho consiste na aplicação da norma ISO 28057:2014 de modo a garantir a exatidão e a precisão indispensáveis na IVD clínica com TLD's aquando da sua aplicação em pacientes e/ou em fantomas.

Neste projeto foram comparados dois lotes de diferentes fabricantes, relacionando as suas propriedades físicas, sendo que cada lote era composto por cem dosímetros (LiF: Mg, Ti), produzidos pela Radcard (MTS-100) e pela Thermo Scientific™ (TLD-100). Para a calibração inicial foram obtidas e analisadas as curvas de brilho de todos os detetores irradiados por um acelerador linear *Varian™ TrueBeam™*. A primeira correção a ser aplicada consistiu na subtração do fundo de cada detector. De seguida, procedeu-se à caracterização da resposta do leitor e, por último, foram aplicadas as correções geométricas devido à heterogeneidade do feixe no caso da irradiação simultânea de mais do que um detector (25 TLD's são sempre irradiados simultaneamente). Para este último ajuste geométrico foi concebido e aplicado um novo método no qual se obtêm os valores de dose da matriz de câmaras de ionização (OCTAVIUS Detector 1500) que se encontra colocada através do feixe durante a irradiação, na área de distribuição dos TLD's. De forma a efetuar uma adequada calibração dos TLD's e, por conseguinte, obter o coeficiente de correção individual de cada dosímetro revelou-se fulcral recorrer ao cálculo da eficiência de cada detector (ECC).

Seguindo as recomendações da norma ISO 28057:2014, cada lote foi caracterizado pela sua homogeneidade, repetibilidade, linearidade, dependência energética e, particularmente, pela incerteza associada à medida da dose absorvida.

Na última etapa deste trabalho confrontaram-se as medidas de dose realizadas *in vivo* num fantoma antropomórfico Rando com o valor da dose calculada pelo sistema de planeamento do tratamento (TPS). As medidas efetuadas no decorrer de uma simulação fidedigna de um plano de Radioterapia Externa e da irradiação correspondente recorrendo a uma configuração clínica real, resultaram na identificação de um lapso no posicionamento do fantoma. Através dos resultados provenientes desta experiência, pode deduzir-se que a aplicação desta metodologia IVD se pode revelar um precioso auxiliar na prática clínica de forma a garantir o incremento da qualidade na execução de um tratamento de Radioterapia. Adicionalmente, o emprego destes dosímetros num protocolo de IVD acarreta ainda a vantagem de evitar a aplicação de uma dose adicional ao

paciente.

Finalmente, através dos resultados obtidos é demonstrável que, atualmente, existe ainda margem de otimização da *performance* dos tratamentos de Radioterapia, o que permitirá de futuro proporcionar ao paciente um tratamento de qualidade consideravelmente superior.

Palavras-chave: Radioterapia Externa; Caracterização Metrológica, Dosimetria *In Vivo*; TLD.

## Publications in Scientific Meetings

- **A. Maia Oliveira**, A. G. Dias, J. A. M. Santos (2017). "Metrological comparison of two thermoluminescent dosimeters (TLD) types using a linear accelerator and a new methodology for beam heterogeneity correction in the clinical dose range." PRS2017 conference, IST, Lisbon, Portugal, 27-29 September 2017.
- **A. Maia Oliveira**, A. G. Dias, J. A. M. Santos (2017). "Comparação metrológica de dois tipos de dosímetros termoluminescentes (TLD) usando um acelerador linear e uma nova metodologia para correção da heterogeneidade do feixe no intervalo de dose clínico." FISMED 2017 conference, Coimbra, Portugal, 6-7 November 2017.



# Contents

<b>Acknowledgments</b>	<b>i</b>
<b>Abstract</b>	<b>v</b>
<b>Resumo</b>	<b>vii</b>
<b>Publications in Scientific Meetings</b>	<b>ix</b>
<b>Abbreviations and Symbols</b>	<b>xix</b>
<b>Terms and Definitions</b>	<b>xxi</b>
<b>1 Introduction</b>	<b>1</b>
1.1 Context . . . . .	1
1.2 Motivation . . . . .	3
1.3 Goals . . . . .	4
1.4 Information and Cases of Study . . . . .	5
1.5 Document Structure . . . . .	5
<b>2 Theoretical Framework</b>	<b>9</b>
2.1 Radiotherapy . . . . .	9
2.1.1 Ionizing Radiation . . . . .	9
2.1.2 Quality Control . . . . .	14
2.2 Detectors Applied for Dosimetry . . . . .	15
2.2.1 Dosimeter . . . . .	16
2.2.2 Dosimetry . . . . .	16
2.2.3 Selection of TLD . . . . .	20
2.3 Thermoluminescence Dosimeters (TLD's) . . . . .	21
2.3.1 Theoretical Basis of Luminescence Phenomena . . . . .	21
2.3.2 Thermoluminescence materials - LiF: Mg, Ti . . . . .	29
2.4 Ionization Chambers . . . . .	31
2.4.1 Principle of Operation . . . . .	31
<b>3 Materials and Experimental Methods</b>	<b>35</b>
3.1 Materials and Instruments . . . . .	35
3.1.1 Measurement System . . . . .	35
3.1.2 Irradiation Equipments and Materials . . . . .	44
3.2 Methods . . . . .	49
3.2.1 ISO 28057:2014 . . . . .	50

3.2.2	Procedures . . . . .	56
<b>4</b>	<b>Experimental results</b>	<b>59</b>
4.1	Calibration Parameters . . . . .	59
4.2	Analysis . . . . .	62
4.2.1	Tests . . . . .	68
4.2.2	Background value . . . . .	72
4.2.3	Repeatability . . . . .	75
4.2.4	Linearity . . . . .	78
4.2.5	Calibration curve . . . . .	81
4.2.6	Energy Dependence . . . . .	82
4.2.7	Estimation of Uncertainty . . . . .	85
4.3	Clinical Application . . . . .	87
<b>5</b>	<b>Conclusion and Future Work</b>	<b>91</b>
5.1	Final considerations . . . . .	91
5.2	Satisfaction of Objectives . . . . .	92
5.3	Future Work . . . . .	92
<b>A</b>	<b>Programmable Oven</b>	<b>95</b>
A.1	Front Panel . . . . .	95
A.2	Commands . . . . .	96
A.2.1	Programmer - 'TM.CFG' = 'ProG' . . . . .	98
<b>B</b>	<b>The operational software, Thermo Scientific™ WinREMS™</b>	<b>101</b>
B.1	Initial Operation . . . . .	101
B.1.1	Power-up . . . . .	101
B.1.2	Initiate Workspace . . . . .	101
B.1.3	Time Temperature Profile Setup . . . . .	104
B.1.4	Acquisition Setup . . . . .	105
B.2	Reading TL Materials . . . . .	106
B.2.1	Start Reader . . . . .	106
B.2.2	Start Reader Process . . . . .	108
B.2.3	Complete Read Process . . . . .	110
	<b>References</b>	<b>111</b>



# List of Figures

1.1	Proportion of global deaths under the age 70 years, by cause of death, 2012. Proportion of global NCD deaths under the age of 70, by cause of death, 2012 . . . .	2
1.2	Structure of the plan of research work. . . . .	6
2.1	Ionizing radiation damages the genetic material (DNA) causing single strand breaks (SSB) or double strand breaks (DSB) in the cells, thus blocking their ability to divide and proliferate further. Mechanisms involved in the decrease of radiosensitivity of the fast doubling cancer cells, while increasing radioresistant of the slow doubling normal cells benefits the cancer patients. . . . .	10
2.2	Direct and indirect actions of radiation. . . . .	11
2.3	Classification of diverse types of radiation. . . . .	12
2.4	Dominant types of interactions as a function of the atomic number $Z$ of the absorber and the energy of the photon radiation. The curves show where two kinds of interactions are equally probable. . . . .	13
2.5	The principle of therapeutic ratio. Curve A represents the TCP and curve B the probability of complications. . . . .	15
2.6	Representative scheme of all radiotherapy procedures and the role of <i>in vivo</i> dosimetry for treatment evaluation in the purple boxes. . . . .	17
2.7	Energy band gaps in different type of materials. . . . .	22
2.8	The energy levels of interest for the thermal equilibrium discussion are shown. This material may have one or several traps or centers. But for this discussion, it's only necessary to refer one to one. . . . .	25
2.9	Energy band model showing the electronic transitions in a TL material according to a simple two-level model: (a) generation of electrons and holes; (b) electron trapping; (c) electron release due to thermal stimulation; (d) recombination ; (e) hole trapping. Solid circles are electrons, open circles are holes. Level T is an electron trap, level R is a recombination center, $E_f$ is Fermi level. . . . .	27
2.10	Example of TL emission curve and some of its descriptive parameters. $I$ is the intensity emitted, $T_m$ is the maximum peak temperature, $\delta$ its width at half height and $T_1$ the temperature at half high in the descent of the curve . . . . .	29
2.11	Structure of dipoles formed by impurity-gap pairs: $Mg^{2+}$ - Li vacancy. . . . .	30
2.12	Typical deconvoluted glow curve of LiF:Mg,Ti TLD-100 following $^{90}Sr/^{90}Y$ irradiation at a dose level of 1 Gy. The insert shows the deconvolution of the high-temperature TL. . . . .	30
2.13	Electrometer in feedback mode of operation. . . . .	32
2.14	Schematic diagram of parallel plate ion chamber, showing drift of ions. Electrons typically drift 1000 times faster than positive ions due to their much smaller mass. . . . .	33

3.1	MTS-100 (red square) and TLD-100 (green square). The point of a finger is in the picture to help in visualization of real dimensions of dosimeters. . . . .	36
3.2	The Thermo Scientific™ HARSHAW TLD™ Model 3500 Manual Reader highlighting its planchet provides manual readout of TL chips, disks, rods and cubes in a broad variety of sizes. . . . .	40
3.3	Block diagram of a simple TLD readout system. The material is slowly heated by a heater supply. The emitted light is filtered and then detected by a photomultiplier tube. The temperature of the material is recorded through the thermocouple. . . .	40
3.4	The oven of Carbolite® coupled to 3204 Process Controller. . . . .	42
3.5	OCTAVIUS® 1500- The New Checkerboard Detector for Patient and Machine QA. . . .	43
3.6	TrueBeam System, Varian Medical Systems, installed in IPO-Porto. . . . .	45
3.7	Design configurations for isocentric medical linacs. The accelerating waveguide and RF power generator are located in the gantry stand; electrons are brought to the movable target through a beam transport system; the machine can produce megavoltage X rays as well as electrons. . . . .	46
3.8	Female Alderson Radiation Therapy phantom (ART). . . . .	47
3.9	Experimental set-up with 20 plates of RW3 phantom, indicated in blue. . . . .	48
3.10	PMMA material board with dimensions of 29.8 cm x 31.5 cm x 1 cm, with excavated circles for the placement of dosimeters from 2 to 2 cm. . . . .	49
3.11	DYMAX 30 Charles Austen Pumps Ltd. with Vaccum Tweezer. . . . .	51
3.12	Numeration of the first 10 Radcard dosimeters. . . . .	51
3.13	Circular and rectangular cases. . . . .	52
3.14	Time-temperature profile and glow curve for LiF:Mg,Ti freshly exposed to 1 Gy. . . .	53
3.15	Time Temperature Profile Setup Dialog Box in edit mode view. . . . .	55
4.1	Representative scheme of experimental steps . . . . .	60
4.2	PMMA material board with numeration of excavated circles for the placement of dosimeters from 2 to 2 cm. . . . .	60
4.3	Dose profile obtained by scanning the beam with a ionizing chamber of a field 10x10 cm <sup>2</sup> and 15x15 cm <sup>2</sup> with a beam of 6 MV and zoom to the central region. . . . .	62
4.4	Example of a curve collected by the reader HARSHAW TLD™ Model 3500 Manual Reader. . . . .	62
4.5	Normalized values obtained by the matrix according to the position of the detector. . . . .	64
4.6	Values of ECC obtained according to the position of the detector to MTS-100 versus TLD-100. . . . .	65
4.7	Values obtained according to the position of the detector and with respective corrections (Group A). . . . .	66
4.8	Values obtained according to the position of the detector and with respective corrections (Group B). . . . .	67
4.9	Values obtained to 11 detectors with respective corrections (Group A). . . . .	69
4.10	Values obtained to 11 detectors with respective corrections (Group B). . . . .	69
4.11	Experimental set-up of the floor irradiation. . . . .	71
4.12	Values obtained according to the position of the detector and with respective corrections (Group A). . . . .	71
4.13	Values obtained according to the position of the detector and with respective corrections (Group B). . . . .	72
4.14	Background value for MTS-100 detectors, for irradiations of 1.36 Gy over 20 cycles of readings (Group A). . . . .	73

4.15	Background value, normalized to the first for TLD-100 detectors, for irradiations of 1.36 Gy over 20 cycles of readings (Group B). . . . .	73
4.16	Background value, normalized to the first for MTS-100 detectors, for irradiations of 1.36 Gy over 20 cycles of readings (Group A). . . . .	74
4.17	Background value, normalized to the first for TLD-100 detectors, for irradiations of 1.36 Gy over 20 cycles of readings (Group B). . . . .	74
4.18	Repeatability achieved in 10 successive measurements, translated by the values of the individual correction factors obtained in each cycle - detectors irradiated at 1.36 Gy, solitary (Group A). . . . .	76
4.19	Repeatability achieved in 10 successive measurements, translated by the values of the individual correction factors obtained in each cycle - detectors irradiated at 1.36 Gy, solitary (Group B). . . . .	76
4.20	Repeatability of the MTS-100 detectors for irradiations of 1.36 Gy (Group A). . .	77
4.21	Repeatability of the TLD-100 detectors for irradiations of 1.36 Gy (Group B). . .	78
4.22	Values obtained to detectors with respective corrections and linear regression in function of quantity of MU (Group A). . . . .	79
4.23	Values obtained to detectors with respective corrections and linear regression in function of quantity of MU (Group B). . . . .	79
4.24	Values obtained to detectors with respective corrections and linear regression (Group A). . . . .	80
4.25	Glow curves obtain after irradiation of 800 MU versus 200 MU (Group A). . . .	80
4.26	Values obtained to detectors with respective corrections and linear regression (Group B). . . . .	81
4.27	Values obtained to detectors with respective corrections and linear regression (Group A). . . . .	81
4.28	Values obtained to detectors with respective corrections and linear regression (Group B). . . . .	82
4.29	Values obtained to detectors with respective corrections (Group A). . . . .	83
4.30	Values obtained to detectors with respective corrections (Group B). . . . .	84
4.31	Experimental set-up of the Alderson RANDO Phantom irradiation. . . . .	88
4.32	Points of measurement in Alderson RANDO Phantom irradiation a) Sketch b) Photograph. . . . .	88
A.1	Front view of the controller. . . . .	95
A.2	The upper section of the display shows the set selected, the lower section shows the five digits which make up the set. . . . .	96
A.3	An example of a program profile. Each ramp consists of a controlled rate of change of setpoint to a target level. Each ramp is followed by a dwell at that level. The ramp rate, target level and dwell time are set by the user. . . . .	98
B.1	Main Menu. . . . .	102
B.2	New Workspace Wizard into view - step 1. . . . .	102
B.3	New Workspace Wizard into view - step 2. . . . .	103
B.4	New Workspace Wizard into view - step 3. . . . .	103
B.5	New Workspace Wizard into view - step 4. . . . .	104
B.6	Password Dialog Box into view. . . . .	104
B.7	Acquisition Setup Dialog Box in edit mode view. . . . .	105
B.8	Read Dosimeters Dialog Box. . . . .	107
B.9	Read Dosimeters Dialog Box - Dosimeter ID Entry. . . . .	107

B.10 Data Acquisition Dialog Box - PMT Noise Reading. . . . .	108
B.11 Results Screen Dialog Box - Glow Curve. . . . .	109

# List of Tables

1.1	Example of cancers treated with radiation therapy. . . . .	3
2.1	Effective atomic number $Z$ and density of some materials present in human body and others for reference. . . . .	14
2.2	Summary of characteristics of detectors used for EBRT <i>in vivo</i> dosimetry, given as the dependence of the detector sensitivity on a specific parameter. . . . .	19
2.3	Analysis of the weaknesses and strengths of the TLD's. . . . .	20
2.4	Half-lives of the LiF:Mg trap peaks and peak temperatures. . . . .	31
3.1	Features of MTS pellets given by manufacture (Group A). . . . .	37
3.2	Full specificatons of manufacture of TLD-100 chips (Group B). . . . .	38
3.3	Full specifications of manufacture of HARSHAW TLD™ Model 3500 Manual Reader. . . . .	39
3.4	Dosimetry performance using LiF:Mg,Ti in conjunction with the HARSHAW TLD™ Model 3500 Manual Reader. . . . .	41
3.5	Full specifications of manufacture of OCTAVIUS® Detector 1500. . . . .	43
3.6	Table of specific conditions for each irradiation. . . . .	54
4.1	Table of results MTS-100 (Group A) versus TLD-100 (Group B) - Calibration. . . . .	68
4.2	Table of results MTS-100 versus TLD-100 - Test 1. . . . .	70
4.3	Table of results MTS-100 versus TLD-100 - Test 2. . . . .	72
4.4	Table of results MTS-100 versus TLD-100 - Background value. . . . .	75
4.5	Table of results MTS-100 (Group A) versus TLD-100 (Group B). . . . .	77
4.6	Table of results MTS-100 versus TLD-100 - Repeatability. . . . .	78
4.7	Table of specific quantity of MU for each irradiation. . . . .	83
4.8	Table of results MTS-100 versus TLD-100. . . . .	84
4.9	Budget of estimates of uncertainties for MTS-100 and TLD-100 dosimeters system utilized as individual chips. . . . .	86
4.10	Table of results MTS-100 versus TLD-100. . . . .	89
A.1	Beacons, operator buttons and their respective functionalities of the front panel. . . . .	96
A.2	To Set Up a Temperature Profile. . . . .	99
A.3	Operations with respective indications and actions. . . . .	100



# Abbreviations and Symbols

<b>ART</b>	Alderson <b>R</b> adiation Therapy phantom
<b>ACQ</b>	<b>A</b> cquisition Set-up
<b>CBCT</b>	Cone <b>B</b> eam <b>C</b> omputerized Tomography
<b>CI-IPOP</b>	Centro de <b>I</b> vestigação do <b>I</b> PO- <b>P</b> orto
<b>CT</b>	<b>C</b> omputerized Tomography
<b>DIRE</b>	<i>Dosimetria Individual de Radiação Externa</i>
<b>DNA</b>	<b>D</b> eoxyribonucleic Acid
<b>DSB</b>	<b>D</b> ouble <b>S</b> trand <b>B</b> reaks
<b>ECC</b>	<b>E</b> lement <b>C</b> orrection <b>C</b> oefficient
<b>EBRT</b>	<b>E</b> xternal <b>B</b> eam <b>R</b> adio <b>T</b> herapy
<b>FCUP</b>	Faculdade de <b>C</b> iências da <b>U</b> niversidade do <b>P</b> orto
<b>FFF</b>	<b>F</b> lattening <b>F</b> ilter <b>F</b> ree
<b>Gy</b>	<b>G</b> ray
<b>IAEA</b>	<b>I</b> nternational <b>A</b> tomic <b>E</b> nergy <b>A</b> gency
<b>ICRP</b>	<b>I</b> nternational <b>C</b> ommission on <b>R</b> adiological <b>P</b> rotection
<b>ICRU</b>	<b>I</b> nternational <b>C</b> ommission on <b>R</b> adiation <b>U</b> nits and <b>M</b> easurements
<b>IMAT</b>	<b>I</b> ntensity <b>M</b> odulated <b>A</b> rc <b>T</b> herapy
<b>IMRT</b>	<b>I</b> ntensity- <b>M</b> odulated <b>R</b> adiation <b>T</b> herapy
<b>IPO-Porto</b>	<b>I</b> nstituto <b>P</b> ortuguês de <b>O</b> ncologia do <b>P</b> orto FG, EPE
<b>IST/CTN</b>	<i>Instituto Superior Técnico / Campus Tecnológico e Nuclear</i>
<b>IVD</b>	<i>In Vivo</i> <b>D</b> osimetry
<b>LINAC</b>	<b>L</b> inear <b>A</b> ccelerator
<b>MLC</b>	<b>M</b> ulti- <b>L</b> eam <b>C</b> ollimator
<b>MOSFET</b>	<b>M</b> etal- <b>O</b> xide- <b>S</b> emiconductor <b>F</b> ield- <b>E</b> ffect <b>T</b> ransistor
<b>MTS-100</b>	Commercial designation of thermoluminescence dosimeter of LiF:Mg,Ti from the company Radcard
<b>MU</b>	<b>M</b> onitor <b>U</b> nits
<b>NCD</b>	<b>N</b> on- <b>C</b> ommunicable <b>D</b> isease
<b>NTCP</b>	<b>N</b> ormal <b>T</b> issue <b>C</b> omplication <b>P</b> robability
<b>OF</b>	<b>O</b> utput <b>F</b> actor
<b>OSL</b>	<b>O</b> ptically <b>S</b> timulated <b>L</b> uminescence
<b>PDD</b>	<b>P</b> ercentage <b>D</b> epth <b>D</b> ose curve
<b>PEEC</b>	<i>Programa de Estágios Extra-Curricular</i>
<b>PMMA</b>	<b>P</b> oly( <b>M</b> ethyl <b>M</b> eth <b>A</b> crylate)

<b>PMT</b>	<b>PhotoMultiplier Tubes</b>
<b>PTV</b>	<b>Planning Target Volume</b>
<b>QA</b>	<b>Quality Assurance</b>
<b>RPL</b>	<b>RadioPhotoLuminescence</b>
<b>SI</b>	<b>International System of Units</b>
<b>SSB</b>	<b>Single Strand Breaks</b>
<b>SSD</b>	<b>Source Skin Distance</b>
<b>TBI</b>	<b>Total Body Radiation</b>
<b>TCP</b>	<b>Tumor Control Probability</b>
<b>TL</b>	<b>Thermoluminescence</b>
<b>TLD</b>	<b>Thermoluminescence Dosimetry</b>
<b>TLD's</b>	<b>Thermoluminescence Dosimetry detectors or TL dosimeters</b>
<b>TLD-100<sup>TM</sup></b>	<b>Commercial designation of thermoluminescence dosimeter of LiF: Mg, Ti from the company Thermo Scientific<sup>TM</sup></b>
<b>TPS</b>	<b>Treatment Planning System</b>
<b>TTP</b>	<b>Time Temperature Profile</b>



# Terms and Definitions

The glossary of terms and definitions was adapted from ISO 28057:2014 [1], Appendix A of the thesis that is referenced in [2] and Glossary of the American Cancer Society [3]. This comprises special terms used in dosimetry of ionizing radiation, in particular in TLD, some radiological quantities and some clinical terms.

<b>Absorbed dose</b>	Energy imparted to matter in a suitably small element of volume by ionizing radiation, divided by the mass of that element of volume.
<b>Background value</b> ( $M_0$ )	Indicated value of a TLD system during evaluation of a non-irradiated TL detector according to the operating instructions.
<b>Batch</b>	Number of TL detectors of the same type originating from the same manufacturing process and corresponding in their entirety both to the requirements defined in the ISO and to the quality proprieties guaranteed by the manufacturer with regard to their response, their individual variation and their non-linearity.
<b>Calibration</b>	Determination of the correlation between the indicated value of a TL detector and the conventional true value of the measured quantity, absorbed dose to water, under reference conditions.
<b>Casing</b>	Capsule in which a small set of TL detectors can be placed in the same plane.
<b>Conditioning</b>	Multiple irradiation and pre-irradiation annealing of a batch of TL detectors.
<b>Correction factor</b>	Factor applied to the indicated value in order to compensate for the measurement deviation caused by an influence quantity or by the measured quantity. Examples for using a correction factor are the corrections for fading, energy dependence, and non-linearity
<b>Correction summand</b>	Summand added to the indicated value in order to compensate for the measurement deviation caused by an influence quantity. The background value is an example for corrections using a correction summand.

<b>Double-strand breaks (DSB)</b>	Double-strand breaks, in which both strands in the double helix are severed, are particularly hazardous to the cell because they can lead to genome rearrangements. Double-strand breaks at the same point are irreparable because neither strand can then serve as a template for repair. The cell will die in the next mitosis or in some rare instances, mutate.
<b>Energy dependence</b>	Dependence of the response of a TL detector on radiation quality.
<b>Fading (F)</b>	Quotient of the alteration of the measured value of the absorbed dose during the time interval between the end of irradiation and evaluation, e.g. caused by the influence of ambient temperature, and the value of the absorbed dose measured immediately after irradiation. Fading is expressed as a percentage. The alteration of the measured absorbed dose may be positive (increment) or negative (decrement).
<b>Field output factors (FOF/OF)</b>	Measurements of the dose rate (or dose per MU) in phantom as a function of field size and it is a necessary step in the commissioning process. The measured in-phantom field output factors are assumed to be the product of two independent effects: phantom scatter factor ( $S_p$ ) and collimator (or head) scatter factor ( $S_c$ ). Measurements of OF should be performed with an ionization chamber in a water phantom and should be at the depth and distance from the source, corresponding to the reference conditions used for calibration.
<b>Glow curve</b>	Measured value of the light emission of the TL detector as a function of the temperature or time during the evaluation process.
<b>Gray (Gy)</b>	The gray is a derived unit of ionizing radiation dose in the International System of Units (SI). It is defined as the absorption of one joule of radiation energy per kilogram of matter.
<b>Indicated value (M)</b>	Numerical value of a parameter displayed by a TL-indicating instrument. The indicated value, M, for a TL detector is assessed from the glow curve by the TL-indicating instrument. The measured value of the dose is determined from the indicated value by applying the calibration coefficient, the correction factors, and the correction summands. The indicated value is also termed the reading of the TL-indicating instrument.

<b>Individual variation of the response</b>	Deviation of the response of single TL detectors from the mean response of a batch of TL detectors under identical irradiation and evaluation conditions.
<b>Influence quantity</b>	A quantity which is not a measured quantity but nevertheless influences the result of a measurement. Influence quantities can develop influences as external disturbances (temperature, humidity, line voltage, etc.), as properties inherent to the instrument, i.e. caused by the instrument itself (zero drift, aging of the system components, post-irradiation stabilization, etc.), or as adjustable quantities affecting the result of the measurement [e.g. radiation quality or direction of radiation incidence during dose measurement]. The correction of the impact of an influence quantity may require the application to the indicated value of a correction factor [multiplicative influence quantity, e.g. fading] or of a correction summand [additive influence quantity, e.g. background value]. If an influence quantity is not taken into account by applying a correction factor or a correction summand, the correction factor is set equal to one or the correction summand is set equal to zero, respectively.
<b>Linear energy transfer (LET)</b>	Average energy locally imparted to a medium by a charged particle of a specified energy along a suitably small element of its path, divided by that element. The value of LET (in keV/ $\mu\text{m}$ ) is usually stated for water as the medium traversed by the charged particle.
<b>Measured quantity</b>	Physical quantity to be determined by the measuring system.
<b>Measured value of a TLD system</b>	Value of the measured quantity, absorbed dose to water, determined with a TLD system at the point of measurement. The measured value is determined as the product of the correction factors and the mean of the indicated values of the single TL detectors, located at and irradiated together at the same time in the TL probe, corrected for the background value, and multiplied by the individual calibration coefficient.
<b>Measurement cycle</b>	Sequence of working steps in TL dosimetry consisting of pre-irradiation annealing, irradiation, post-irradiation annealing and evaluation of TL detectors.
<b>Measuring range</b>	Range of dose values in which the TLD system meets the requirements for the operation characteristics. The limits of the measuring range of a TLD system are within the interval spanned by the smallest and the highest measured value.

<b>Noncommunicable diseases (NCD's)</b>	NCD's also known as chronic diseases, tend to be of long duration and are the result of a combination of genetic, physiological, environmental and behaviors factors. The main types of NCDs are cardiovascular diseases (like heart attacks and stroke), cancers, chronic respiratory diseases (such as chronic obstructive pulmonary disease and asthma) and diabetes.
<b>Nonlinearity of response</b>	Change in response to dependence on dose. Linearity means constant response, supralinearity denotes an increase in response, and sublinearity denotes a decrease in response with increasing dose.
<b>Parameters for tests</b>	Values of influence quantities agreed upon for testing the impact of other influence quantities.
<b>Percentage Depth Dose (PDD)</b>	In radiotherapy, a percentage depth dose curve relates the absorbed dose deposited by a radiation beam into a medium as it varies with depth along the axis of the beam. The dose values are divided by the maximum dose, referred to as $d_{max}$ , yielding a plot in terms of percentage of the maximum dose. Dose measurements are generally made in water with an ionization chamber, since water is very similar to human tissue with regard to radiation scattering and absorption.
<b>Point of measurement</b>	The point on or in the patient's body or water phantom at which the absorbed dose to water is measured.
<b>Post-irradiation annealing</b>	Controlled heat treatment (annealing) of a TL detector after irradiation and before evaluation. Post-irradiation annealing serves to reduce the fading.
<b>Pre-irradiation annealing</b>	Controlled heat treatment of already evaluated TL detectors before reuse. Pre-irradiation annealing serves to delete the radiation-induced TL signal remaining after evaluation and approximately restores the original response.
<b>Radiation damage</b>	Permanent alteration of the response of a TL detector due to pre-irradiation beyond a detector-specific dose. The value of this dose may depend on the temporal pattern of pre-irradiations (dose fractionation, dose protraction).

<b>Reference/calibration conditions</b>	Set of reference values of all influence quantities and of the measured quantity. If one or more influence quantities or the measured quantity deviate from their reference values, the conditions of measurement are denoted as non-reference conditions.
<b>Reference/calibration detector</b>	TL detector used to determine the correction factor for the change in response during successive measurement cycles.
<b>Reference point of a TL probe</b>	Point located within or on the surface of the TL probe whose spatial coordinates serve to specify the position of the TL probe in its surroundings. In clinical dose measurements, the reference point of a TL probe is placed at the point of measurement either on or in the phantom or the patient's body. For calibration, the reference point of a TL probe is placed at the point at which the absorbed dose to water under reference conditions is known.
<b>Response</b>	Difference between the indicated value for a single TL detector $i$ and the background value divided by the conventional true value of the causing absorbed dose to water. The response of a TL detector does not only depend on the absorbed dose, but also on the radiation quality, the direction of radiation incidence, the material and size of the detector, the type of the detector, the casing, and the TL-reading instrument.
<b>Single strand break (SSB)</b>	When only one of the two strands of a double helix has a defect, the other strand can be used as a template to guide the correction of the damaged strand. In order to repair damage to one of the two paired molecules of DNA, there exist a number of excision repair mechanisms that remove the damaged nucleotide and replace it with an undamaged nucleotide complementary to that found in the undamaged DNA strand.
<b>Stability check device</b>	Instrument for checking the dosimeter response.
<b>Test conditions</b>	Set of parameters for tests of all influence quantities.
<b>Test light source</b>	Light source with constant illuminance used for operation checks of the TL-indicating instrument.

<b>Thermoluminescence (TL)</b>	Light emission in a visible or adjacent spectral range, based on the radiation-induced occupation of trapping centers by the charge carriers of certain ion crystals, and emitted when the transition of these charge carriers into activator levels occurs as a consequence of heating.
<b>Thermoluminescence detector (TLD's)</b>	Quantity of TL material of a certain chemical composition in homogeneous, e.g. crystalline or polycrystalline form. The properties of a TL detector are determined by its material composition, mass, and shape, as well as by pre-irradiation or special thermal pretreatment.
<b>Thermoluminescence dosimetry system (TLD system)</b>	TLD system consisting of a number of TL detectors of a certain type, which are placed, if necessary, in groups forming TL probes, as well as of the associated TL-indicating instrument, and, if there is a need, the supporting instruments, the operating instructions containing the description of the evaluation procedure, and the calibration instructions for the TLD system.
<b>Thermoluminescence-indicating instrument (Reader)</b>	Instrument for measuring the thermoluminescence light emitted by a TL detector. The instrument is equipped with devices for heating the TL detector, for recording the light emitted by the TL detector, and for the indication of a measurement signal proportional to the TL light emission.
<b>Thermoluminescence probe (TL probe)</b>	Setup consisting of one or more TL detectors and the corresponding casing.

**Tissue-equivalent**

Tissue equivalent denotes a substance, with absorbing and scattering properties for a given radiation that sufficiently match those of a certain biological tissue.

**Type of thermoluminescence detector**

Characteristic type of all TL detectors which have been manufactured from the same material and according to the same specifications (shape, size) and have the same dosimetric properties except for some minor differences (batch variation) due to the manufacturing process.

**Uncertainty of measurement**

Parameter obtained by measurement or calibration which, together with the measured value, marks the range of values in which the true value of the measured quantity lies. The uncertainty of measurement is the positive root obtained from the sum of the squares of the standard uncertainties, for all uncertainty components.





# Chapter 1

## Introduction

The present work intends to answer the question: “How can we be sure of the actual dose that is being administered to a patient during a given treatment with ionizing radiation in External Beam Radiotherapy (EBRT)?”. The answer to this question will necessarily address the ways and detectors that are available to measure dose in-vivo, such as ionization chambers, diodes, metal–oxide–semiconductor field-effect transistors (MOSFET’s), TLD’s, optically stimulated luminescence (OSL) dosimeters, etc. The work developed in this thesis consists in the preparation of an in-vivo verification system using TLD in the Instituto Português de Oncologia - Porto FG, EPE (IPO-Porto), according to ISO standard 28057:2014.

### 1.1 Context

Cancer is the second leading cause of non communicable diseases (NCD) deaths worldwide and was responsible for 8.8 million deaths in 2015. Globally, just about 1 in 6 deaths are due to cancer. Besides that the number of new cases is expected to rise by about 70% over the next 2 decades. [4] In the Figure 1.1, it is notorious the big portion, 27%, that malignant neoplasm occupies in NCD deaths.

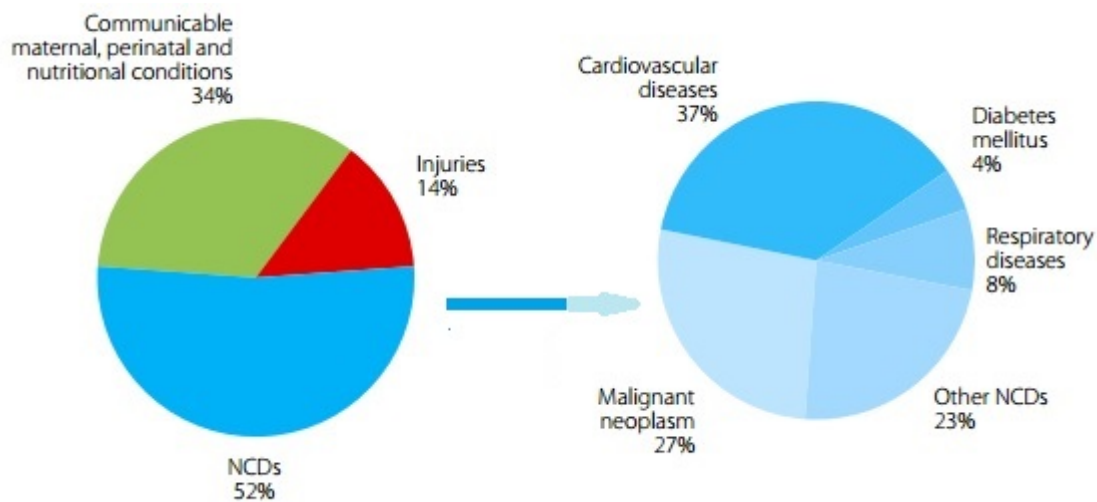


Figure 1.1: Proportion of global deaths under the age 70 years, by cause of death, 2012. Proportion of global NCD deaths under the age of 70, by cause of death, 2012. Adapted from [5].

The goal of Radiotherapy is to precisely and efficiently administer radiation to treat various types of malignant and non-malignant anomalies and consequently, reduce the number of deaths by cancer. Unfortunately, these objectives are not always achieved. Over the last few years, numerous radiation accidents in several countries have been reported. Basic Safety Standards defines the radiological accident as: ACCIDENT is any severe unintended event, including an operating error, equipment failure or other mishap, the consequences of which cannot be ignored from the protection or safety point of view, and which usually leads to potential overexposure or to abnormal exposure conditions for treated patient, staff or general public. [6]

Unfortunately, the recent history is full of many examples of such accidents throughout history since the discovery of x-rays (and, consequently, radiography) on November 8, 1895 by German physicist Wilhelm Conrad Röntgen. [7]

The first example described the use of an incorrect decay curve for  $^{60}\text{Co}$  (USA, 1974-76). As a consequence 34 % of the patients who survived had several complications, such as redness of the skin, ulcerations and blistering. Later, as a second example, there was an incorrect accelerator repair and communicative problem that led to the death of at least 15 of the patients from the accidental exposure (Spain, 1990). The last example reported an untested change of procedure for data entry into TPS that leading to 100% overdose (Panama, 2000). This error affected 28 patients, of whom at least 5 died due to overexposure. [8]

Besides the overdose incidents, suboptimal patient treatments also happen since one or more of the parameters involved in a patient irradiation may have a systematic error or can be originated by human errors. [9]

In order to avoid more accidents such as those reported above, the direct and causing reasons of radiological accidents have been inferred from each incident, when it was possible and classified into 9 categories: mistakes in procedures (30%), professional mistakes (17%), communication

mistakes (15%), lack of training (8.5%), interpretation mistakes (7%), lack of supervision (6%), mistakes in judgment (6%), hardware failures (5%), software and other mistakes (5.5%). Three types of direct and contributing causes responsible for almost 62% of all accidents are directly associated to the quality assurance (QA) of treatment. [10]

In conclusion, most accidents could have been avoided if a comprehensive QA program was established and applied correctly in all radiotherapy departments.

## 1.2 Motivation

First of all, an accurate cancer diagnosis is crucial for adequate and effective treatment since every cancer type requires a particular therapy that involves one or more modalities such as surgery, radiotherapy, chemotherapy or immunotherapy. [11]

The major goal in this field is usually to cure or control cancer and substantially prolong patient life. The International Agency for Research on Cancer defends that improving the patient's quality of life is also an important goal. This can be accomplished by palliative care and psychosocial support given by health services that should be integrated and people-centered. [12]

However, each method has its particularities which undertakes special role in cancer treatment. Radiotherapy is one of the modalities most commonly used for disease control. [13] It is possible to observe in Table 1.1 the several carcinomas in which this modality is selected by the teams in hospital centers around the world.

Table 1.1: Example of cancers treated with radiation therapy. Adapted from [14].

Early cancers curable with radiation therapy alone	Cancers curable with radiation therapy in combination with other modalities
Skin cancers (Squamous and Basel cell)	Breast carcinomas
Prostate carcinomas	Rectal and anal carcinomas
Lung carcinomas (non-small cell)	Local advanced cervix carcinomas
Cervix carcinomas	Locally advanced head and neck carcinomas
Lymphomas (Hodgkin's and low grade Non-Hodgkin's)	Locally advanced lung carcinomas
Head and neck carcinomas	Advanced lymphomas
	Bladder carcinomas
	Endometrial carcinomas
	CNS tumors
	Soft tissue sarcomas
	Pediatric tumors

EBRT aims to shape the optimal isodose curve to the tumor volume while indulging normal tissues. The profits of this purpose are threefold: patient cure, organ preservation and cost-efficiency. [15] Effectiveness of irradiation is based on the accuracy by which the dose is planned and delivered to the patient. Consequently, the dose and dose distribution evaluation administered to patients during treatment is a fundamental quality control process; the percentage difference between the prescribed and administered dose recommended by the International Commission on

Radiation Units and Measurements (ICRU), should be between -5% and +7%. [16]

*In vivo* dosimetry, that is, the set of measurements that are carried out during the course of the treatment and where the dosimeters are placed in the skin of the patient or in existing cavities is one way of verifying the quality of the treatment. Usually, IVD is used for the detection of errors in individual patients, as well as errors in the procedures applied in the clinic. In addition, this technique has important applications, specifically in the evaluation of the quality of a specific treatment technique or in the evaluation of the dose in situations in which its calculation is more imprecise or even impossible depending on the software of dose distribution optimization (TPS). Thus, it can be concluded that the IVD routine is an added value for the patient. [17]

The IVD will be the object of study of the present work and in the same will be analyzed, in particular, the typical characteristics of the thermoluminescence detectors that can be used. In addition, the advantages and disadvantages of this type of device will be analyzed as well as its basic operating principle and the motivations that will lead to its use in clinical practice.

### 1.3 Goals

The purpose of this work is to guarantee the reliability and the accuracy indispensable in clinical *in vivo* dosimetry when applied in the patient or phantom. In order to achieve these main goals, the following requisites have been identified:

- To have a global perspective of the dosimetry systems existing and their application in the clinical practice;
- To understand the phenomenon and study the theoretical basis behind thermoluminescence dosimetry;
- To learn how to handle the equipment that compose the thermoluminescence dosimetry system, namely the reader and associated software, the programmable oven controller, the linear accelerator and the matrix of ionization chambers (this point will be explained later in the thesis);
- Analyze the ISO standards and understand the requirements necessary to implement a thermoluminescence dosimetry system according to these standards;
- To establish a calibration procedure approaching the ISO 28057:2014 standard using a last generation linear accelerator and a novel beam heterogeneities correction;
- To compare the physical characteristics of two TLD (LiF: Mg, Ti) batches from different manufactures - Radcard (MTS-100) and Thermo Scientific™ (TLD-100) - leading to a reliable clinical dosimetry protocol;
- To test the TLD system in a clinical application on a particular pathology.

## 1.4 Information and Cases of Study

The research that supports this thesis was conducted during the years 2016 and 2017 in the context of the Masters in Medical Physics of *Faculdade de Ciências da Universidade do Porto* (FCUP). This dissertation was carried out following the establishment of a contract for an Extra-Curricular Internship Program (named PEEC) between the master's degree student, the FCUP and the IPO-Porto, which was carried out at the latter's facilities.

Thus, to perform the experimental activities presented in chapters 3 was available a dosimetry system (Medical Physics service of IPO-Porto) and a Varian Truebeam® accelerator (External Radiotherapy service of IPO-Porto). Additionally, the lab DIRE (*Dosimetria Individual de Radiação Externa*) at *Campus Tecnológico e Nuclear* of IST/CTN (*Instituto Superior Técnico/Campus Tecnológico e Nuclear*) provided their valuable assistance for some initial experimental methodological approach.

In chapter 3, in addition to the data obtained in phantoms, it was necessary to obtain data from real treatments. These data was obtained with the collaboration of IPO-Porto.

Furthermore the collaboration of IPO-Porto, it stands out the role of the *Centro de Investigação do IPO-Porto* (CI-IPOP), in particular to *Grupo de Física Médica, Radiobiologia e Proteção Radiológica*.

## 1.5 Document Structure

The diagram of the Figure 1.2 shows the structure of the various phases of this work, from the bibliographic review, including the detailed reading of the ISO standards, being the starting point to develop the next approach in the implementation of the dosimetry system. This was followed by a visit to the DIRE laboratory that provided an insight into what is necessary in a dosimetry laboratory and allowed the experimentation of its system. In addition, they also provided some theoretical knowledge, namely the PhD thesis of Dr. João Alves and provided the commands to be used in the software associated with the reader HARSHAW TLD™ Model 3500 Manual Reader, Thermo Scientific™ WinREMS™. After that, the IPO-Porto implementation proved to be challenging, since a traditional calibration  $^{60}\text{Co}$  source was not available in its installations, for example. After a few attempts and a high data collection it was concluded that the use of a OCTAVIUS Detector 1500, a matrix of 1405 vented ionization chambers, would correct the geometric deviations associated to the linear accelerator. Besides that, the need to learn how to program the controller of the oven emerged from the requirement to create a reproducible annealing cycle. Once the calibration process was completed and functional, some tests were implemented. Then, it was carried out an application in a phantom. The results were obtained and discussed, highlighting comparison between two batches available. Finally the conclusions were reached.

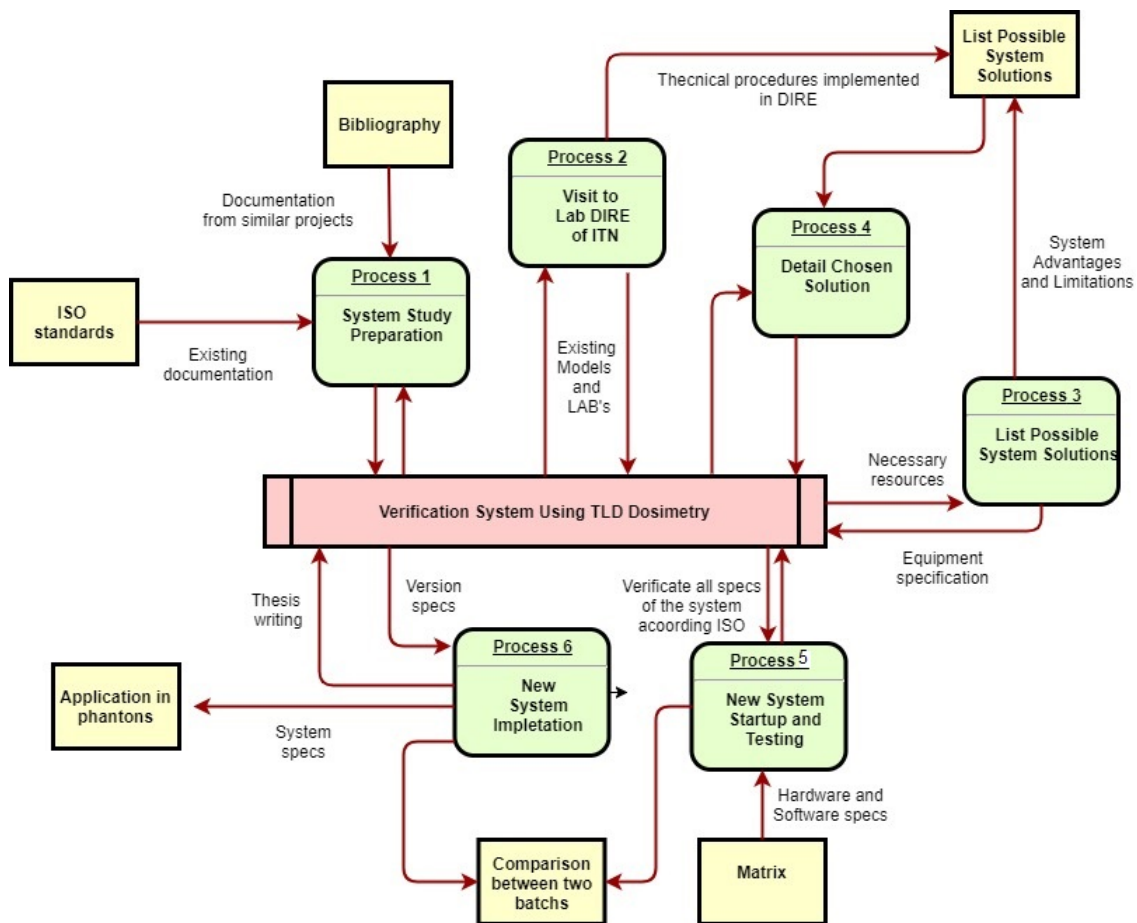


Figure 1.2: Structure of the plan of research work.

All this research and operational work culminated in this document. Therefore, the present thesis is divided in 5 main chapters and two appendices pertaining to the controller of the oven and the operational software of the reader HARSHAW TLD™ Model 3500 Manual Reader, Thermo Scientific™ WinREMS™.

Initially, in Chapter 1 a brief framework is given to the subject of the work, the objectives and motivations that led to its realization are described, and the support for obtaining the data and material necessary to carry out the presented work of investigation is also mentioned.

Then, the Chapter 2 presents the essential concepts about ionizing radiation and a theoretical framework on radiotherapy (this chapter aims to clarify concepts and approaches determinant to the work). It also presents the physical processes inherent to the dosimetry systems used in the dissertation: ionization chamber and thermoluminescence detectors, presenting a more detailed description for the TL detectors, object of study of this work.

After, in the Chapter 3 a description of the materials and methods used in the fieldwork of this thesis is provided. In particular, it describes the details of this investigation, the characteristics of the detectors under study, the measurements and a collection of ISO standards.

The Chapter 4 encompasses the experimental results obtained, their respective analysis and,

consequently, their discussion. The calculation of dose, evaluation and comparison of the results of the both batches are also approached.

Finally, in Chapter 5, a critical analysis is pursued through the satisfaction of the objectives initially proposed, the main conclusions are presented through this dissertation, as well as some references to possible future work which seems to be interesting for the development of the application of TL (Thermoluminescence) IVD in the IPO-PORTO.





## Chapter 2

# Theoretical Framework

The purpose of this chapter is to accomplish a bibliographical review that allows someone with a basic academic background to be introduced to the necessary concepts for the understanding of the developed work.

To accomplish this objective, at the beginning, it presents the essential concepts about ionizing radiation and a general theoretical framework beyond Radiotherapy. It also demonstrates the importance of quality control as well that precision and accuracy are essential in this area. Then a generalized approach to dosimetry and existing dosimeters is introduced. In the final stage of the chapter, the physical processes inherent to the dosimetry systems used in the dissertation, ionization chamber and thermoluminescence detectors, are presented and a more detailed description for the TLD detectors, principal object of study of this work, is explained.

### 2.1 Radiotherapy

EBRT uses high-energy particles or photons, such as x-rays, gamma rays, electron beams, or protons, to destroy or damage cancer cells. Other designations for radiation therapy are x-ray therapy, radiation oncology, therapeutic radiology, irradiation or - the most popular - Radiotherapy. [3]

#### 2.1.1 Ionizing Radiation

In the human body, the majority of cells raises and divide to form new cells. But, in most types of cancer, some of the body's cells begin to divide without stopping - an uncontrolled growth - and can spread into surrounding tissues or metastasise all the way through the body. However, every cancer type requires a particular treatment procedure that implies one or more modalities such as surgery, radiotherapy, chemotherapy and immunotherapy. Each method has its unique proprieties which assume a distinct role in cancer treatment; nevertheless, Radiotherapy is a crucial component of cancer management.

A concrete proof of that is the fact that around 50% of all patients with localized malignant tumors are treated with ionizing radiation at some time in the progression of their illness. [18]

In addition, as it can be seen in the Table 1.1, in Chapter 1 this modality is chosen for the treatment of the most diverse types of cancer, since it destroys cancer tissues by depositing high energy radiation on them.

### 2.1.1.1 Radiobiology

Radiation mechanism of the treatment is the creation of small breaks in the DNA chains inside cells nucleus. These breaks retain can prevent cancer cells from growing and dividing, and often cause them to die. But, the primary goal is the radiobiological death of cell (loss of reproductive ability- reproductive death) is abortive cell divisions after irradiation. Nearby normal cells can also be affected by radiation, but most recover and go back to function the way they were meant to.

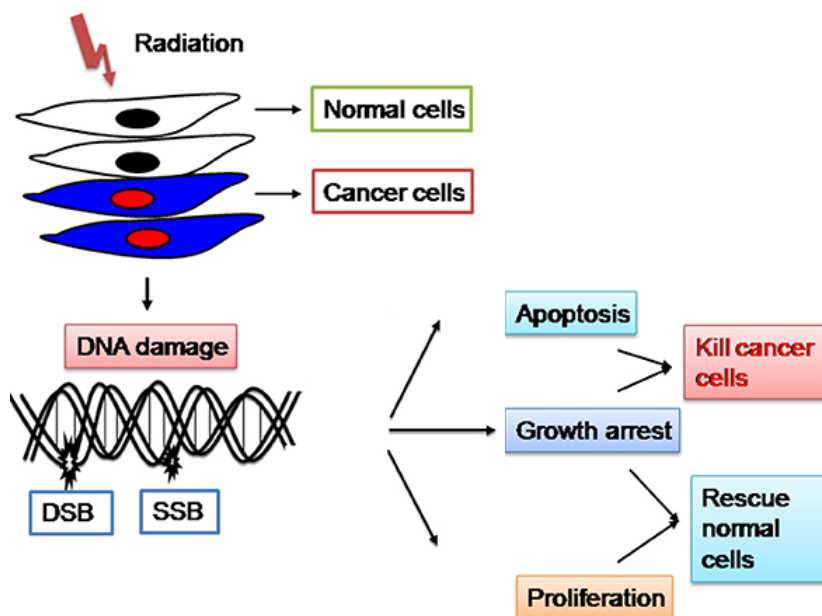


Figure 2.1: Ionizing radiation damages the genetic material (DNA) causing single strand breaks (SSB) or double strand breaks (DSB) in the cells, thus blocking their ability to divide and proliferate further. Mechanisms involved in the decrease of radio-sensitivity of the fast doubling cancer cells, while increasing radio-resistant of the slow doubling normal cells benefits the cancer patients. Adapted from [19].

Damages to the cell due to ionizing radiation can be caused by the direct or indirect action of radiation on the DNA molecules, as explained in Figure 2.2. In the direct action, the radiation impact on the DNA molecule directly, disrupting the molecular structure. This process becomes predominant with high-LET radiations such as  $\alpha$ -particles and neutrons, and high radiation doses. In the indirect action, the radiation interacts mainly with the water molecules, the major constituent of the cell, and other organic molecules in the cell, where by free radicals such as hydroxyl ions are generated. [20]

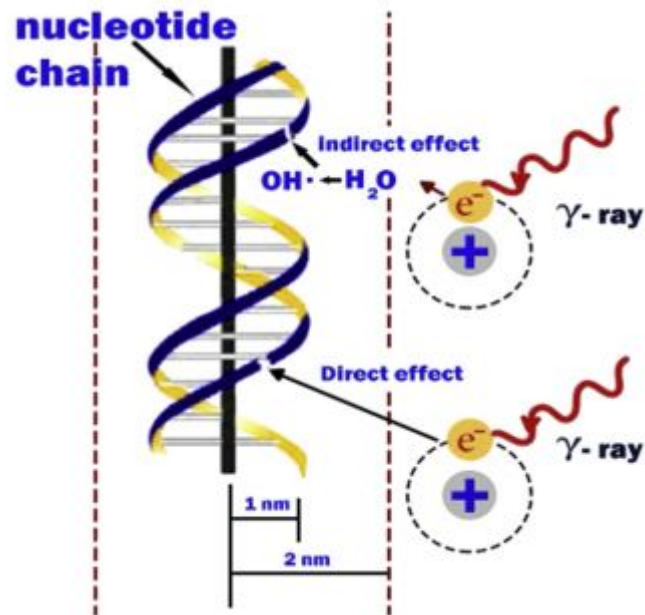


Figure 2.2: Direct and indirect actions of radiation. Adapted from [20].

Unfortunately, premature and late toxicity restricts the deliverable intensity of radiotherapy, and possibly will have an effect on the long term health-related quality of life of the patient. This is a subject of considerable interest on the part of researchers and clinicians, so several projects have been carried out in order to know complications after radiation therapy. [21, 22, 23]

Primary consequences manifest themselves in only some weeks of the conclusion of a course of fractionated radiotherapy and they are transient. These effects include skin erythema, dry or moist desquamation of the skin, mucositis, nausea and diarrhea. Late effects of radiation include radiation induced second malignancies among others.

Late effects are usually expressed after latent periods of months to years, and besides radiation induced neoplasias, can involve radiation-induced fibrosis, atrophy, vascular damage, neural damage and a range of endocrine and growth-related consequences. They tend to be irreversible or even progressive in severity and the pathophysiological and functional expression of these injuries is influenced by the tissue or organ irradiated. Radiation-induced second malignancies are of some apprehension, specifically in patient populations with a long life expectancy like children and young adults. [24]

### 2.1.1.2 Radiological physics

The physical process by which DNA damage occurs is named ionization and it is the process by which an atom or a molecule acquires a negative or positive charge by gaining or losing electrons to form ions. As the energy required to a valence electron escape from an atom is in the region of 4-25 eV, radiations must carry kinetic or quantum energies in extra of this magnitude to be titled "ionizing." So, the significant forms of ionizing radiations to take into consideration are:  $\gamma$ -rays;

X-rays; neutrons; fast electrons; heavy charge particles (proton, deuteron, triton, pions, alpha particles, etc.). The ability of radiation to induce ionization allows the categorization into non-ionizing and ionizing and in turn ionizing radiation can ionize matter either directly or indirectly, as exposed in Figure 2.3.

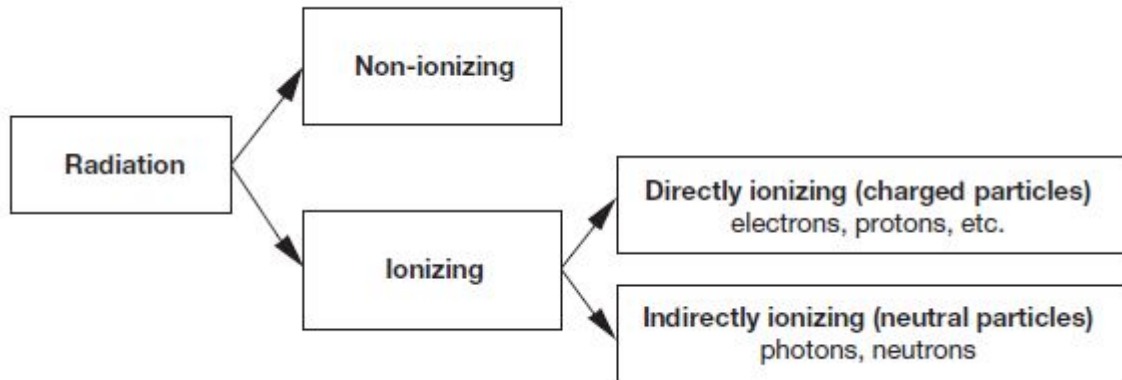


Figure 2.3: Classification of diverse types of radiation. [25]

Directly ionizing radiation deposits energy in the medium because of direct Coulomb interactions, involving the orbital electrons of atoms in the medium and directly ionizing charged particles. Indirectly ionizing radiation happens when neutral particles increase energy in the medium via a two-stage course of action: in the earliest stage a charged particle is released in the medium (photons release electrons or positrons, neutrons release protons or heavier ions); in a second stage the free charged particle have the exactly same behavior that a directly ionizing charge particle. [25]

There are five varieties of ionizing radiation interactions with matter which must be considered:

1. Compton effect;
2. Photoelectric effect;
3. Pair production;
4. Rayleigh (coherent) scattering;
5. Photonuclear interactions.

Considering the transfer of energy to electrons, the earliest three of these are the most significant, since Rayleigh scattering is elastic and photonuclear interactions are only significant for photon energies above a few MeV. Nevertheless, as explain in the graph of Figure 2.4, the relative prominence of Compton effect, photoelectric effect, and pair production depends on both the atomic number  $Z$  of the absorbing medium and photon quantum energy ( $E_\gamma = h\nu$ ). [26]

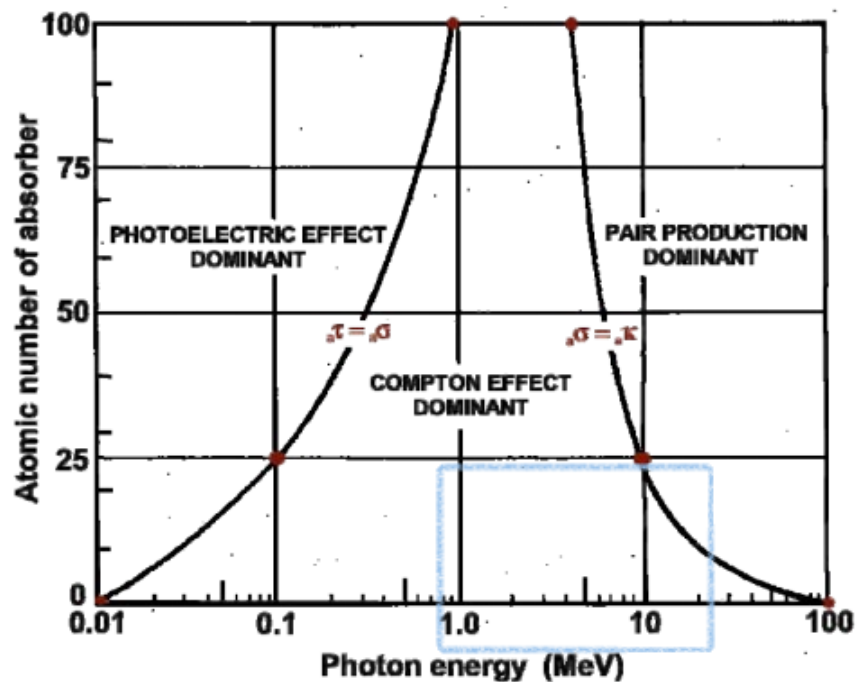


Figure 2.4: Dominant types of interactions as a function of the atomic number  $Z$  of the absorber and the energy of the photon radiation. The curves show where two kinds of interactions are equally probable. Adapted from [26].

It can be concluded that the photoelectric effect is most important at inferior photon energies, the Compton Effect is dominant at intermediate energies, and pair production is dominant at the higher energies.

Human tissue, fat, muscle, etc., are low- $Z$  medium as can be verified in Table 2.1. Consequently, this region (low- $Z$ ) is the one with more interest in the area of EBRT. In terms of energies, beams with the voltage range of 4-25 MV are used to treat deeply cancers and lower energy x-rays, called orthovoltage X-rays, are used to treat more superficial cancers. Conjugating these two conditions, it is concluded that the area highlighted in blue in 2.4 is one that presents a greater interest. [27]

Table 2.1: Effective atomic number  $Z$  and density of some materials present in human body and others for reference. [28]

Material	Effective Atomic Number $Z$	Density $\text{g cm}^{-3}$
Soft Tissue	7	1
- Fat	6	0.9
- Water	7.4	1
- Muscle	7.5	1
Air	7.6	0.00129
Bone	14	1.85
Calcium	20	1.55
Tooth		2.4
Iodine	53	4.9
Barium	56	3.5
Barium Contrast Media	56	4.25
Lead	82	11.3

Another conclusion that can be derived from the graph of the previous figure is the Compton-effect wide supremacy, extending from 20 keV to 30 MeV, for low  $Z$  medium. Nevertheless, this domain decreases gradually with the increase of  $Z$ .

As different interactions between radiation and the medium generate different responses, it can be stated that the response of each volume irradiated depends strongly on its composition.

### 2.1.2 Quality Control

Unfortunately, the response of tumor cells and living healthy tissue to radiation are not very diverse from each another, and as such, radiation therapies are undoubtedly more effective when the dose distribution is optimized. This principle is demonstrated in figure 2.5 by two curves, the first one being representative of the probability of tumor control (TCP) (curve A) while the second one is illustrative of the occurrence of normal tissue (NTCP) complications (curve B). [25]

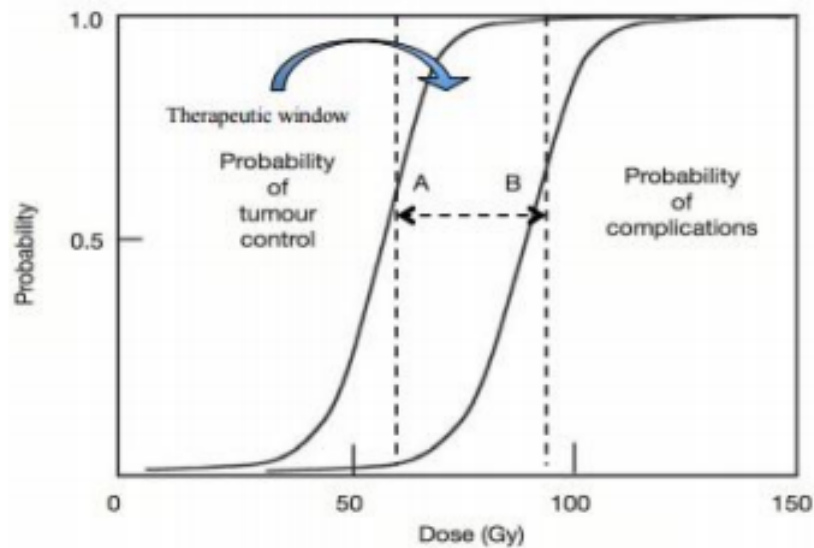


Figure 2.5: The principle of therapeutic ratio. Curve A represents the TCP and curve B the probability of complications. Adapted from [25].

EBRT aims to shape the optimal isodose curve to the tumor volume while sparing normal tissues. The profits of this purpose are threefold: patient cure, organ preservation and cost-efficiency.

The potential side effects, acute (occur during treatment) or chronic (occur months or years after treatment is completed), of radiotherapy depend on the area of the body being treated, the dose given per day, the total dose delivered, the patient's general medical condition, and other treatments given at the same time. So, any variation in the position and condition of the patient (such as body weight, pain or discomfort, stomach/intestine/bowel content, colon, bladder, etc.) can influence and therefore degrade the quality of the treatment thereby reducing therapeutic window. As a result, to overcome any adverse effects on the treatment, the movement of the patient or even the simple movement of their internal organs, especially their respiration, must be checked and can be compensated during treatment, so that a high accuracy can be achieved. [15]

Effectiveness of irradiation is based on the accuracy by which the dose is planned and delivered to the patient. Consequently, the dose and dose distribution evaluation administered to patients during treatment is a fundamental quality control process; the percentage difference between the prescribed and administered dose recommended by the ICRU, should be between -5% and +7%. [16]

Daily checks using *in vivo* dosimetry have the potential to detect variation in most of the parameters mentioned above, thus achieving a rigorous control that allows the patient to receive the correct dose of radiation at the exact position at each moment.

## 2.2 Detectors Applied for Dosimetry

In order to function as a radiation dosimeter, the dosimeter must have at least one physical property that is a function of the measured amount and that can be used for radiation dosimetry with an

adequate calibration. In practice for a dosimeter to be useful, it should have several desirable features characterized by their respective proprieties. Obviously, not all dosimeters can satisfy all desirable characteristics and therefore the choice of a dosimeter and its reader must be carefully designed considering the specific requirements of the measurement situation.

### **2.2.1 Dosimeter**

A radiation dosimeter is a device, instrument or system that measures and evaluates, directly or indirectly, exposure, absorbed dose or equivalent, kerma or any physical quantity that relates to ionizing radiation. A dosimeter along with his reader and measurement/calibration protocols is referred as a dosimetry system. [25]

Radiation dosimeters and dosimetry systems appear in numerous shapes and forms, and they depend on several physical effects for storage and readout of the dosimetric signal. The four most commonly used radiation dosimeters in Medical Physics in clinical environment are: ionization chambers; radiographic films; TLD's and diodes. New types of passive or active dosimeters such OSL dosimeters or other scintillation dosimeters are starting also to be used more broadly. [29]

Signal stability after irradiation, intrinsic accuracy, sensitivity, dose and dose rate response, temperature and energy influence and directional dependence are physical proprieties that characterize a dosimeter. It is necessary to take into account the variation of all of them according to the conditions of measurement and then apply the respective correction factors and thus obtain valid measurements. Furthermore, dosimeters can be categorized as one-dimensional, if they allow only dose measurement at one point - ionization chambers, semiconductors, and thermoluminescent detectors- , two-dimensional, by permitting the construction of the dose distribution map - radiosensitive films- and three-dimensional, capable of performing a 3D measurement of the dose. Ionization chamber matrices are considered two-dimensional or three-dimensional, depending on their distribution. [30]

Considering all the proprieties described above, the dosimeter that best fits the desired quality control parameters should be the one selected.

### **2.2.2 Dosimetry**

There are many steps in the chain of processes that determine the dose a patient will undergo in radiation therapy, as outlined in Figure 2.6.



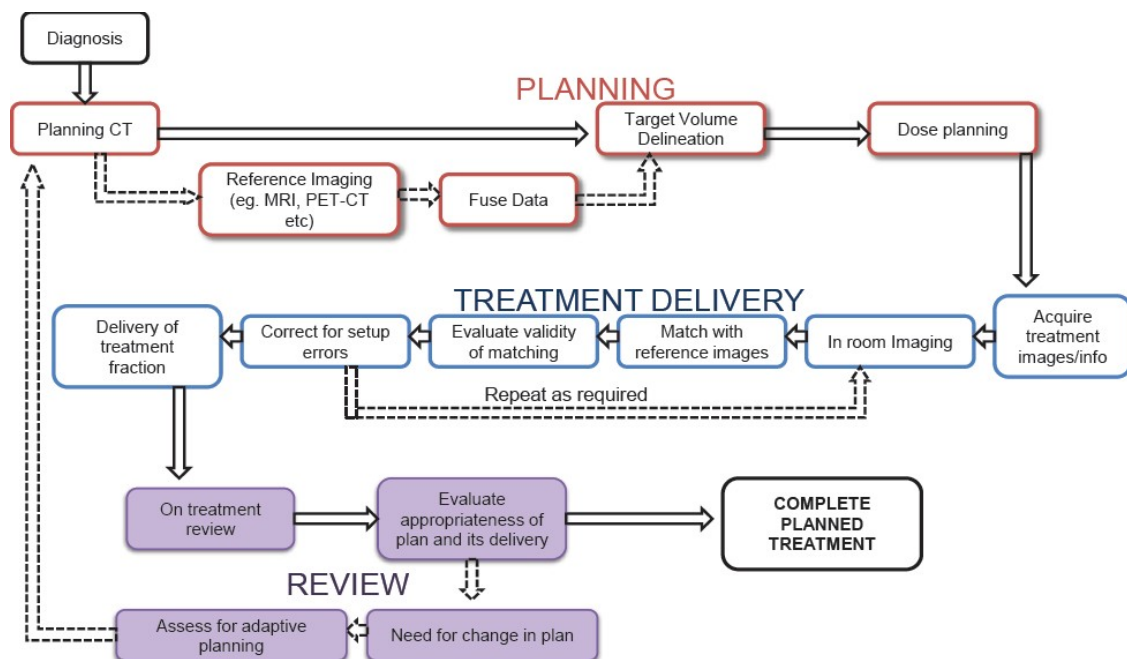


Figure 2.6: Representative scheme of all radiotherapy procedures and the role of *in vivo* dosimetry for treatment evaluation in the purple boxes. [31]

Initially, the oncologist begins by evaluating the patient's clinical situation to determine the indication for the treatment model. Then, before the start of treatment, there is a planning phase. A CT-scan (Computerized Tomography) is performed by radiotherapy technologist and references are obtained regarding the patient positioning to the isocenter.

The physician draws all the volumes in the CT previously obtained necessary to the elaboration of treatment plans and, defines the prescription dose to each volume and the fractionation (per fraction, for day and total). The elaboration of a specific plan performed by the dosimetrist and/or medical physicist depends on these indications. The treatment plan consists in the arrangement of the radiation beams to be used and dose to be administered, considering the tolerance levels of organ at risk. All these data are the basis of the treatment that will later be carried out by the radiotherapy technologists. Following this phase, the treatment is approved by the oncologist and a quality control is performed by the medical physicist.

After the planning stage and dosimetric verification, the therapeutic phase depends on the radiotherapy technologists, who works directly with the patient in the treatment centers.

During treatment, the duration of which may vary from one day to eight or more weeks, depending on the treatment modality, the medical radiotherapist performs several appointments of routine or motivated by occurrence of secondary effects due to irradiation. After conclusion of the prescribed treatment, a reference query is performed by the physician, in which the technical data is transcribed into the clinical process of the patient. [31]

Since the ICRU established, in 1976, that each of these steps until treatment delivery may introduce an uncertainty therefore, it may even be necessary for specific groups of patients or under unusual treatment conditions to perform a final check of the actual treatment using *in vivo*

dosimetry. [32]

### 2.2.2.1 Measurements *in vivo*

The ICRU Publication 24 specifies the parameters that the IVD should include, so dose measurements can be divided into:

- Intake dose measurements: Used to verify the output and performance of the treatment apparatus as well as the accuracy of patient positioning;
- Exit dose measurements: Used to check the algorithm for calculating the dose and determining the influence of size, shape and changes in patient body density in the dose calculation process; Sometimes it is also possible to determine the intracavitary dose in readily accessible body cavities.

A "first approach" method is to compare the values calculated by the treatment planning system (TPS) with the converted dose values of the signals from the detectors placed on the skin or in the patient's natural cavities. However, the computational precision of the algorithms present in the commercial TPS of the dose on the skin is questionable, including the cases where it is intended to perform a specific treatment on the skin. By placing a detector on the skin at the entrance and another at the exit it is possible to determine the inlet and outlet doses, respectively, and then apply corrections to validate the results of the comparison with the input and output values obtained in the planning. It is therefore an indirect determination of the dose at the intended target, in a phantom or a patient. A more ambitious method aims to directly verify whether the absorbed dose, usually in PTV, the target volume of the planning, is the one intended. For this purpose, it is advised if the radiation is being delivered correctly. However, except in cases where the possibility exists for the detectors to be inserted into the natural cavities, such as the rectum, esophageal tube, vagina, etc., it is impossible to perform measurements *in vivo* and locally. [32]

Generally, *in vivo* dosimetry is limited to measurements on the surface of the patient, being that one of the objectives of the IVD is to compare the doses measured from the signal of the dosimeters placed on the skin of the patient with the theoretical values calculated by the planning system.

If there is a significant deviation between the data, and assuming that the experimental values were correctly obtained, the target dose is incorrect. Having this information in mind it is necessary to subsequently find the source responsible for the deviation. Errors in radiation parameters, incorrect patient positioning, unexpected variations in the outputs of the devices and errors in the calculations are some of the several factors that can cause discrepancies in the desired values. [33]

*In vivo* dose measurements are not only used to verify dose delivery in the target volume but may also be employed in the evaluation of dosage for at-risk organs (eg: eye lens, gonads and lungs) or in situations where the dose is difficult to predict (eg: source-skin distance (SSD) in non-standard modalities like total body irradiation (TBI) or when using bolus).

If only input dose measurements are performed, it will have to be converted to the corresponding target dose using information on patient setup and treatment. A combination of measurements of dose in and out is a more accurate method of obtaining the dose at the target volume.

Several methods are currently available for obtaining the mid line dose from the inlet and outlet dose values. These methods generally show favorable results for homogeneous situations, but, however, if there are non-homogeneities, there is a risk of considerable deviations. These deviations can be tested in phantoms in which there is the possibility of placing dosimeters inside. [34]

TLD's and semiconductor detectors (silicon diodes) are the most commonly used dosimeter types for IVD because of their advantages. These are summarized in Table 2.2

Table 2.2: Summary of characteristics of detectors used for EBRT *in vivo* dosimetry, given as the dependence of the detector sensitivity on a specific parameter. Adapted from [9].

Parameter	Diode	MOSFET	TLD	OSLD	Film		EPID
					Radiographic	Radiochromic	
Dose	0	+	0	0	+	+	0
Accumulated dose	+	+	+	++	Not applicable	Not applicable	+
Dose rate	+	+	0	0	0	0	0
Energy	+ <sup>c</sup>	+ <sup>c</sup>	+	+	++	+	+ <sup>c</sup>
SSD	+ <sup>d</sup>	+ <sup>d</sup>	0	0	0	0	0
Field size	+ <sup>d</sup>	+ <sup>d</sup>	0	0	+	0	+
Linearity	0	0	+	+	+	+	0
Reproducibility (1SD)	0(<1%)	+(<2%)	+(<2%)	+(<2%)	+(<2%)	+(<3%) <sup>e</sup>	0(<1%)
Orientation	+ <sup>d</sup>	+ <sup>d</sup>	0	0	0	+ <sup>f</sup>	0
Temperature	+	+ <sup>g</sup>	0	0	0	+	0
Readout delay	0	0	++	+	+	++	0
Intervening with patient setup	+	+	+	+	+	+	0
Correction factors	++	++	+	+	+	+	++
Estimated dose uncertainty (1SD) <sup>h</sup>	1.5% – 3% <sup>l</sup>	2% – 5% <sup>l</sup>	2%–3% <sup>l</sup>	2%–3% <sup>l</sup>	3% <sup>l</sup>	3% <sup>e</sup>	1.5%–3% <sup>l</sup>
Main advantages	Good reproducibility, immediate readout	Immediate reading, minor fading	No cables, reusable after annealing, few corrections	No cables, readout 10 min postirradiation, reusable after optical bleaching	2D dose distribution, resolution, reread, permanent record, various shapes	2D dose distribution, resolution, reread, various shapes, light insensitive	2D and 3D dose distribution, resolution, immediate readout, permanent record
Main disadvantages	Cumbersome calibration, many corrections, cable	Limited lifetime, high cost	Labor intensive, specific TLD equipment	Short lifetime, dependence on accumulated dose, specific OSDL equipment	Light sensitive, processing equipment and maintenance, specific scanning equipment	Cost, specific scanning equipment, strict readout protocol	Cost, limited availability of commercial software

Note: 0 no concern; + minor concern; ++ serious concern. a) Information of the entries was taken from International Atomic Energy Agency (IAEA) Human Health Report No. 8. b) Because the experience with plastic scintillation detectors and radiophotoluminescence (RPL) glass dosimeters for IVD during EBRT is still limited, these detector types are not included in the table. c) Assumes calibrations at a particular energy. d) Varies depending on the build-up encapsulation. e) Assumes following a strict readout protocol. f) Orientation plays a role at readout. g) Not of concern for dual MOSFET's that correct for temperature differences. h) Relative to cali-

brated ionization chamber dose measurements. i) Lower values are applicable for dosimeters that are regularly calibrated and have well-known correction factors. j) Assumes a well-maintained processor.

However, other systems have also been used, in particular films, gel dosimeters, electronic devices (MOSFET's) or alanine.

### 2.2.3 Selection of TLD

Thermoluminescence dosimetry was one of the primary techniques to be applied for *in vivo* dosimetry in radiotherapy and it is still widely used currently. The various methods applied in the TLD's are documented and due to the availability of automatic readers, the wide applicability of this method in dosimetry, especially for *in vivo* measurements, has increased considerably due to the advantages they present (left side of Table 2.3)

Table 2.3: Analysis of the weaknesses and strengths of the TLD's. Adapted from [35].

Advantages	Limitations and disadvantages
Re-usable	Precision can be affected by poor handling and storage
Automated read-out	Immediate read out is not possible
Energy independent over a wide range of the energies	'Fading'– unintentional release of trapped electrons, may be caused by exposure to heat or light (particularly UV)
Similar atomic number to soft tissue (except those containing calcium)	Some types may liquefy if left in humid conditions
Capable of measuring over a wide range of doses	Scratches on the surface of the TLD or reduction in mass will affect the light emission characteristics
Small physical size	May become contaminated by grease or adhesives

Table 2.3 resumes some advantages, disadvantages and limitations. Although the major disadvantage of TLD is that it is very time consuming and needs a highly trained professional who specializes in the pre-irradiation and annealing procedure. There are several practical examples of the desirability of TLD's to *in vivo* dosimetry, including *in vivo* dosimetry in Intensity-Modulated Radiation Therapy (IMRT) (Burmanq et al., 1997; Van Esch et al., 2002; Engström et al., 2005) and there is documented scientific work of the possibility of the implementation of an *in vivo* dosimetry routine in head and neck cancers (Viegas, C.C.B. "Dosimetria in Vivo Com Uso de Detector Termoluminescente Aplicada Ao Câncer de Cabeça E Pescoço") or in TBI treatments

(Sánchez-Doblado F1, Terrón JA, Sánchez-Nieto B, Arráns R, Errazquin L, Biggs D, Lee C, Núñez L, Delgado A, Muñiz JL. Verification of an on line *in vivo* semiconductor dosimetry system for TBI with two TLD procedures. Radiotherapy Oncol. 1995 Jan;34(1):73-7).

## 2.3 Thermoluminescence Dosimeters (TLD's)

In this Sub-chapter, it will be presented some of the physics behind different luminescent behaviors and therefore described conjunctions of rate constants based on Chapter 2- "Theoretical Basis of Luminescence Phenomena" - of the book entitled "Thermally and Optically Stimulated Luminescence: A Simulation Approach". [36]

### 2.3.1 Theoretical Basis of Luminescence Phenomena

The thermoluminescence (TL) is, in brief, the emission of light as a result of the heating of the materials after previous absorption of energy from the ionizing source. Thus, thermoluminescence dosimetry is based on this ability of imperfect crystals to absorb and store the energy of ionizing radiation. The emitted light is then detected by a photomultiplier and correlated with the absorbed dose received by the TL material.

#### 2.3.1.1 Crystals: Energy Bands and Levels

Initially, it is exposed an explanation of the basic proprieties of a crystal that allows a wide range of conductivity and luminescence proprieties. The basic theory of all types of luminescence in solids, particularly TL, has to do with the band energy of solids. The solution of the Schrödinger equation for electrons in a periodic potential results in allowed bands separated by forbidden bands.

In a pure insulating and semiconducting crystal, the last band that is totally occupied is termed the valence band. Then, there is a gap between the valence band and the next allowed band, the conduction band, called the forbidden band. To reach the conduction band must be given enough energy to the electrons. If the electron is in the conduction band, electronic conduction in crystal happens and this electron can contribute to electrical conductivity. Therefore, in valence band there is missing a negative charge, and this can be described as a positive charger carrier or a "hole" that can move through the crystal and, consequently contribute to the conductivity. The energy necessary for the occurrence of the elevation of the electron in a crystal with a band gap,  $E_g$ , can be due to different causes, nominally thermic or optical excitations. In optical absorption, the light might have photon energies higher than  $E_g$  and, consequently, frequencies above  $E_g/h$  ( $h$  = Planck constant). The capability of the electrons to be thermally raised into the valence band allowed us to distinguish and categorize crystals in semiconductors or insulators. For the first group, relative low temperatures are required for this effect to occur, since they have a relativity narrow band gap. However, for insulators, the object of study that matters for this thesis, their broader band gap makes the the transition harder to occur.

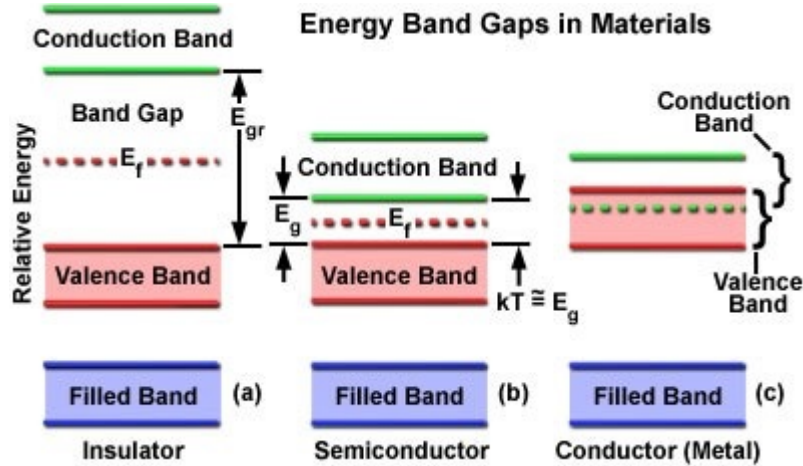


Figure 2.7: Energy band gaps in different type of materials. Adapted from [37].

Any real crystal contains imperfections, such as impurities and defects. Due to these local changes that are incorporated in ideal periodic systems, new energy levels are generated in the forbidden bands, which make possible the “trapping” of electrons and holes. So, these trapping states hold energies that would otherwise be forbidden in an ideal crystal. Consequently, photon with energies inferior to the band-to-band energy may be absorbed, thus new absorption bands are detected. But this is not the only change that is observed, the existence of trap states alters conductivity proprieties as well as the characteristic of luminescence.

New acceptable energy levels can be dependent by the host lattice of the crystal and the imperfections. For example, the proprieties of impurities also depend on the neighbor atoms and ions and in their position in the host material. On a sample exposed to radiation, low-energy and even high-energy particles might not yield new defects. However, they perform a decisive role in the filling of traps or centers. On the other hand, the absorption of photons may photo-stimulate earlier trapped charge carriers into the conduction band for example, as a result this leads to a decrease of a predictable TL effect. Transitions of this type and the connection of the effects of excitation and de-excitation to the luminescence phenomena are the theory that is beyond this thesis.

### 2.3.1.2 Capture Rate Constants

#### General Considerations

First, let's consider an electron (or a hole) traveling in a solid at a speed of  $v$ .  $r_c$  is the minimum distance of a trap that an electron can be and not be captured. If a trap exist in the volume  $V$  of a hypothetical cylinder with high of  $vt$ , that is the distance that an electron travels over a time  $t$ , the electron is captured. Considering the density of traps,  $N$ , the number of traps that is expected in a volume  $V$  is  $NV$ . The probability of capture per unit of time, which is the capture rate, denoted by

A can be written as:

$$A = Nv(\pi r_c^2). \quad (2.1)$$

Since free electrons, condition that is of interest, have a velocity distribution characterized by a temperature  $T$ , a substitution of  $v$  for  $\bar{v}$  will be performed, where mean thermal speed is given by

$$\bar{v} = \sqrt{\frac{8k_B T}{\pi m}}, \quad (2.2)$$

where  $T$  is temperature,  $k_B$  is Boltzmann's constant, and  $m$  is the effective mass of the electron. As a result and moreover simplifying the area that can be titled as a cross-section and symbolized by sigma, the capture rate for a free electron is written as

$$A = \bar{v}\sigma \quad (2.3)$$

To study the orders of magnitude, it will be theoretical accepted that capture radius is its physical radius. Suppose that the trap has the size of a atom, then  $rc \sim 2 \times 10^{-8}cm$ . Well ahead, the effective masses range from  $0.05 m_e$  to  $2 m_e$  according with the crystal structure, where  $m_e$  is the mass of an electron in free space  $m_e = 9.1 \times 10^{-31}kg$ . So, a typical mean thermal speed has an order of magnitude  $10^{-7}cm s^{-1}$ . Having in mind all these values, a typical rate constant would be

$$A = \bar{v}\sigma \sim 10^{-7}cm s^{-1} \times [3.14 \times (2 \times 10^{-8}cm)^2] \sim 10^{-8}cm^3 s^{-1} \quad (2.4)$$

Experiments corroborate the magnitude obtained in equation 2.4 for rate constants, if the trap is neutral. For instance, Bemski measured a cross section of  $5 \times 10^{-16}cm^2$  for electrons being captured by a neutral Au trap in a silicon crystal at room temperature. In case the traps have a net charge, are measured very divergent values. Values of  $10^{-15}$  to  $10^{-12}$  are observed from cross-sections when the free particle is electro statically attracted to the trap, witch happens if they have opposite signs. By dissimilarity, there is an electrostatic repulsion, if both charges of free particle and traps have the same sign. As a result, the probability of capture is reduced and in this case experimental sigma is, approximately,  $10^{-21}cm^2$ . The electron lose a significant amount of energy in the capture process, since a trapped electron is at a minor energy state than a free electron. Then, it is believed that phonons, the corresponding particles of vibrations of the lattice, absorbed that difference of energies. [38] The discussion of this sub chapter focuses on capture by a trap. Before the initiation of the study of inverse process, the thermal de-trapping, is necessary to review some thermodynamic processes.

### 2.3.1.3 Thermal Equilibrium

The huge number of quantum states that an electron may possibly occupy leads to not considerate them individually but instead, their distribution  $N(E)$ . So,  $N(E)dE$  is the number of states per

unit volume with energies between  $E$  and  $E+dE$ . The probability that an electron state is full, in thermodynamic equilibrium, is given by function  $f(E)$  of Fermi-Dirac distribution.

$$f(E) = \frac{1}{1 + e^{\frac{(E-E_f)}{k_B T}}} \quad (2.5)$$

$E_f$  represents the energy of the Fermi level,  $k_B$  is the Boltzmann constant,  $E_f$  is Fermi energy and  $T$  is the absolute temperature of the solid. So, the predictable number of electrons occupying a state between  $E$  and  $E+dE$  is the number of states with that specific energy per unit volume versus the probability that those electron states are full, this is  $f(E)N(E)dE$ . The estimated total number of electrons in the solid,  $N_e$ , is the integration of previous quantity over all energies.

$$N_e = \int N(E)f(E)dE \quad (2.6)$$

Whole electrons in the solid  $N_e$  may counterpart the total number of positive charges in the nuclei, since under normal circumstances, solids are approximately electrically neutral. Consider the case when a solid is sustained at a temperature of absolute zero:  $T = 0K$ , the Fermi distribution, equation 2.6 simplifies to

$$N_e = \begin{cases} 0, & \text{if } E > E_f \\ 1/2, & \text{if } E = E_f \\ 1, & \text{if } E < E_f \end{cases} \quad (2.7)$$

For  $T \sim 300K$ , at the room temperature,  $k_B T \sim 1/40$  eV and materials with band gap energies of 1–12 eV, it is convenient to establish approximations in which temperature is small. The term  $e^{\frac{(E-E_f)}{k_B T}}$  is considerably smaller than one, for energies higher than a few  $k_B T$  below the Fermi energy. Otherwise, this exponential is larger than one, for energies more than a few  $k_B T$  beyond the Fermi energy. These remarks lead to advantageous approximations for the Fermi–Dirac distribution

$$f(E) = \begin{cases} \frac{e^{-(E_f-E)}}{k_B T}, & \text{if } k_B T \ll E - E_f \\ 1/2, & \text{if } E = E_f \\ 1 - \frac{e^{(E-E_f)}}{k_B T}, & \text{if } k_B T \gg E - E_f \end{cases} \quad (2.8)$$

This equation shows that traps with energies sufficiently under the Fermi level are practically complete with electrons, that is to say traps “hole-type”. Let us consider a luminescent material with a valence band, a conduction band, and one or more traps in the bang gap as shown in Figure 2.8.



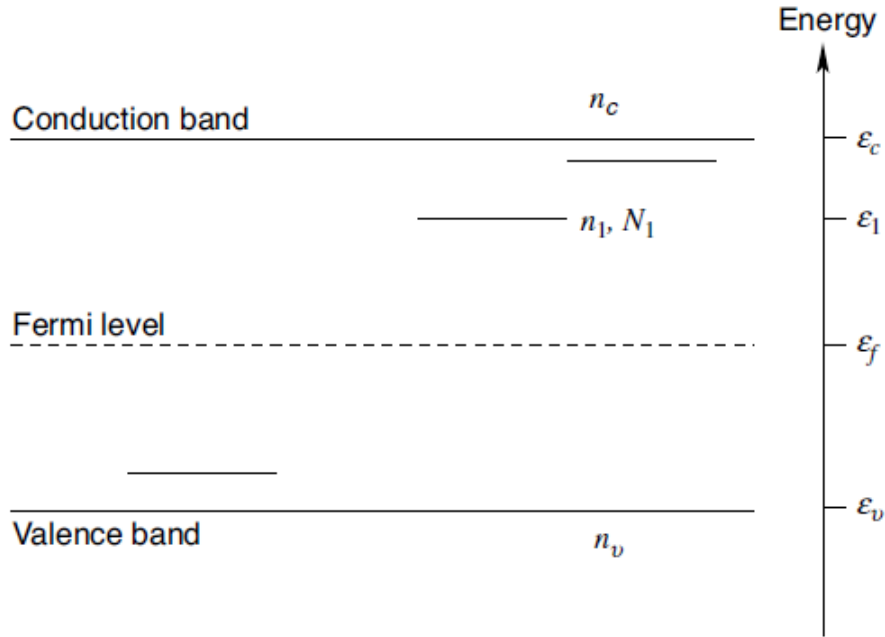


Figure 2.8: The energy levels of interest for the thermal equilibrium discussion are shown. This material may have one or several traps or centers. But for this discussion, it's only necessary to refer one to one. Adapted from [36].

The ratio of trap states  $N_1$  that are occupied with electrons can be calculated by substituting  $E$  for  $E_1$ , energy of the trap, in equation 2.5. So, assuming that the material is in equilibrium at temperature  $T$  and define  $n_1$  as the number of electrons in the state of energy  $E_1$ , Fermi–Dirac statistics says that

$$\frac{n_1}{N_1} = f(\epsilon_1) = \frac{1}{1 + \frac{e^{(\epsilon_1 - \epsilon_f)}}{k_B T}} \approx \frac{e^{-(\epsilon_1 - \epsilon_f)}}{k_B T}. \quad (2.9)$$

In the conduction band, a difficulty is added for the determination of the population of free electrons,  $n_c$ , because there is a large variety of energy levels accessible to free electrons. Nevertheless, when taking into account the density of states in the conduction band and integrating over energy, the calculation of the quotient is simpler as it is showed in the next equation

$$\frac{n_c}{N_c} = f(\epsilon_c) = \frac{1}{1 + \frac{e^{(\epsilon_c - \epsilon_f)}}{k_B T}} \approx \frac{e^{-(\epsilon_c - \epsilon_f)}}{k_B T}, \quad (2.10)$$

where  $E_c$  is the energy of the edge of the conduction band and  $h$  is Planck's constant. Discriminating the equation 2.10, the quotient of the free electron population  $n_c$  to the trapped electron population  $n_1$ , is influenced by only on material proprieties and temperature, in equilibrium.

Furthermore, it is convenient to define a representation for the energy difference  $E_c - E_1$ , because it occurs relatively often in luminescence studies. So,  $E_1$  is the quantity of energy that would be necessary to upgrade an electron in the trap up into the conduction band; it is the binding

energy of the electron trap. Using this notation, equation 2.10 becomes as simple as

$$\frac{n_c}{n_1} = \frac{N_c}{N_1} e^{\frac{E_1}{k_B T}}. \quad (2.11)$$

#### 2.3.1.4 Detailed Balance

Looking again to Figure 2.8, it will be considered two distinct process: an electron trap N1 which is able to capture electrons from the conduction band with rate  $AN_1n_c$  or the inverse process, that is, the electron trap lose electrons back to the conduction band, can happen through thermal excitation with rate  $\gamma$ . As a result, the charge conservation differential equation is

$$\frac{dn_1}{dt} = AN_1n_c - \gamma n_1 \quad (2.12)$$

If this trap is in thermal equilibrium, at some fixed temperature T, the concentration of trapped electrons is obviously constant so that  $dn_1/dt = 0$ . Therefore, the first term of equation 2.12 is null and with a simple reorganization it can be written as

$$\frac{n_c}{n_1} = \frac{\gamma}{AN_1}. \quad (2.13)$$

So, analyzing the previous equation, the quotient of free electrons to imprisoned electrons is determined by the material proprieties  $\gamma$ , A, and  $N_1$ . Additionally, in equilibrium this identical quotient is determined by the Fermi–Dirac distribution as per equation 2.11. So, merging equation 2.11 with equation 2.13 and finally write

$$\gamma = s e^{\frac{-E_1}{k_B T}} \quad (2.14)$$

where  $s$  is the frequency factor linked with the trap, it finds

$$s = AN_c \quad (2.15)$$

The two quantities  $s$  and  $\gamma$  are not independent. This relationship applies under the very general condition that the material can be described as having a temperature. An exception to the requirement that the material has “a temperature” can occur if the capture or de-trapping processes have an important step that involves emission or absorption of radiation, and the optical radiation field is not in equilibrium at the same temperature as the material.

#### 2.3.1.5 The one trap-one center model

In a simple TL model two levels are presupposed, one positioned below the bottom of the conduction band and the other situated above the top of the valence band as specified in Figures 2.8 and 2.9. In the latter figure, as can be seen below, the transitions between the various levels are highlighted and identified by different letters.

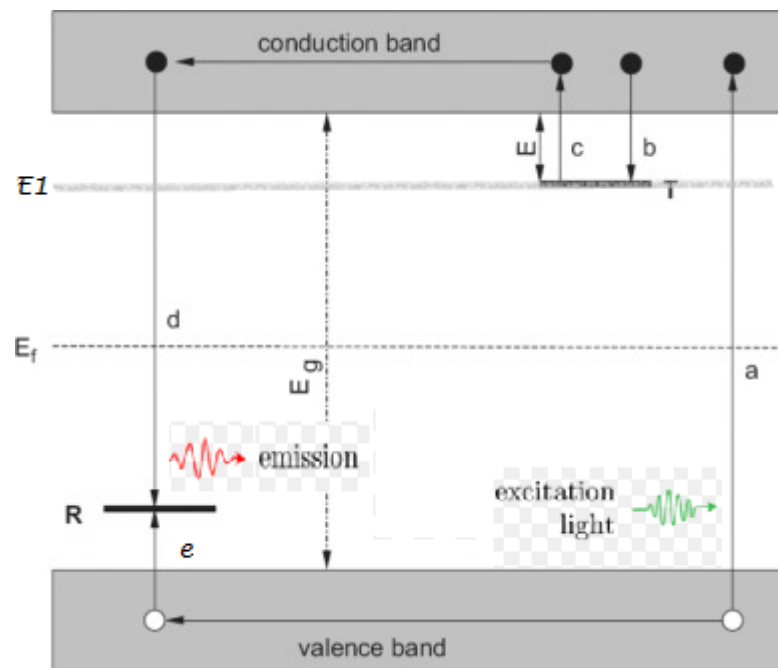


Figure 2.9: Energy band model showing the electronic transitions in a TL material according to a simple two-level model: (a) generation of electrons and holes; (b) electron trapping; (c) electron release due to thermal stimulation; (d) recombination; (e) hole trapping. Solid circles are electrons, open circles are holes. Level  $T$  is an electron trap, level  $R$  is a recombination center,  $E_f$  is Fermi level. Adapted from [39].

The uppermost level designated by  $T$ , trapping center, is located above the equilibrium Fermi level,  $E_1 > E_f$  and therefore unfilled in the equilibrium state, i.e. previously the exposure to radiation and the formation of electrons and holes. It is consequently a potential electron trap. The other level designated by  $R$ , recombination center, is a potential hole trap and can function as a recombination center.

The absorption of radiant energy with higher energy than the difference between the delocalized bands leads to excitation of valence electrons, producing energetic electrons and holes which will, after thermalization, create free electrons in the conduction band and free holes in the valence band (transition a).

While the material is exposed to radiation the carriers may undergo recombination with each other or remain trapped. The recombination can occur indirectly involving the localized states  $T$  and  $R$  associated with defects in the network and / or to the presence of impurities purposely incorporated for that purpose or directly between the conduction band and the valence band, but the probability of such transition is low due to the width of the gap. For the recombination to occur, the holes initially retained in the center  $R$  (transition e) are annihilated with the electrons coming from the conduction band (transition d). If it is a radiative combination, there is emission of a luminescence photon. However, in semiconductors and insulators a certain percentage of the charge carriers is trapped: the electrons at  $T$  and the holes at  $R$  (transition b). The probability of release of an electron from the trap per unit time is expected to be described by the equation 2.14.

In the case of direct recombination an amount of energy will be released which could excite a luminescent center which may coincide with the re-combination center). The luminescent center revenues to the ground state - relax - under the emission of light.

During relaxation the electrons may be retained in the trap T (transition b), characterized by an activation energy and representing the energy difference between the state and the threshold of the conduction band. The electrons will remain trapped until by some process the energy E is given, allowing them to re-enter the conduction band (transition c), from which recombination can take place. In this case, the emission is delayed by a time  $\tau$  representing the mean time that the electrodes remain trapped at the temperature T, which is given by equation

$$\tau = \gamma^{-1} = s^{-1} e^{\frac{E_1}{k_B T}} \quad (2.16)$$

If the depth of the trap, i.e. its energy, is much higher than the thermal energy, i.e. if it is such that for the irradiation temperature  $T_0$  if it has  $E_1 \gg k_B T$ , the electrons will remain retained for a long time after removal of the excitation source, maintaining a significant population of trapped electrons. But, this configuration is not in equilibrium because the Fermi level is between the state T and the R. The temperature at which irradiation occurs is very low when compared to  $E_1/k_B T$  and consequently the rate of relaxation,  $\gamma$ , is very low. Thus, the configuration achieved constitutes a metastable state, existing for a period of time governed by the parameters E, S and T.

The return to the equilibrium configuration can be accelerated by increasing the temperature of the material above  $T_0$  until  $E_1 k_B T$ , as with the increase in temperature also increases the probability of the electrons being released into the conduction band. If during this process the released electrons are recombined with the holes and the radioactive recombination, a thermoluminescence photon is emitted.

During heating, the intensity of the thermoluminescence signal  $I(t)$  is proportional to the recombination rate of the holes and electrons in the R:

$$I(t) = -\frac{dn_h}{dt} \quad (2.17)$$

Where  $n_h$  represents the concentration of holes in the R. Linearly varying the temperature of the materials with a heating rate, according to equation 2.17, the intensity  $I(t)$  increases as the electrons are being released and undergoing recombination. As it might be expected, simultaneously, the concentration of holes in the center R decreases with increasing intensity. As the traps become empty, the rate of recombination decreases, and the thermoluminescence intensity decreases as well. Then a thermoluminescence peak appears. [39]

### **The Emission Curve - Glow Curve**

TL is usually recorded in the form of a curve of intensity of light emitted in function of the material temperature. The existence of traps in different depths (E) results in the occurrence of emission peaks at different temperatures, since the probability of releasing complies with the

equation 2.14 varies with  $E$ . Thus, the number of peaks observed reflects the amount of different levels of traps, as shown in Figure 2.10.

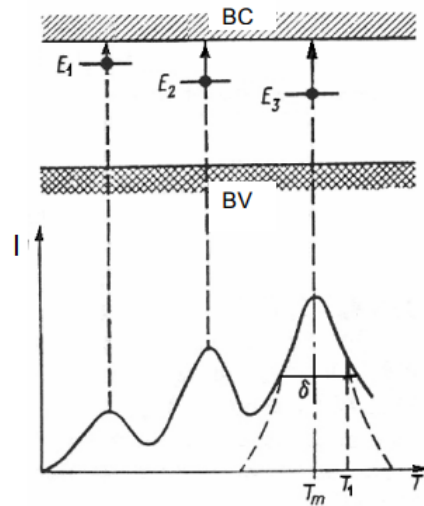


Figure 2.10: Example of TL emission curve and some of its descriptive parameters.  $I$  is the intensity emitted,  $T_m$  is the maximum peak temperature,  $\delta$  its width at half high and  $T_1$  the temperature at half height in the descent of the curve. Adapted from [40].

Each  $T_m$  temperature where a maximum emission occurs is related to a certain level. The maximum emitted intensity (area under an emission peak), or alternatively the high of the peak is proportional to the number of traps previously occupied, and therefore, is a function of the radiation dose.

The model that has been presented is the one that involves the smallest possible number of states to describe the process of thermoluminescence. But, in reality, the energy band diagram of any material is more complex and the type of states  $T$  and  $R$  accessible to the charge carriers are also more diverse, thus leaving other possibilities of interaction. [40]

### 2.3.2 Thermoluminescence materials - LiF: Mg, Ti

The most promising material that emerged in the 1950s since the first efforts to find materials with application in the TLD was the LiF. Later, it was found that the desirable dosimetry proprieties of this material originated in the impurities of Magnesium (Mg) and Titanium (Ti).

The introduction of magnesium in the material causes a redistribution in the crystal lattice so that the crystal remains neutral, that is, the  $Mg^{2+}$  is incorporated in the network and there are cationic voids that are absences of  $Li^+$ , thus making the charge compensation, like explained in Figure 2.11 and "impurity-gap" pairs are formed.

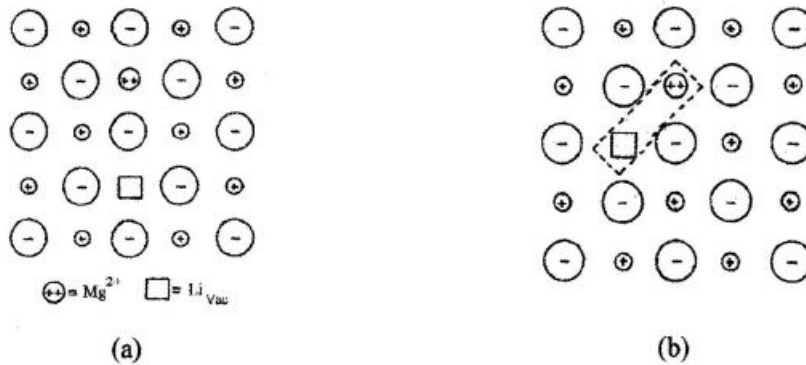


Figure 2.11: Structure of dipoles formed by impurity-gap pairs:  $Mg^{2+}$  - Li vacancy. Adapted from [41].

These pairs then form more stable aggregates (dimers and trimers) moving in the lattice. The role generally attributed to Mg in the crystal lattice is to capture/retain excited electrons during irradiation: it is a trap.

Similarly to Mg, Ti is also incorporated in the network forming "impurity-gap" pairs with  $Li^+$  but since Ti has +3 or +4 oxidation state the charge compensation can still be done by association to ions,  $O^{2-}$  ions, to  $OH^-$  ions (or combinations of these) occupying substitution positions of  $F^-$ . The most frequent are the titanium-hydroxyl complexes. The role that has been assigned to Ti is that of recombination center. [42]

The TL emission curve of LiF:Mg,Ti is complex because of its intricate trap dynamics, as can be seen in Figure 2.12.

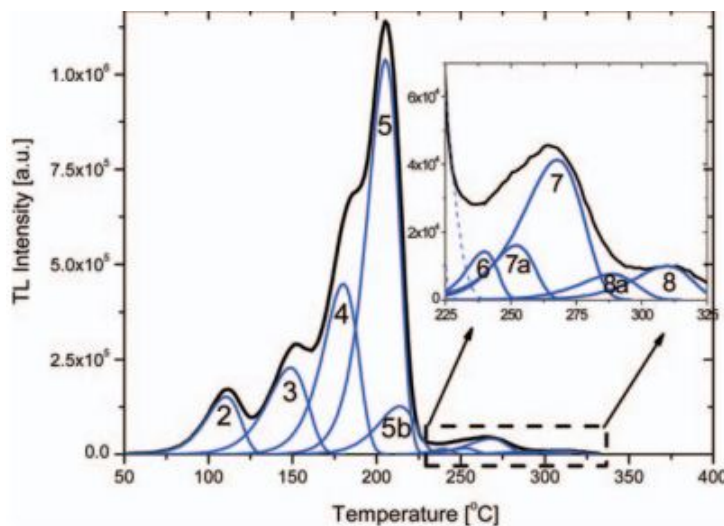


Figure 2.12: Typical deconvoluted glow curve of LiF:Mg,Ti TLD-100 following 90Sr/90Y irradiation at a dose level of 1 Gy. The insert shows the deconvolution of the high-temperature TL. Adapted from [43].

The principal peak typically exploited for dosimetric purposes, entitled the dosimetry peak,

is peak 5 at a peak temperature of 225 °C, since the corresponding trap level is very stable, as can be verified in Table 2.4, although, peak 4 and 6 are sufficiently stable for most dosimetric applications. The low-temperature peaks 1 and 2 are relatively unstable and must be suppressed by a thermal regeneration process. Finally, peak III only presents difficulties for integration times exceeding several weeks.

Table 2.4: Half-lives of the LiF:Mg trap levels and peak temperatures. Adapted from [44].

Peak number	Emission temperature (°C)	Half-life
1	70	5 min
2	130	10 h
3	170	0.5 yr
4	200	7 yr
5	225	80 yr
6	275	-

Until nowadays many other materials with specific characteristics for use in dosimetry such as magnesium or calcium sulfate oxides, for example, have emerged. However, lithium fluorides have been the most popular and best characterized materials for clinical as well as environmental and individual dosimetry because LiF based TLD materials are near tissue-equivalent and provide excellent energy response, eliminating the need for extensive mathematical computations to determine dose, improving overall accuracy and reducing the potential for costly errors. They are also sensitive in a sufficient range of doses, have a behavior independent of the dose rate and the possibility of being reusable. [44]

## 2.4 Ionization Chambers

Ionization chambers are an essential type of radiation dosimeter as the principal device applied for calibration of radiotherapy beams. [45]

### 2.4.1 Principle of Operation

The ionization chamber is a gas-filled radiation detector used for the detection and measurement of certain types of ionizing radiation, such as X-rays, gamma rays and beta particles. There are several types of ionization chamber, especially cylindrical and flat-parallel plates. Despite the

variety, all are constructed according to the same basic operating principle, which is based on measuring the amount of charged particles present in a medium generated by each interaction between the incident radiation and the gas, and does not include the gas multiplication mechanisms used by other radiation instruments, such as the Geiger-Müller counter or the proportional counter; as a result, there is no avalanche effect and no dead time problem. [46]

The indispensable constituents of the ionization chamber are its two collecting electrodes: the anode and cathode (the anode is positively charged with concerning to the cathode). The potential difference between the anode and cathode is often in the 100 to 500 Volt range. [47]

The simplest ionization chambers consist of a central electrode -anode- and the wall of the chamber which is coated by a conductive material and which functions as a cathode. The sensitive volume of the detector is delimited by the wall of the chamber and forms a cavity filled with a gas or a mixture of gases with a relatively low pressure. Between the anode and the cathode is applied a difference of potential, to separate the pairs of produced ions, causing the negative ions migrate to the anode and the positives to the cathode. This ion flux produces a extremely low current, on the order of  $10^{-9}A$ , that can be measured by a high-precision device called an electrometer. [29]

Electrometers are devices for measuring small currents, of the order of  $10^{-9}A$  or less. An electrometer used in conjunction with an ionization chamber is a high gain, negative feedback, operational amplifier with a standard resistor or a standard capacitor in the feedback path to measure the chamber current or charge collected over a fixed time interval, as shown schematically in Figure 2.13. [48]

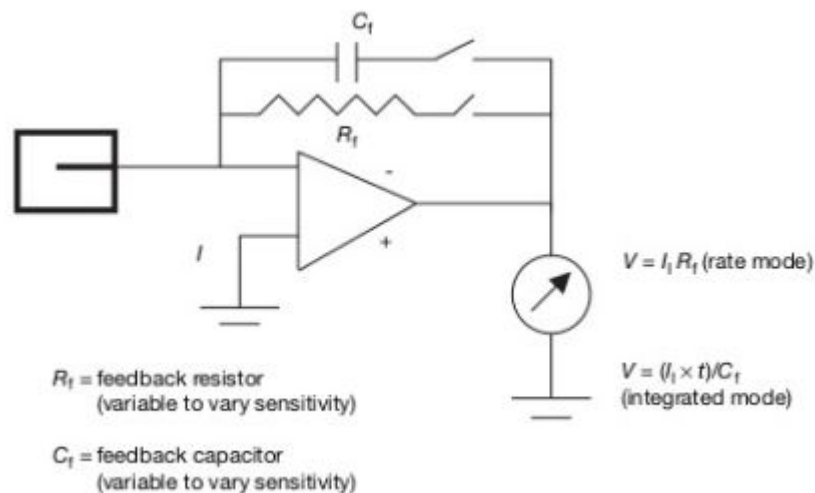


Figure 2.13: Electrometer in feedback mode of operation. Adapted from [25].

The design most commonly used for photon beams is the thimble chamber, also called a Farmer chamber, which has a cylindrical geometry with central linear and outer cylindrical electrodes. Parallel-plate chambers are also used and are the recommended chamber geometry for electron beam dosimetry. The Figure 2.14, in a simple way, presents the experimental set-up scheme required of parallel plate ion chamber. [49]



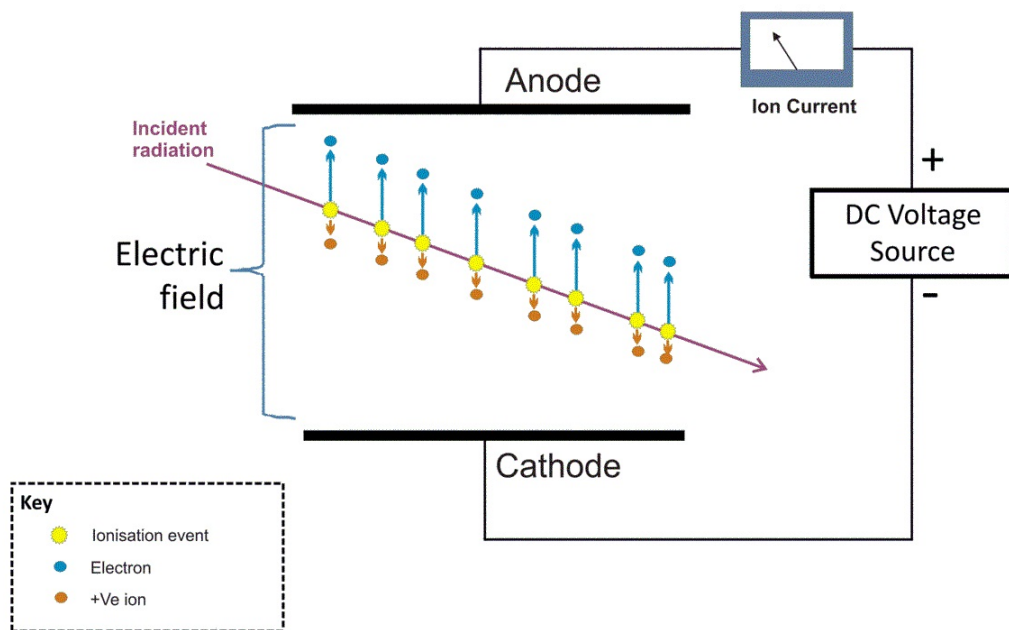


Figure 2.14: Schematic diagram of parallel plate ion chamber, showing drift of ions. Electrons typically drift 1000 times faster than positive ions due to their much smaller mass. Adapted from [49].

A prerequisite for operation of all ionization chambers is that the chamber be operated under conditions of electronic equilibrium. In disequilibrium conditions, the amount of ionization measured is incorrect, as will be the exposure or dose calculation. Measurements with open air ionization chambers necessitate temperature and pressure corrections to account for the alteration in the mass of air in the chamber volume, which fluctuates with the ambient temperature and pressure. Besides that, an ionization chamber and electrometer require calibration before use and with a triaxial connecting cable are required tools for radiation beam calibration. [25]



## Chapter 3

# Materials and Experimental Methods

This chapter begins the experimental part. It describes the domain of application of this thesis and therefore the materials, equipment and methods used in the development of the experimental work. Briefly, the experimental work consists in comparison of two TLD (LiF: Mg, Ti) batches (100 units each) from different manufactures: Radcard (MTS-100) and Thermo Scientific™ (TLD100) using a linear accelerator and a novel beam heterogeneities correction. The purpose was to compare the TLD physical characteristics leading to a reliable clinical dosimetry system (0.1 Gy to 5 Gy) and to establish a calibration procedure approaching the ISO 28057:2014 standard. Thus, the chapter is developed around the main dosimetric characteristics of both types of detectors. Then, the measuring and irradiation equipment is described. Finally, the chapter ends with the presentation of the ISO 28057:2014 standard that ensures the choice of two procedures adopted during this work- Initial General Procedure and One Complete Cycle Annealing Irradiation-Readout Procedure - and supports the subsequent results.

### 3.1 Materials and Instruments

The IPO-PORTO dosimetry system is composed by the measurement system and by the equipments and materials necessary for irradiation.

#### 3.1.1 Measurement System

The IPO-PORTO measurement dosimetry apparatus is similar to most of the equipment that exists in the market, including the one at the DIRE from IST/CTN, and is therefore based on three essential equipment: the dosimeters (MTS-100 and TLD-100), the reader and the programmable oven. Besides that, it was utilized an extra device during the calibration, a matrix of vented ionizing chamber, OCTAVIUS Detector 1500.

### 3.1.1.1 TL Dosimeters

This project used two new batches with one hundred dosimeters each. One batch is made from a specific mass of material, in this particular case LiF:Mg,Ti, with uniform composition, fabricated in a single production run under controlled, consistent conditions and having a unique identification code, by definition. [1]

The Figure 3.1 shows the two different types of dosimeters available. The crystals of LiF: Mg, Ti, are marked with a red and a green square, and are approximately  $3.2 \times 3.2 \times 0.90 \text{ mm}^3$  (they are easily seen as the two white squares); on the left is one example of MTS-100 (Group A - red) and on the right an example of TLD-100 (Group B - green).

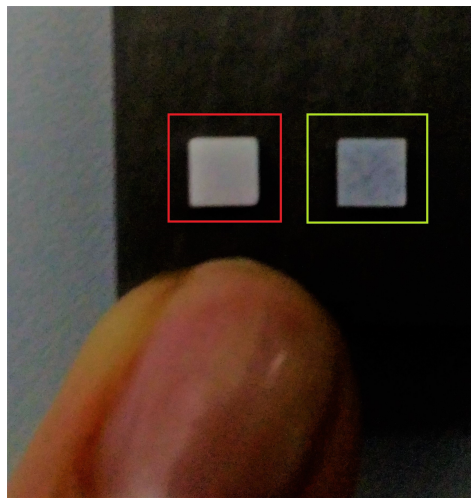


Figure 3.1: MTS-100 (red square) and TLD-100 (green square). The point of a finger is in the picture to help in visualization of real dimensions of dosimeters.

As can be seen in the previous figures, the dimensions of both dosimeters are similar, so the visible distinction is only possible by their differences in opacity. Detectors from Thermo Scientific™ are more transparent, while the other pieces are more opaque and therefore they present a whitened color.

In terms of features, each producer provides their table. Therefore, main features of MTS-100 pellets given by manufacture are in the Table 3.1 and the characteristics of TLD-100 detectors given by the manufacture, Thermo Scientific™, are in the Table 3.2 .

Table 3.1: Features of MTS pellets given by manufacture (Group A). Adapted from [50].

<b>Detector type</b>	<b>MTS-100</b>
<b>Phospor</b>	Li:F: Mg,Ti
<b>Form</b>	solid disc 3,2×3,2 mm thickness 0,90±0,05 mm
<b>Effective atomic number Z</b>	8,2
<b>Density [g.cm-3]</b>	2,5
<b>TL emission spectrum [nm]</b>	400
<b>Relative sensitivity to TLD-100</b>	1
<b>Sensitivity spread</b>	±3,0 % SD
<b>Main peak temperature [oC]</b>	210
<b>Zero dose reading [μGy]</b>	15
<b>Detection threshold [μGy]</b>	10
<b>Linearity range [Gy]</b>	5×10-5 - 5
<b>Repeatability</b>	< 2%
<b>Photon energy dependence 30 keV - 1.3 MeV</b>	< 30 %
<b>Batch No.</b>	RS 1860/16
<b>Quantity</b>	100 pieces
<b>Batch homogeneity [1 SD]</b>	< 5 %
<b>Thermal fading [% at room temperature]</b>	< 5% / yr
<b>Fluorescent light effect on fading and zero reading</b>	negligible at laboratory light intensity
<b>Reusability</b>	unlimited
<b>Dose rate influence</b>	independent

A very significant characteristic of these detectors is that they are interchangeable with other LiF:Mg,Ti phosphors and pellets generally utilized in a lot of laboratories (e.g. TLD-100). They may be read out with any typical TL reader, both with hot gas (e.g. Alnor DOSACUS or Harshaw 5500) and ohmic (e.g. Harshaw 4000, Toledo or Solaro) heating systems. Radcard proclaim that their "MTS-N, MTS-6 and MTS-7 pellets can easily replace materials produced by other manufactures in all cases when their virtues such as higher sensitivity and lower prices are crucial".

Table 3.2: Full of specifications manufacture of TLD-100 chips (Group B). Adapted from [51].

Detector Type	TLD-100 chip
Emission Spectra	3500 to 6000Å (4000 maximum)
Energy Response	1.25 keV/6°Co
Height (Metric)	0.89mm
Material	Lithium Fluoride (Li natural) LiF:Mg, Ti
Sensitivity	1.0 at 6°Co relative to LiF
Width (Metric)	3.2mm
Item Description	chip (Area: 3.2 x 3.2 x 0.89mm)
Length (Metric)	3.2mm
Accuracy	±15 (±2 sigma) %
Measurement Ranges	10pGy to 10Gy

Both producers sustain that these materials are durable and indefinitely re-usable and have low fading, as well as high TL efficiency.

As explained in Sub-chapter 2.3.2 Lithium Fluoride based TLD materials exhibits tissue-equivalence and offer an exceptional energy response, abolishing the need for mathematical computations to determine dose, improving global precision and reducing the potential for errors. According to the manufactures, high quality lithium fluoride based materials exhibits low background, resistivity against environmental conditions (not light sensitive) and tissue-equivalence to offer flexibility in handling the dosimeters and assurance in analyzing results and, consequently, improved productivity and efficiency. Therefore, the detectors present are best suited for health and medical physics dosimetry applications, namely, clinical/research dosimetry and radiotherapy planning verification, such as:

- CT dose measurement;
- Diagnostic dose studies;
- Stereotactic beam output factor measurement;
- Total body irradiation dose verification;
- Skin irradiation dose verification;
- Critical organ dose verification;
- Quality assurance;
- Extremity dosimetry;
- Environmental dosimetry;
- High dose applications (radiation hardness testing);

- Irradiated food analysis;
- Radiocarbon dating.

### 3.1.1.2 Readout System

The readout system consists in one HARSHAW TLD™ Model 3500 Manual Reader and the producer certifies that the reader disposes the characteristics mentioned on Table 3.3.

Table 3.3: Full specifications of manufacture of HARSHAW TLD™ Model 3500 Manual Reader. Adapted from [52].

Part Number Description	3500TLDREADER Model 3500 with Heating Temperature Capability to 400°C
Warm-up time	30 minutes
Heating cycles	Pre-read anneal, acquire and post-read anneal
Typical cycle time per detector	Typically 35 seconds (based on standard LiF: Mg, Ti)
Size (Height x Width x Depth)	31 × 32 × 47cm
Weight	25kg
Dynamic range	7 decades
HV stability	±0.005% per hour, ±0.02% per 8 hours
Photronics linearity	Better than 1%
Stability	Better than 1.0 µGy, based on one standard deviation of ten consecutive measurements
Light exposure	Tested to withstand a minimum of 1,000 W/m2
Test light	1 mGy (100mrad) 137Cs)
Electrical supply	Selectable: 110/120VAC ±10%, 60Hz or 220/240VAC ±10%, 50Hz
Nitrogen supply	Purified (99.995%), dry
Pressure	1.5 to 3kg/cm2
Flow Rate	130 liters/h, subject to external regulation
Operating temperature	15° to 40°C
Storage temperature	-10° to 60°C
Humidity	Functions within specification after 24 hour exposure to 90% humidity and subsequent 6-hour recovery with use of the nitrogen supply
Ambient light exposure	Functions within specifications when exposed to ambient light up to 1,000 W/m2 with cover on the reader
Shock	Withstands a 1-cm drop onto a concrete surface
Computer requirements	Any commercially available PC system with Windows™ 7, XP, 2000, or NT 4. 32 bit OS only. RS232 strongly recommended. (Please contact your sales representative for approved USB to RS232 converters)
Compatible with	Thermo Scientific TLD Materials, Thermo Scientific TLD Accessories

Note: a) The use of nitrogen is optional. Absence of nitrogen will result in understated performance. b) Options include glow curve deconvolution software (WinGCF Software), various types of neutral density filters to extend the high measurement range, and TL element specific planchets for best possible reproducibility. Easy to operate, service and maintain.

Besides that, this reader contains a sample drawer for a solitary element TL detector, as exhibited in Figure 3.2.



Figure 3.2: The Thermo Scientific™ HARSHAW TLD™ Model 3500 Manual Reader and highlighting planchet provides manual readout of TL chips, disks, rods and cubes in a broad variety of sizes.

The planchet heating on which the detector is positioned integrates a fused thermocouple for greatest temperature reproducibility. Further it is connected to a dedicated computer with its own operational software designed by Harshaw - Thermo Scientific™ WinREMS™ - to provide the user interface, to control the heating cycle of the readers and, consequently, the cycles of reading and anneal and also for the recording of the readings, cycles of anneal and still with other functionalities that at the moment are not in use. In Appendix B there is an overview of how to use the software. It also includes a linear, programmable heating system that is required to the heating cycle of the detectors according to the temperature profile and temperature rate (TTP - Time Temperature Profile) appropriate for the reading cycle and a cooled photomultiplier tube with supplementary electronics to measure the TL light output. The main build blocks of any TLD readout system are show in Figure 3.3.

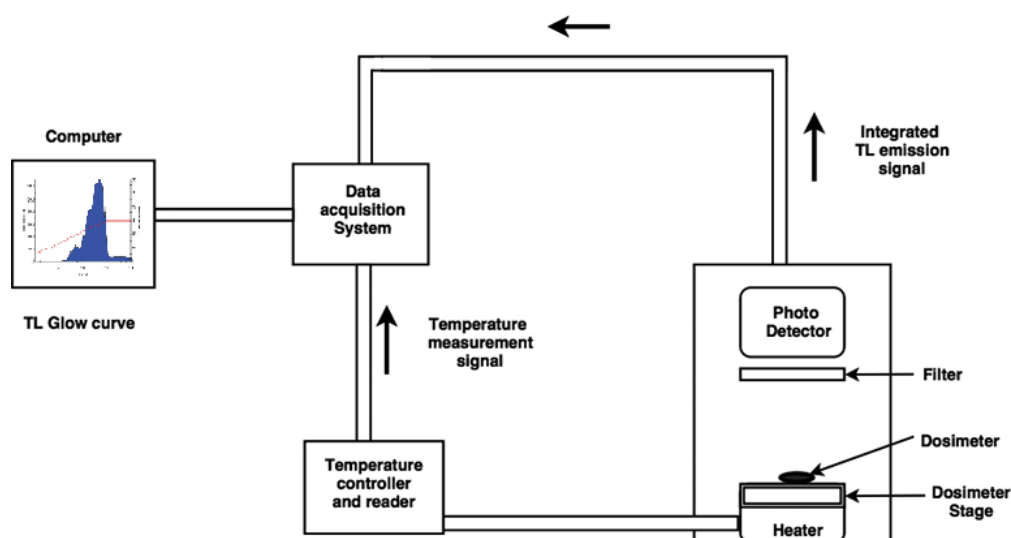


Figure 3.3: Block diagram of a simple TLD readout system. The material is slowly heated by a heater supply. The emitted light is filtered and then detected by a photomultiplier tube. The temperature of the material is recorded through the thermocouple. Adapted from [53].



According to the manufacturer, this equipment was constructed for reading dosimeters using a planchet heating technique and it is perfect for medical physics, health physics, material research, food irradiation and industrial applications. As well, the producer affirm that it reads quickly and accurately with precise temperature control, due to thermoelectric photomultiplier tube (PMT) cooler for maximum gain stability. Finally, they assert that the exclusive "glow curve and temperature heating profile provided by Harshaw TLD readers affords verification of read quality. The glow curve is independent of potential inaccuracies induced by environmental conditions in reading, storage and handling to provide trustworthy record keeping. In case of errors in reading or a faulty/ damaged dosimeter, glow curve analysis could help determine validity of the reading and drive appropriate corrective or preventative actions."

To support these claims Harshaw -Thermo Scientific™ presents some facts listed in the Table 3.4, in particular measurements performed with the TLD-100.

Table 3.4: Dosimetry performance using LiF:Mg,Ti in conjunction with the HARSHAW TLD™ Model 3500 Manual Reader. Adapted from [53].

Dosimetry Performance Using LiF:Mg,Ti (TLD-100/600/700)	
Measurement range	10 $\mu$ Gy to 1 Gy (linear), 1 Gy to 20 Gy (supralinear)
Detection threshold	<10 $\mu$ Gy based on 2.26 standard deviations for 10 sequential readings of an unexposed dosimeter
Repeatability	Less than 2% variation based on one standard deviation for 10 sequential measurements of 1 mGy 137-Cs
Residual TL signal	<0.2% of reading
Fading	<20% in 3 months without thermal treatment; <5% in 3 months using pre-read anneal or glow curve deconvolution software (WinGCF Software)
Batch uniformity	$\pm$ 30% from the factory standard

It is important to emphasize that with this reader it is possible to perform not only the measurements of the TLD-100 but also of MTS-100 detectors, since they may be read out with any typical TL reader, both with hot gas and ohmic heating systems.

### 3.1.1.3 Programmable Oven

The oven of Carbolite® coupled to 3204 Process Controller, as show in Figure 3.4, provide precise temperature control.



Figure 3.4: The oven of Carbolite® coupled to 3204 Process Controller.

The controller may be configured, initially, with ‘Quick Configuration’ codes. This is a built-in tool which enable the configuration of the input type and range, the output functions and the display format. All the process of configuration is explained in detail in Appendix A.

#### 3.1.1.4 Extra: OCTAVIUS® Detector 1500

Since precise and meticulous dose measurements are necessary it is common practice to call upon ionization chambers due to their small variation in response to energy, dose, dose rate, and reproducibility. [54] International dosimetry procedures such as AAPM TG-51 or IAEA 398 involve measurements with ionization chambers, since their well-known performance and their outstanding accuracy and stability. [55, 56]

According to its manufacturer, the OCTAVIUS® Detector 1500 is a pioneering conception of an ion chamber matrix in a plane for patient plan verification and machine QA in radiation therapy. Using ion chambers prevents radiation defects, the main disadvantage of solid-state detectors. The 1405 vented plane-parallel ion chambers are 4.4 mm x 4.4 mm x 3 mm in size, and the center-to-center spacing is 7.1 mm. In overall there are placed 1405 ion chambers in a chessboard matrix, affording a maximum field size of 27 cm x 27 cm showed in Figure 3.5

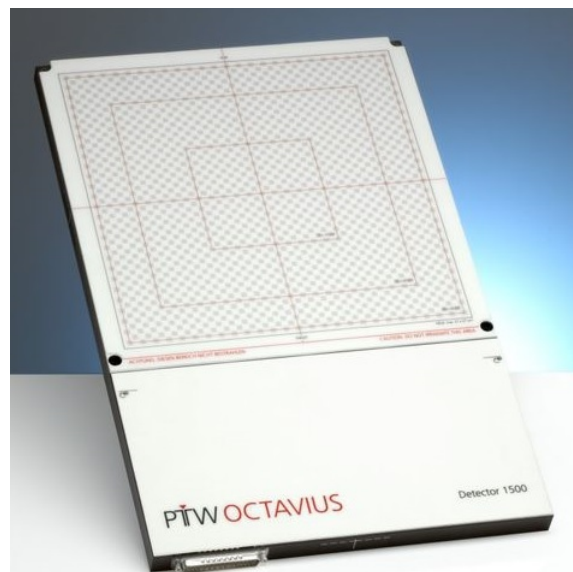


Figure 3.5: OCTAVIUS® 1500- The New Checkerboard Detector for Patient and Machine QA. [57]

The package also includes an interface - VeriSoft® Patient Plan Verification Software - for fast data acquisition and smart visualization tools like multiple dose display options, 2D/3D graphs, zoom functions and slice sliders to analyze measured data more efficiently. Full specifications of manufacture of OCTAVIUS® Detector 1500 are presented in Table 3.5.

Table 3.5: Full specifications of manufacture of OCTAVIUS® Detector 1500. Adapted from [57].

<b>OCTAVIUS® Detector 1500</b>	
Detector type	Plane-parallel vented ionization chambers
Number of detectors	1405
Detector size	4.4 mm x 4.4 mm x 3 mm (0.06 cm <sup>3</sup> )
Detector spacing	7.1 mm center-to-center
Max. field size	27 x 27 cm <sup>2</sup>
Reproducibility	≤± 0.5%
Dead time	zero
Repetition rate	100 ms
Measured quantities	absorbed dose to water (Gy), absorbed dose rate to water (Gy/min)
Resolution	0.1 mGy or 0.1 mGy/min
Measurement range	(0.5 ... 48 Gy/min)
Reference point	7.5 mm below the surface of the array
Housing material	PS, GRP (frame)
Dimensions (W x D x H)	30 cm x 46.7 cm x 2.2 cm
Weight	6 kg
Power supply	(100 ... 240) VAC; (50 ... 60) Hz
PC connection	Ethernet, RS232
Part No.	L981382

Ionization chamber panel is not affected by accumulated dose, since gold standard ionization chambers have not a representative aging or degradation and it only needs a relative factory cal-

ibration once to match the individual responses. Besides that, the finite geometric dimensions of ionization chambers benefits the measurement of hot spots and high dose gradients, presenting an enormous advantage in what concerns IMRT/IMAT (Intensity Modulated Arc Therapy) plan verification measurements. The field coverage with ion chambers is radically greater than that of diodes, e.g. PTW's OCTAVIUS Detector 1500 50% vs. Sun Nuclear's MapCHECK 0.6% [57]

Application highlights in brochure of PTW's OCTAVIUS Detector 1500 are:

- Largest field coverage - better detection of hot spots;
- Highest detector density - better error detection;
- Extended dose rate range for FFF beams;
- Machine QA with FFF analysis (optional);
- Optional 4D dosimetry.

### 3.1.2 Irradiation Equipments and Materials

Irradiation equipment and materials provided for the IPO-PORTO consists in one Linear Accelerator TrueBeam® Radiotherapy System, one Alderson RANDO female phantom and other auxiliary materials such as water-equivalent RW3 slab phantoms, PMMA material board for placing and irradiating the detectors and a OPUS 10 TPR - DOSTMANN-electronic® to measure the air pressure and the temperature.

#### 3.1.2.1 Linear Accelerator TrueBeam® Radiotherapy System

A LINAC is the election equipment for administering external radiotherapy treatments due to its high versatility. The use of LINAC's has the advantage of being able to treat various areas of the human body, since it contains sophisticated radiation production, administration and control systems, patient positioning equipment and systems for locating and verifying the fields to be irradiated. [58]

In this this work, TrueBeam® Radiotherapy System - the most recent acquisition of IPO-Porto - was the one selected to perform the necessary irradiations.

An image of the equipment is presented in Figure 3.6.



Figure 3.6: TrueBeam System, Varian Medical Systems, installed in IPO-Porto.

To the LINAC are associated: patient support assembly, i.e. a specific treatment table, where the patient is positioned; a system of location lasers; a real time image acquisition system of the irradiated field; a collimator system (multileaf collimator); a closed circuit video system for patient surveillance during treatment and computerized command equipment. Particularly, central to the TrueBeam™ system's superior performance is Maestro that dynamically directs, synchronizes and monitors the performance of all TrueBeam's fully integrated functional components. [59]

Although the Trubeam™ exhibits superior performance and new capabilities, in essence it has the basic components of any accelerator as schematized in Figure 3.7

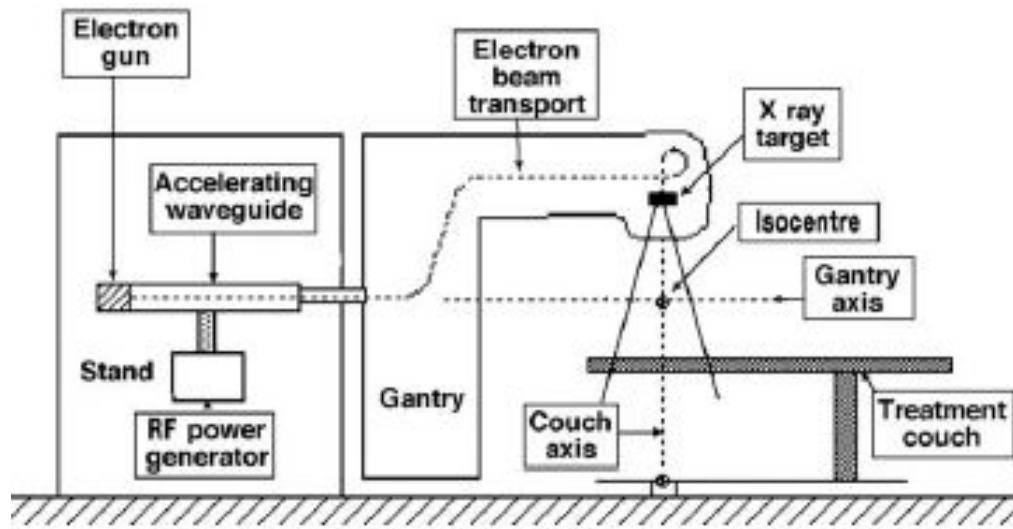


Figure 3.7: Design configurations for isocentric medical linacs. The accelerating waveguide and RF power generator are located in the gantry stand; electrons are brought to the movable target through a beam transport system; the machine can produce megavoltage X rays as well as electrons. Adapted from [25].

This accelerator has two types of collimators, the traditional collimator and the multi-leaf collimator (MLC). Traditional collimators are composed of two pairs of metallic blocks (jaws), oriented almost perpendicularly to each other and that allows to adjust the size of the irradiation field to each treatment. The MLC collimation system consists of multiple small monitored blades that allows the treatment using irregular fields without the need to resort to individually manufactured custom protections. Since most tumors do not present regular forms, this last system is an asset. Besides that, the gantry enables the radiation source to rotate along a horizontal axis. The isocenter is defined as the point of intersection between the axis of rotation of the gantry, the collimator and the bed.

So, these devices can direct several beams with a determined dose at different angles. It also has several photon and electron energies, depending on the depth of each treatment; quite of few photon energies, for deep treatments, and various electron energies, for more superficial treatments. Both beams are produced when electrons are speeded up to nearly the speed of light in a straight track. When these high-speed electrons hit a tungsten target, they release a stream of photons that then is directed at the patient after passing a flattening filter for field homogeneity correction. If the tungsten target is not added, then the electrons themselves reach the patient. If the flattening filter is removed (flattening filter free - FFF-beam), the photon flux is increased and, in this way, a high dose rate can be applied to the tumor, but a dose much lower than the other tissues. [29]

### Monitor Units (MU)

Since in the LINAC the beams of ionizing radiation are pulsed, it is necessary to constantly monitor these beams to ensure the effectiveness of the treatment and safety of the patient. This

is done through ionization chambers localized in the gantry. When the desired dose is deposited, these chambers communicate to the system that the dose was reached, and the treatment is finished. [60]

Thus, in radiotherapy, it is used the term MU which is associated with the dose in cGy by means of correction factors. It is common practice to adjust the LINAC calibration, so that a monitoring unit is equivalent to 1 cGy delivered to a point at the depth of maximum dose in a water-equivalent phantom whose surface is at the isocenter of the machine (i.e. usually at 100 cm from the source) with a field size at the surface of 10 cm × 10 cm. [61]

### 3.1.2.2 The Alderson RANDO Phantom

The Alderson RANDO phantoms are molded of tissue-equivalent material; they are designed within highly sophisticated technological constraints and follow ICRU-44 standards, according to the manufacture.

The female ART available in IPO-Porto represents a 155 cm (5 ft. 1 in.) tall, 50 kg (110 lb.) female as can be seen in Figure 3.8. Besides, breasts attachments are available in various sizes. They can be sliced in frontal planes (drilled or undrilled for film dosimetry). Breasts of male and female ART phantoms are contoured to blend realistically with the thoraxes. They are attached to the thorax with nylon screws. The male chest with breasts attached serves as a large female.



Figure 3.8: Female Alderson Radiation Therapy phantom (ART). [62]

The ART phantom is transected-horizontally into 2.5 cm thick slices. Each slice has holes which are plugged with bone-equivalent, soft-tissue-equivalent or lung tissue equivalent pins which can be replaced by TLD holder pins. The holder pins are ordered separately.

Phantoms are shipped with all dosimetry holes filled with blank pins. Pins for TLD chips have recesses at one end 3.2 x 3.2 x 0.9 mm, so the dimensions are perfected for dosimeters of both batches. Pins for TLD rods have 1 mm-diameter holes cross-drilled at the centers of the pins. All pins are 2.50 cm long unless otherwise specified. [62]

### 3.1.2.3 Auxiliary Materials

For the accomplishment of this work, in addition to materials already presented, other materials such as the Water-equivalent RW3 slab phantoms, a Poly(methyl methacrylate) (PMMA) material board and OPUS 10 TPR - DOSTMANN-electronic® were also used.

#### Water-Equivalent RW3 Slab Phantoms

The RW3 phantom is appropriate for high energy photon and electron dosimetry, since it is water-equivalent in the energy varieties from  $^{60}\text{Co}$  to 25 MV photons and from 4 MeV to 25 MeV electrons. To provide for backscatter, slabs are placed below the radiation detector. So, usually the phantoms are applied in monitor calibration and quality assurance measurements. The slab phantoms each includes of 1 plate 1 mm thick, 2 plates each 2 mm thick, 1 plate 5 mm thick and 29 plates each 10 mm thick, that makes it conceivable to implement monitor calibrations and depth dose measurements by varying the measuring depth in a solid state phantom. The dimensions of the whole phantoms is 30 cm x 30 cm x 30 cm and each plate is accurately machined for a thickness tolerance of  $\pm 0.1$  mm. [63]



Figure 3.9: Experimental set-up with 20 plates of RW3 phantom, indicated in blue.

#### PMMA Material Board

The irradiations were carried out using a PMMA material board (custom made) with a thickness of 1 cm, with excavated circles for the placement of dosimeters from 2 to 2 cm. Although the detectors are square, this plate served perfectly as can be seen in Figure 3.10.



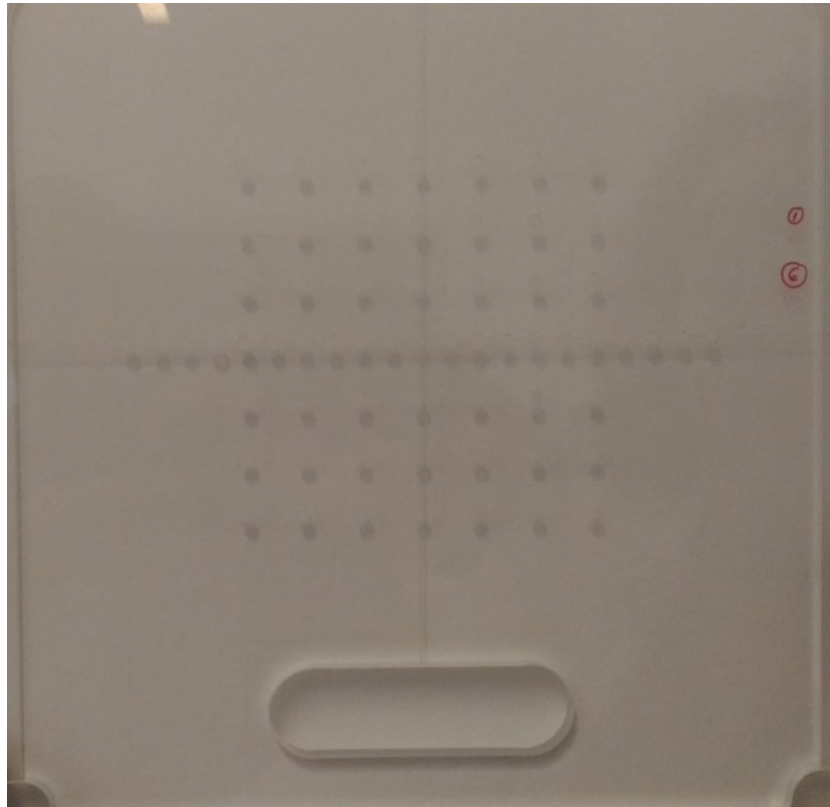


Figure 3.10: PMMA material board with dimensions of 29.8 cm x 31.5 cm x 1 cm, with excavated circles for the placement of dosimeters from 2 to 2 cm.

#### **OPUS 10 TPR - DOSTMANN-electronic®**

The OPUS 10 TPR produced by DOSTMANN-electronic® enables the measurement of the air pressure as well as of the temperature. [64]

## **3.2 Methods**

During this project were compared two new batches, with one hundred dosimeters each, produced by distinct producers: crystals of LiF:Mg,Ti from Radcard (MTS-100) and its equivalent Thermo Scientific™ TLD-100. Glow curves of all TLD irradiated by a *Varian™ TrueBeam™* linac using reference conditions were obtained using a HARSHAW TLD™ Model 3500 Manual Reader. A fixed annealing protocol was established. For each irradiation, 25 dosimeters were exposed. Since the field is not homogeneous, it was necessary to apply a geometric correction factor in order to irradiated the 25 dosimeters at once. For this purpose, were used the dose values obtained with the matrix - OCTAVIUS 1500 - placed during the irradiation just below the TLD plane. To accomplish the calibration of the TLDs, the efficiency of each detector, the Element Correction Coefficient (ECC) was determined for each dosimeter. To test the validity of the calculated ECC, 11 dosimeters were randomly selected. Each TLD was individually submitted to the same anneal-irradiation-readout procedure, with a fixed dose (1.36 Gy). Then, a second test was performed.

The dosimeters/solid water slabs set-up were placed on the floor, so that the field in the central zone where the dosimeters were distributed would be much more homogeneous. Batch heterogeneity, linearity, repeatability and sensibility were determined in this case.

### 3.2.1 ISO 28057:2014

The authors assume that the role of any International Standard is to provide trustworthy concepts, terms and definitions, and rules for good practice for the application of TLD methods, which include requirements for TLD system, by medical physics and instrument producers. In particular, it is applicable to solid “TL detectors” like chips made from LiF:Mg,Ti in crystalline or polycrystalline form. [1] The specifications and procedures described in International Standard can be applied in the next conditions:

- [0.020; 50] MeV for photon radiation;
- [4; 25] MeV for electron radiation;
- Brachytherapy with photon-emitting radionuclides;
- [0.001; 100] Gy.

With the purpose of the determination of the values of the absorbed dose, the TL detectors have to go through numerous measurement cycles for the determination of an individual calibration coefficient for each detector.

The user must be very careful and gentle while handling the dosimeters.

Detectors should not be cleaned regularly, however if the response of TLD's get altered, frequently it is reduced, it is suggested to be uncontaminated by means of an ultrasonic bath using ethanol. The entire batch has to be cleaned as fast as possible, then a pre-irradiation annealing of the whole batch has to be carried out. One of the most important recommendations of ISO/ASTM 51956:2013 is that TLD's should not be handled with the bare fingers to avoid getting dirt or oils on them. There are strong reasons for this caution: dirt and/or grease on surfaces of TLD's can affect their response and can contaminate the heating chamber of the TLD reader, since human fat melts at 42 °C in maximum and higher temperatures are reached in TLD reader, approximately 350 °C. [65]

So, a vacuum pen or tweezers coated with TFE-fluorocarbon should be used in handling the chips. The choice was the last once, since the DYMAX 30 Charles Austen Pumps Ltd. with Vacuum Tweezer, in Figure 3.11 was the equipment that existed in laboratory.



Figure 3.11: DYMAX 30 Charles Austen Pumps Ltd. with Vacuum Tweezer.

Other recommendation that is important to have in consideration is always to handle them in a manner that minimizes mechanical stress and the possibility of starching or chipping the TLD.

First, TLD's must be identified. Numeration seems to be a good method, because besides it provided an appropriately mark for distinction it also helps in the positioning of the dosimeter. So, in each one was written a number between 1 and 100 on top of the face of the detector with a pencil, as exemplified in Figure 3.12 for the first 10 dosimeters of Radcard.

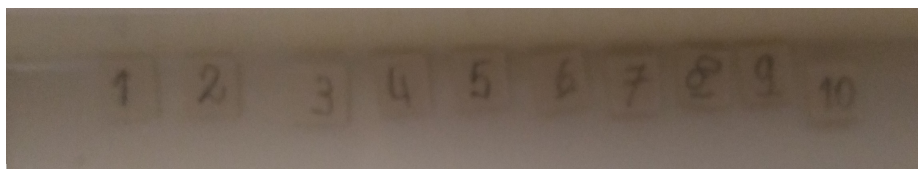


Figure 3.12: Numeration of the first 10 Radcard dosimeters.

The next step consisted in realizing the first cycle anneal-irradiation-readout procedure. TL detectors should be placed in casings for any thermal treatment that they receive. Preferably, the material of election for annealing casings is aluminum, because chemical reactions with TLD's were not detectable at high temperatures. It is important to note, that the maximum temperature that aluminum casings may reach is 420 °C. In laboratory of IPO-Porto, there were available two annealing casings, which are show in Figure 3.13.

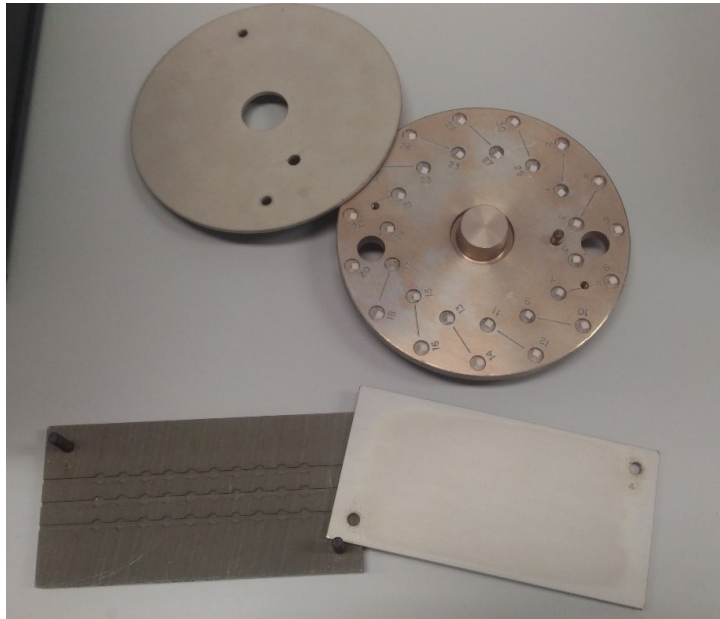


Figure 3.13: Circular and rectangular cases.

Obviously, the sizes of the annealing casings must be adjusted to the dimensions of the annealing oven. Otherwise, they should be as small as conceivable to reach fast heating and cooling down of TLD's. Besides that, it is necessary that they have a lid made of the same material to cover the TLD's, since this guarantee homogeneous heating of all pieces and avoids adulteration.

In the event of contamination of annealing casing, it may be washed with acetone first, then methyl alcohol, and finally, submitted to a heat treatment without TLD's inside. The objective of pre-irradiation annealing is to eliminate the effects of preceding irradiation and to readjust the sensitivity of the dosimeter.

The annealing procedure should include a reproducible temperature cycle of the annealing oven, accurate timing of the annealing period and a reproducible cooling rate as demonstrated in [Figure 3.14](#).

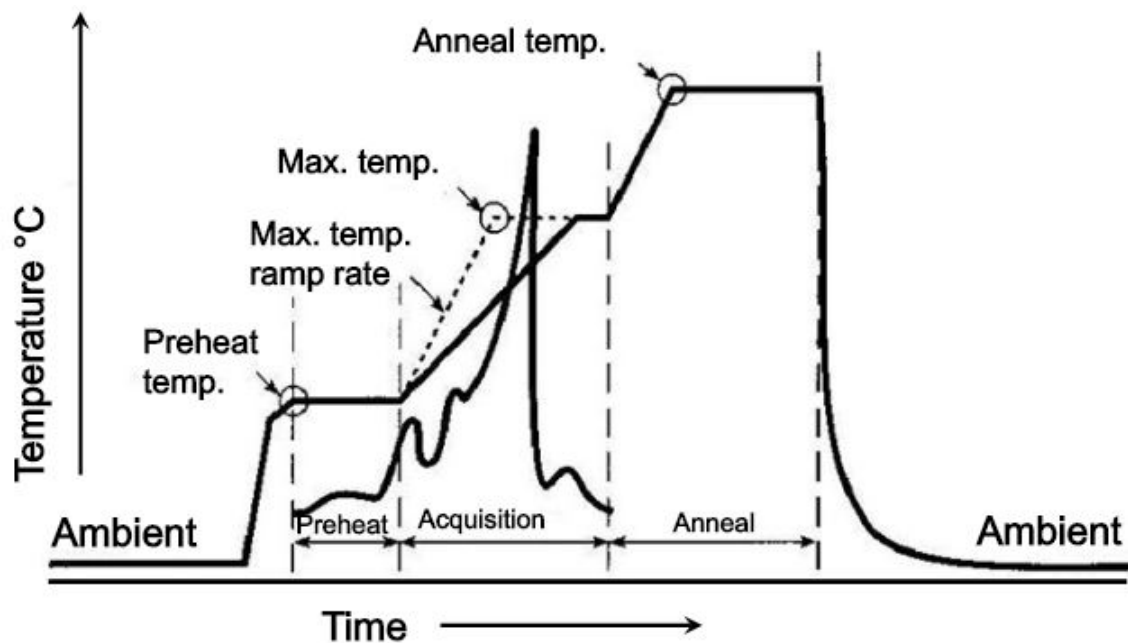


Figure 3.14: Time-temperature profile and glow curve for LiF:Mg,Ti freshly exposed to 1 Gy. Adapted of [66].

For this purpose, has been resorted to an oven with a controller associated. The temperature must be selected depending on the detector type, since it influences the response of TLD's. The recommended full anneal for LiF(Mg:Ti) is 400 °C for one hour followed by a longer anneal at a lower temperature—e.g., two hours at 100 °C, or 24 hours at 80 °C, or 18 hours at 75 °C. They have all been used with success, but taking into account efficiency the first alternative was selected. [67]

The necessity of many parameters definition, including the parameters of annealing, lead to a TTP that define the temperature cycle. For controller programming bases, refer to the Appendices A and B at the end of this thesis. But there is another important factor that may alter the response of detectors, which is the time interval between pre-irradiation annealing and the irradiation. Therefore, it may not surpass one week. A limitation of space in the oven and in the platform of irradiation condition implied the formation of four groups: A/B<sub>1</sub> (1-25); A/B<sub>2</sub> (26-50); A/B<sub>3</sub> (51-75); A/B<sub>4</sub> (76-100). The next step was the readout of the background of each dosimeter. The parameters used are the same defined in a normal readout after irradiation. For photon irradiation, the dosimeters must be surrounded with enough material to achieve charged-particle equilibrium condition in the TLD's. It is necessary to measure the temperature and air pressure of the room, since temperature is an influence quantity of the dosimeter response. For that it was used the OPUS 10 TPR for both measurements. [68]

For irradiation, dosimeters have to been placde in defined and precise positions, that depend of the settings established. Consequently, it depends on the specific radiation processing application. To record the specific conditions of each irradiation, the user should complete a table as Table 3.6.

Table 3.6: Table of specific conditions for each irradiation.

<b>Irradiation</b>	
<b>Date</b>	
<b>Quality of radiation</b>	
<b>Dose</b>	
<b>Dose rate (optional)</b>	
<b>Field size</b>	
<b>Phantom</b>	
<b>Depth of measurement</b>	
<b>Type and desing of the probe</b>	

After irradiation, it is applied a post-irradiation analysis procedure that is also named stabilization since most of the fading is suppressed by this treatment. But before any treatment, it is important to verify the setting of each dosimeter and account for all, followed by the recollection to the compartments and inspection for imperfections. Any irregularity must be documented. Prior to measurement, TLD's are retained in a drawer in the laboratory of readout inside their respective pocket during 24 hours until the pre-readout or post-irradiation annealing, which temperature depends on the detector type. LiF chips require annealing at low temperatures between irradiation and readout to remove unstable low temperature peaks in the response output, when it is used the entire response output glow curve. The post-irradiation annealing is not required when using the peak-high response or for readers with regulating temperature discrimination. Given that the reader has not that peculiar characteristic and the access to the values for each canal of the readout is not available, the entire response output glow curve is used. The manufacturers recommend a post-irradiation annealing of about 100 °C for 10 minutes, but there are another procedure that is quicker and the most important remove the undesirable unstable low temperature peaks. Taking advantage of the functionalities of the reader, the parameters must be adjusted for a fast-post-irradiation annealing: 10 s at 130 °C.

Simultaneously, other reader parameters had to be adjusted to obtain reproducible responses through several cycles of anneal-irradiation-readout procedure. Consequently, they generate reproducible glow curves, since the shape of those depends on the heating profile used. The manufacturer mention that they may be read out with any typical TL reader, either with heated inert gas flow (e.g. Alnor DOSACUS or Harshaw 5500) and ohmic - heated "planchet"- (e.g. Harshaw 4000, Toledo or Solaro) heating systems. The reader available in the IPO-Porto laboratory is the HARSHAW TLD™ Model 3500 Manual Reader and belongs to the second group mentioned above, namely contact heating. Therefore, the sample compartment must be flushed with inert gas to suppress air-related combustion of surface contaminations of the heated support or TLD's. The gas used in the available reader is nitrogen ( $N_2$ ) and its inertia is more important the lower the dose being measured, since this prevents combustions that can mimic a signal. In addition, the recommendations of ISO/ASTM 51956:2013 for readers that use resistively heated planchets to heat the chips, a heating rate of approximately 30 °C per second is satisfactory and the TLD's

should be heated until a temperature of about 350 °C.

The combination of previous recommendations with some experiments performed at IST/CTN and other documentation lead to the selection of reader parameters demonstrate in the Figure 3.15. [69, 70]

The screenshot shows the 'Time Temperature Profile Setup' dialog box with the following settings:

- Setup Info:** Title: leitura, Date Edited: 15-12-2016, Number: 1, Edited by: system
- Regions:** ROI 1 [ 0, 0 ], ROI 2 [ 0, 0 ], ROI 3 [ 0, 0 ], ROI 4 [ 0, 0 ], Calibration Region [ 1, 200 ]
- Preheat:** Temperature: 130 °C, Time: 10 sec
- Acquire:** Temperature Rate: 10 °C/sec, Maximum Temperature: 300 °C, Time: 20 sec
- Anneal:** Temperature: 350 °C, Time: 20 sec
- Calibration:** Date Calibrated: (none), Units: nC / nC, RCF: 0, Average Noise: 0 nC, Light: 0 nC
- Factors:** Background: 0, Quality: 1
- Current TTP:** Buttons: New, Delete, Copy, Paste
- Buttons:** OK, Cancel, Help

Figure 3.15: Time Temperature Profile Setup Dialog Box in edit mode view.

To prevent that the response has a dependence on the orientation of the TLD in the reader chamber, the chips are positioned always with the same orientation and face marked down. Besides that, the integrated light output eliminates this effect. The reader available is furnished with a light source and it is used to check the stability for the light measuring section and its associated electronics. For that reason, this reference light-check is applied prior to the reading and after ten consecutive readouts. However, the test of performance and stability of the heating and, conse-

quently, of the temperature measuring section is missing. So, to fill this need it is suggested to choose some calibration TLD's to this purpose.

The user's dosimetry system calibration shall consider the influence quantities associated with pre-irradiation, irradiation, and post-irradiation conditions applicable to the process. Nevertheless, the calculation of the limits of detection was not considered during this work since the clinical applications for which the dosimeters will be used present very high doses when compared with the limits already obtained in other projects. The fading factor was also not taken into consideration, since all readouts are performed in the same time after irradiation (approximately  $24 \pm 1$  hours).

If reusable TLD's are irradiated to high accumulated absorbed-dose levels ( $> 10^2$  Gy) recalibration may be required because of possible changes in absorbed-dose sensitivity. To identify detectors in this situation and others it is important to record the conditions to which each of the dosimeters was submitted.

### 3.2.2 Procedures

The procedures of an annealing-irradiation-readout cycle and the steps to be taken when receiving a new batch of dosimeters are presented in the following sub chapters. The elaboration of procedures for calibration and other protocols is a recommendation of ISO/ASTM 51261:2013. [71]

#### 3.2.2.1 One Complete Cycle Annealing-Irradiation-Readout Procedure

The detailed procedure of a complete cycle Annealing-Irradiation-Readout is described as follows:

##### 1. Annealing

- (a) Turn off the room lighting and turn on the small lamp that exists in the laboratory;
- (b) Switch on the air conditioner at a low temperature (at  $18^\circ\text{C}$  for example);
- (c) Place the dosimeters in the casings indicated for annealing;
- (d) Place the filled casings with the detectors in the oven and start the annealing process;
- (e) Remove the casings when the ambient temperature is the same as that indicated on the oven controller.

##### 2. Irradiation

- (a) Place each detector in the desired position on the irradiation plate by checking the integrity of each one;
- (b) Note in the laboratory notebook which dosimeters will be subjected to irradiation and the conditions (see Table 3.6);
- (c) Transport, with the help of the cars available in the IPO-Porto, the plate with detectors covered with solid water plates, the remaining plates needed, the OPUS 10 TPR and the matrix to the bunker where the LINAC is located;



- (d) Fix the dosimeters and the matrix when necessary the set up intended with the help of lasers, front pointers and bright field;
- (e) Connect the matrix, enter the correction factors in the program VeriSoft® (temperature and air pressure) and measure the "zero". Click start;
- (f) Insert the parameters in the software of the accelerator and check that they are correct before starting the irradiation. Irradiate;
- (g) Stop the matrix acquisition mode. Fill the conditions of the irradiation and save the data of VeriSoft®;
- (h) Transport the plate with detectors covered with solid water plates and the remaining materials to the laboratory;
- (i) Transfer the detectors from the plate to the containers in the drawers of the laboratory. Write on the container lid the date of irradiation and the group that was submitted to it.

### 3. Readout

- (a) Connect the reader half an hour before the readout. Turn on nitrogen gas. Wait 24 hours to read the dosimeters;
- (b) Create a folder with the date and the ID to save the glow curves and the file ASCII with the data;
- (c) Inserted the TLD's in the reader one by one, where they subjected to the desired and preset heating cycle;
- (d) Save the data in the specific folder;
- (e) Store the dosimeters in the containers in the drawer of the laboratory and note "readout check and no annealing".

#### 3.2.2.2 Initial General Procedure

The detailed initial general procedure is described as follows:

1. Setting the oven and inserting the reading parameters in the software of the reader;
2. Numeration of dosimeters;
3. Determination of the value of Element Correction Coefficient (ECC) and decision of what will be the use of the detector (field or calibration):
  - (a) Perform 3 consecutive cycles of annealing, irradiation with the calibration conditions (detailed in Sub-chapter 4.1) and readout;
4. Tests for the verification of calculated ECC:

- (a) Perform 3 consecutive cycles of annealing, irradiation and readout with the particularity that each dosimeter was irradiated in the center of the support solitary;
  - (b) Perform 3 consecutive cycles of annealing, irradiation and readout with the particularity that sets of dosimeters were placed on the floor;
5. Study of linearity:
- (a) Perform 3 consecutive cycles of annealing, irradiation with the calibration conditions and readout, except the quantity of MU. Repeat this step for diverse doses (MU);
  - (b) Perform 3 consecutive cycles of annealing, irradiation with the calibration conditions and readout and determinate the new ECC;
6. Study of repeatability:
- (a) Perform 4 consecutive cycles with 25 dosimeters of annealing, irradiation with the calibration conditions and readout;
7. Study of energy dependence:
- (a) Perform 3 consecutive cycles of annealing, irradiation with the calibration conditions and readout, expect the selected energy. Repeat this step for diverse energies;
8. Application in the phantom;
9. Application in the clinical practice.

## Chapter 4

# Experimental results

The objective of this chapter is to present all the results of this investigation and a detailed analysis of them in a succinct way.

Initially, the calibration parameters are described, and a detailed analysis is performed on the results obtained, namely the individual and geometric correction factors calculated, always focusing on the comparison of the two types of dosimeters. Then the results of two experiments formulated to test these factors are presented and discussed.

Besides that, it is exposed the results obtained for the linearity and, consequently, the calibration curves that must be highlighted. Next, a study on energy dependence is presented.

Finally, an estimate of the uncertainty is performed and the results of the clinical application in the phantom are revealed.

### 4.1 Calibration Parameters

In view of the purpose of calibration, glow curves of 100 TLD's of each brand, 200 in total, irradiated by the linear accelerator with TrueBeam® Radiotherapy System were obtained and analyzed. The cycle in Figure 4.1 summarizes the different steps.

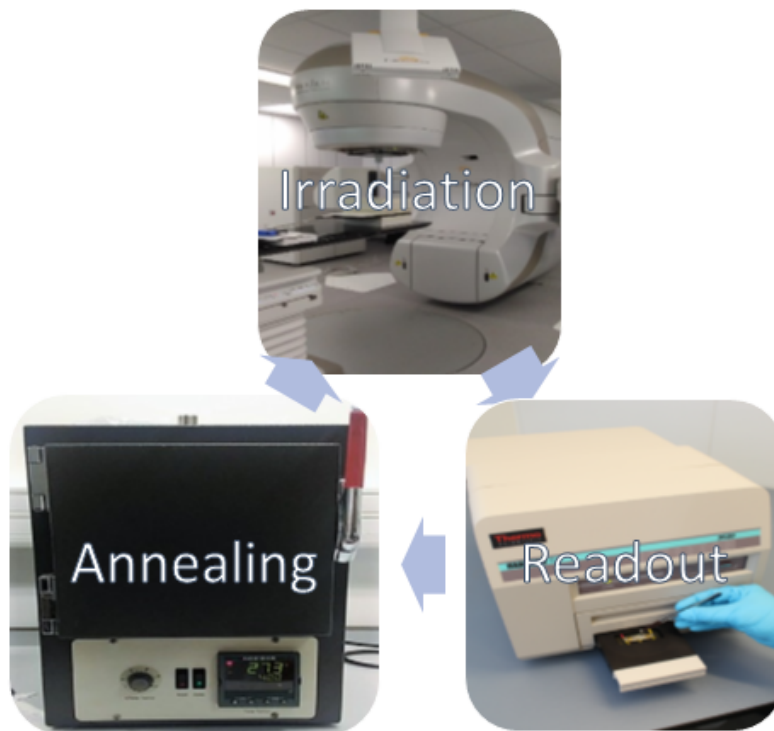


Figure 4.1: Representative scheme of experimental steps.

To do the calibration, TLD's were placed orderly on a previously drilled PMMA material plate. To each drill it was attributed a number from 1 to 25 from top to bottom and from left to right, as represented in Figure 4.2 .

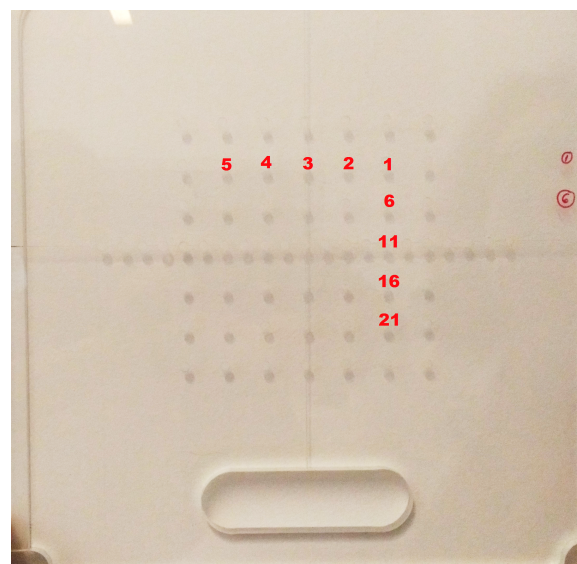


Figure 4.2: PMMA material board with numeration of excavated circles for the placement of dosimeters from 2 to 2 cm.

There are two marks (number 1 and 6) in the plate to help the user to correspond the position

of the detector in the plate with the number of identification of the detector. A line is completed with 5 dosimeters and there are five lines.

In turn, this is centered on the top of 10 plates of solid water with 1 cm plus a matrix between the 8th and 9th plates. Besides that, they are covered with more ten plates (10 cm). The lower plates prevent the back scattering and the upper plates allows to place the dosimeters at the reference depth of the dose measurements performed with the ionization chambers. Then, the TLD's were irradiated with the linear accelerator with a photon beam having the following characteristics:

- Field size =  $12 \times 12$  cm;
- Energy = 6 MV;
- Dose = 200 monitor units (1.36 Gy);
- Dose rate = 600 MU/min;
- Gantry rotation =  $0^\circ$ ;
- Rotation of the collimator =  $0^\circ$ ;
- SSD = 100 cm;
- Depth = 10 cm.

**Conversion to dose:**

$$OF(12 \times 12)_{10cm} = 1.014$$

$$PDD(12 \times 12)_{10cm} = 67.1\%$$

$$Dose = 200 \times 0.671 \times 1.014 = 136cGy = 1.36Gy$$

To study the behavior of TLD's and possible variations, these pieces were irradiated under the same conditions three successive times. The need to introduce the matrix is due to the fact that the irradiation field is not perfectly homogeneous in the region where the dosimeters are placed (-4 cm to 4 cm) as can be seen in the graph of dose profile in the Figure 4.3.

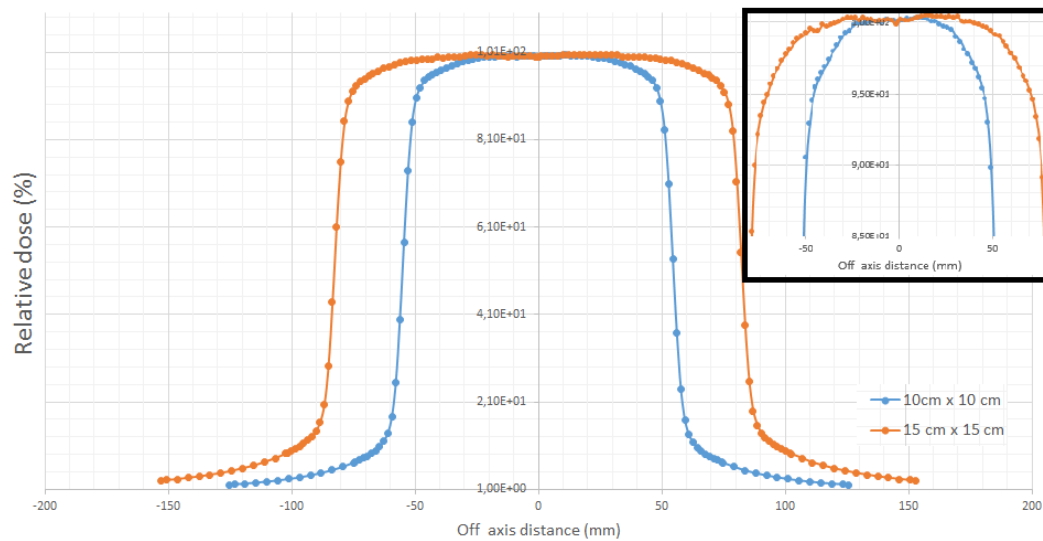


Figure 4.3: Dose profile obtained by scanning the beam with a ionizing chamber of a field 10x10 cm<sup>2</sup> and 15x15 cm<sup>2</sup> with a beam of 6 MV and zoom to the central region.

## 4.2 Analysis

Having obtained the readings of all the dosimeters of the first cycle, it is time to analyze the data. These can be extracted directly from a text file by simply changing the definitions in Acquisition Set-up (ACQ) creation (see Appendix B). But firstly, to determine variations in the response within the group of available TLD's, the total intensity value obtained per channel, in nA, is plotted to each dosimeter in question as showed in Figure 4.4.

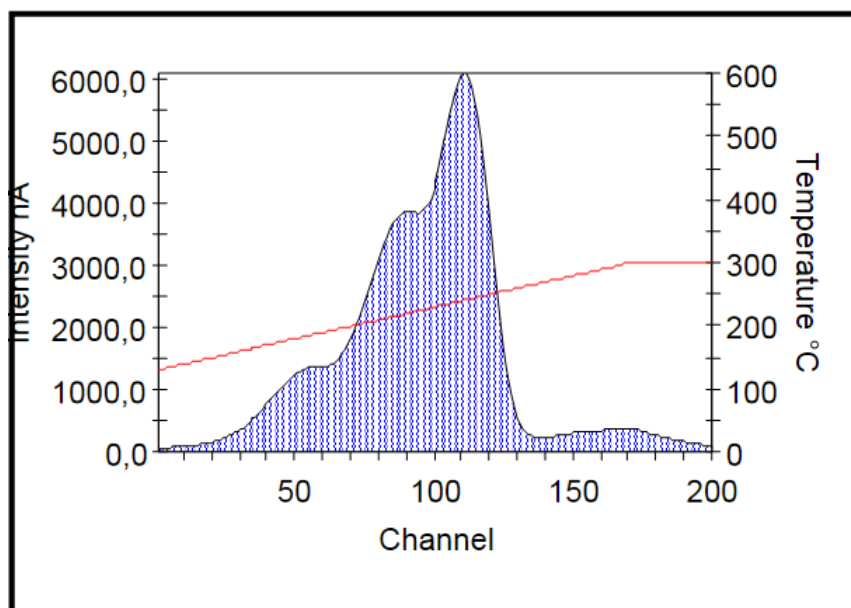


Figure 4.4: Example of a curve collected by the reader HARSHAW TLD™ Model 3500 Manual Reader.

Then, with the help of the Excel spreadsheet, a table was constructed with the read values,  $M_i$ , total integration of the collected load curve, and the background values -  $M_{0_i}$  - for the respective dosimeters in nC. First correction to apply is subtraction of the background of each TLD, so reduced reading value is obtain as exemplified in equation 4.1.

$$M_{red_i} = M_i - M_{0_i} \quad (4.1)$$

Then, it was necessary to proceed with the correction factor of the reader. The changes in the response of the measuring equipment must also be considered. depending on the application under study, the measurement sessions can be extended by several hours and it is therefore necessary to consider the sensitivity fluctuations of the reader within that time. With this aim, a set of five dosimeters randomly selected and always irradiated at the same reference dose (calibration conditions) were considered at each reading session. They were always read under the same conditions as the dosimeters of measurements and interspersed with them, so that the variations in the reader could be better quantified.

Thus, by generating a normalized correction factor for each readout,  $f_r$ , a corrected value,  $M_{l_i}$ , can be obtained by multiplying the values respectively by the reduced reading value.

$$M_{l_i} = (M_i - M_{0_i}) \frac{\overline{R}_{t_0}}{\overline{R}_t} = M_{red_i} \cdot f_R \quad (4.2)$$

In this equation,  $\overline{R}_{t_0}$  and  $\overline{R}_t$  represent, respectively, the mean value of the readings of the control group at a reference instant  $t_0$  and at a later time  $t$ . Each of which is obtained by the mean of the readings obtained for the sets of 5 dosimeters. So, the reader correction factor determined in each work session affects all measurements taken in that session. Besides that, it is necessary to compare the values obtained with the previous ones and to report if their relative deviation is greater than 5%. Otherwise a new calibration is recommended.

Then, it is necessary to proceed with the geometric corrections. For this it is used the values of the matrix placed during the irradiation as exemplified in Figure 3.9.

The graph of Figure 4.5 traduces the values obtained by the matrix and then normalized according to the position of the detector in the PMMA dosimeter plate (4.2).

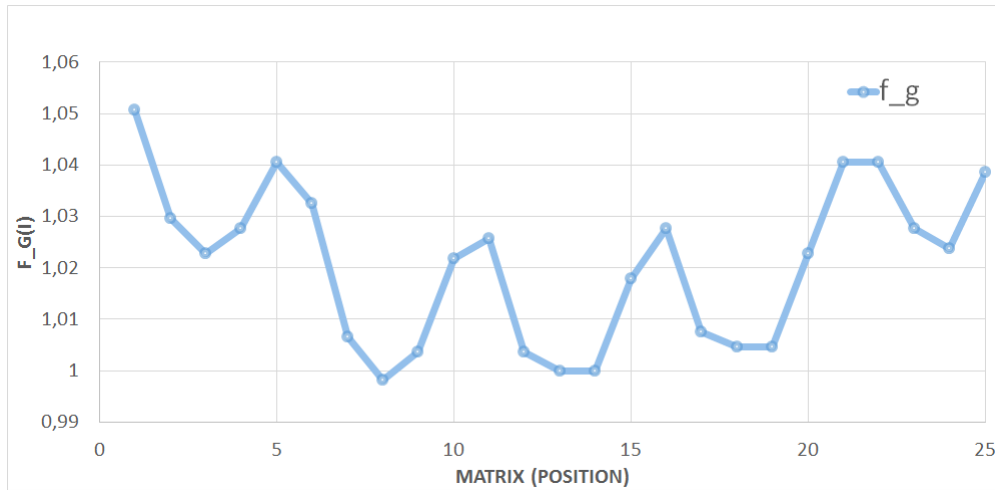


Figure 4.5: Normalized values obtained by the matrix according to the position of the detector.

The dosimeter plate is centered in relation to the matrix, the dosimeters are separated by 2cm and the resolution of the matrix is 0.5cm, so it was enough to make the correspondence between the value of the matrix and the number of the dosimeter to obtain a factor for non-uniformity of the beam. Then, this factor  $f_i$ , was normalized in relation to the mean central value of the 4 groups,  $f_n$ , and is calculated as

$$f_{g_i} = \frac{f_n}{f_i} \quad (4.3)$$

Thus, by generating a normalized geometric correction factor for each detector, a corrected value,  $M_{ge_i}$ , can be obtained by multiplying the values respectively by the reduced reading value.

$$M_{ge_i} = (M_i - M_{0_i}) \frac{\overline{R_{t_0}}}{R_t} \times \frac{f_n}{f_i} = M_{t_i} \cdot f_{g_i} \quad (4.4)$$

Being excluded the geometric dependence, it remains to calculate the efficiency of each detector, the ECC. Initially, to determine the ECC, the mean of all values read already corrected is calculated and divided by the read value already run of each dosimeter,  $M_{ge_i}$ :

$$ecc_i = \frac{\overline{M_{ge_i}}}{M_{ge_i}} \quad (4.5)$$

Then the four best dosimeters, i.e. those with an ecc closer to 1 are selected as calibration dosimeters. With the average value of their readings, the ECC of the remaining dosimeters is recalculated as follows:

$$ECC_i = \frac{\overline{M_{ge_{cal}}}}{M_{ge_i}} \quad (4.6)$$

The Figure 4.6 allows the comparison between the ECC values obtained for each one of the batches.



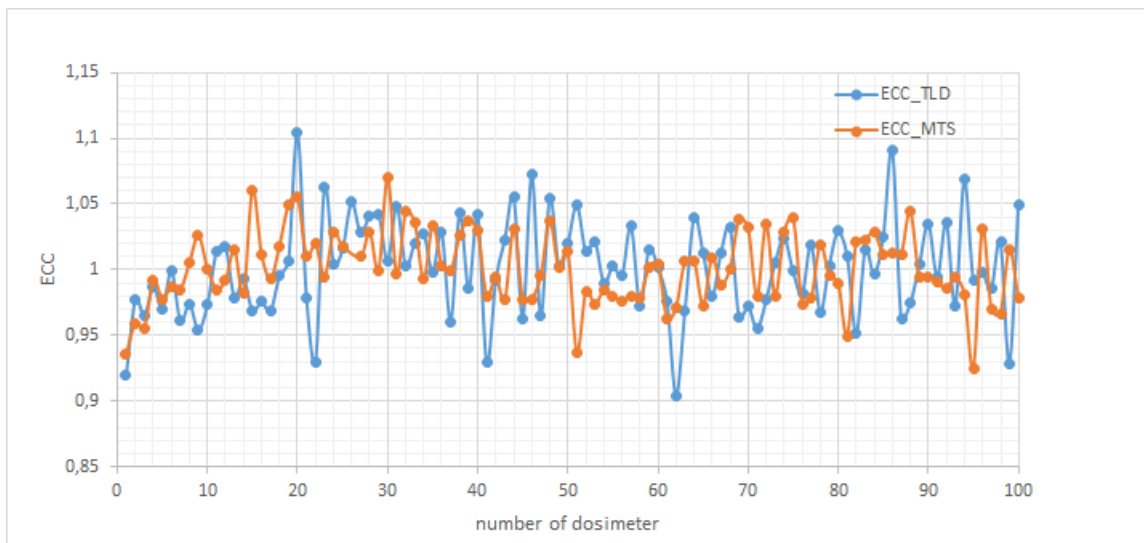


Figure 4.6: Values of ECC obtained according to the position of the detector to MTS-100 versus TLD-100.

The obtained data leads to the following graphics of Figures 4.7 and 4.8 to Group A and B, respectively. In conclusion, if each reading value is multiplied by the respective ECC and by the geometric correction factor, a constant value should be reached.

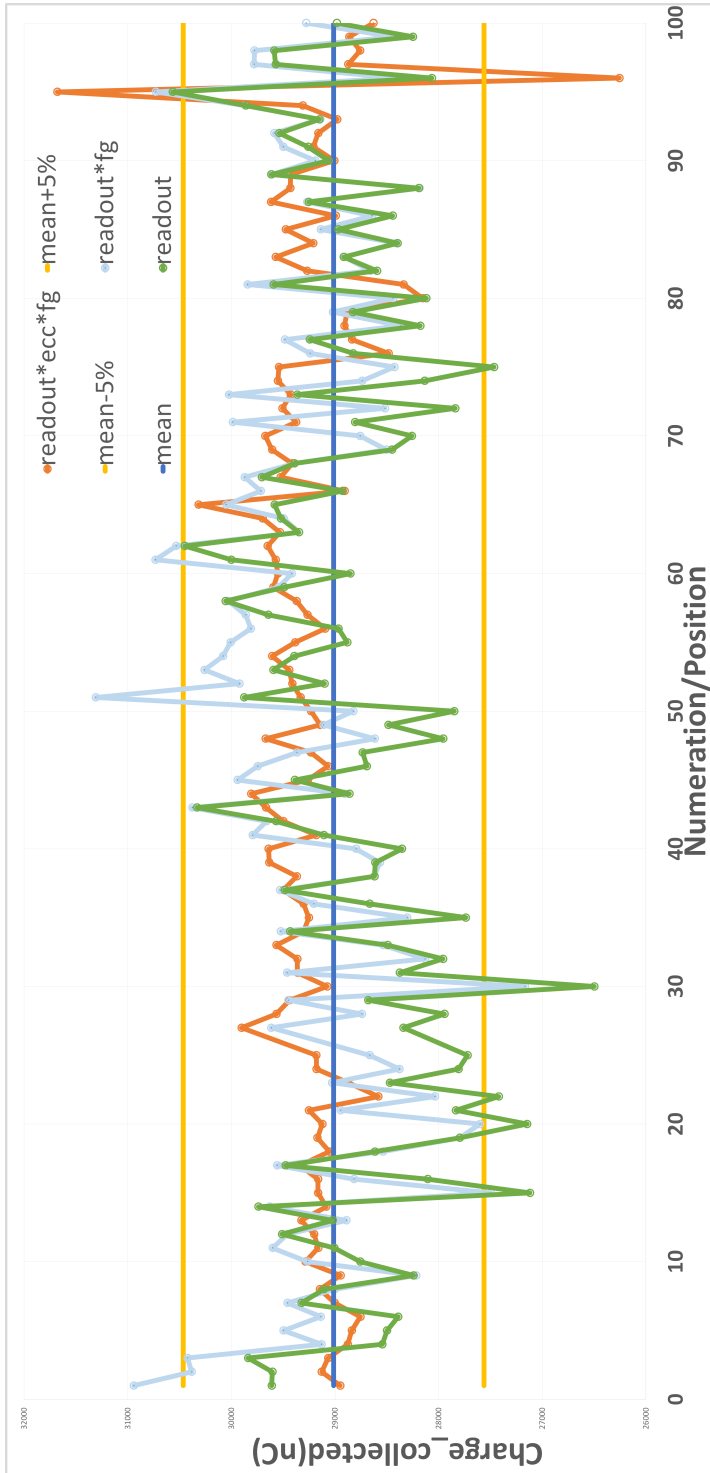


Figure 4.7: Values obtained according to the position of the detector and with respective corrections (Group A).

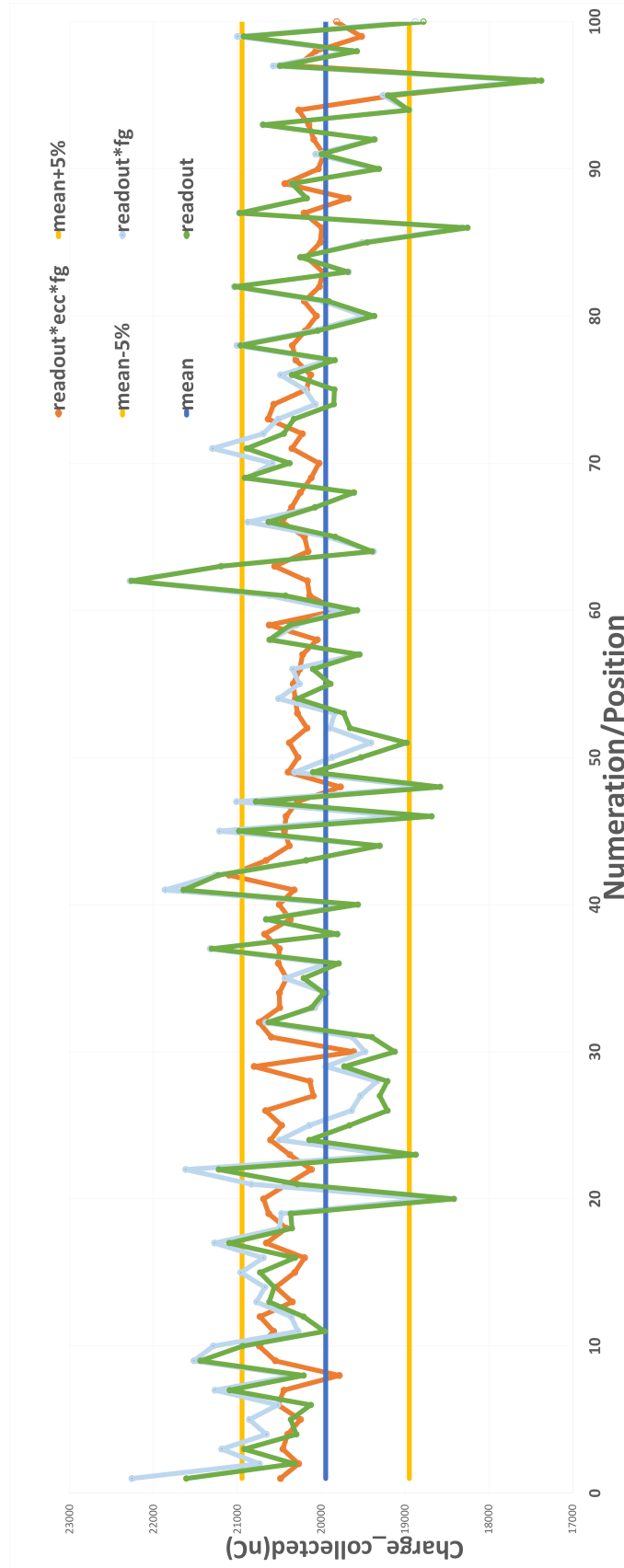


Figure 4-8: Values obtained according to the position of the detector and with respective corrections (Group B).

In Table 4.1, they are presented the results for MTS-100 versus TLD-100.

Table 4.1: Table of results MTS-100 (Group A) versus TLD-100 (Group B) - Calibration.

	MTS-100	TLD-100
mean_charge (nC)	29122	20179
$\sigma_{\text{readout}}$ (%)	2.8	3.6
$\sigma_{\text{after\_fg}}$ (%)	2.6	3.5
$\sigma_{\text{after\_ECC\_fg}}$ (%)	1.1	2.1
$\sigma_{\text{ECC}}$ (%)	2.8	3.6

Exactly under the same conditions, the average value obtained from the readings for the dosimeters MTS-100 is more than 45% compared to pieces TLD-100 and the standard deviation calculated of the first batch is 2.8% and for the second batch is 3.6%. The mean of variability between two consecutive cycles in the ECC value was 0.9% for the MTS-100, while the value obtained for the TLD-100 was 2.2%.

So, the MTS-100 (Group A) dosimeters show higher sensitivity, better uniformity and lower variability. After applying the geometric correction factor to all measurements, it was found that the standard deviation was reduced 0.1% and 0.2% for the Group A and Group B detectors, respectively, which supports the use of the matrix.

#### 4.2.1 Tests

To test the calculated ECC, it was programmed two different essays; one that involved 11 dosimeters and other with 25 detectors selected randomly.

##### Test 1 - Solitary Irradiation

For the first one, each TLD was submitted to the same cycle anneal-irradiation-readout procedure, with the particularity that each dosimeter was irradiated in the center of the support solitary. This set-up eliminates the necessity of using the geometric correction factor.

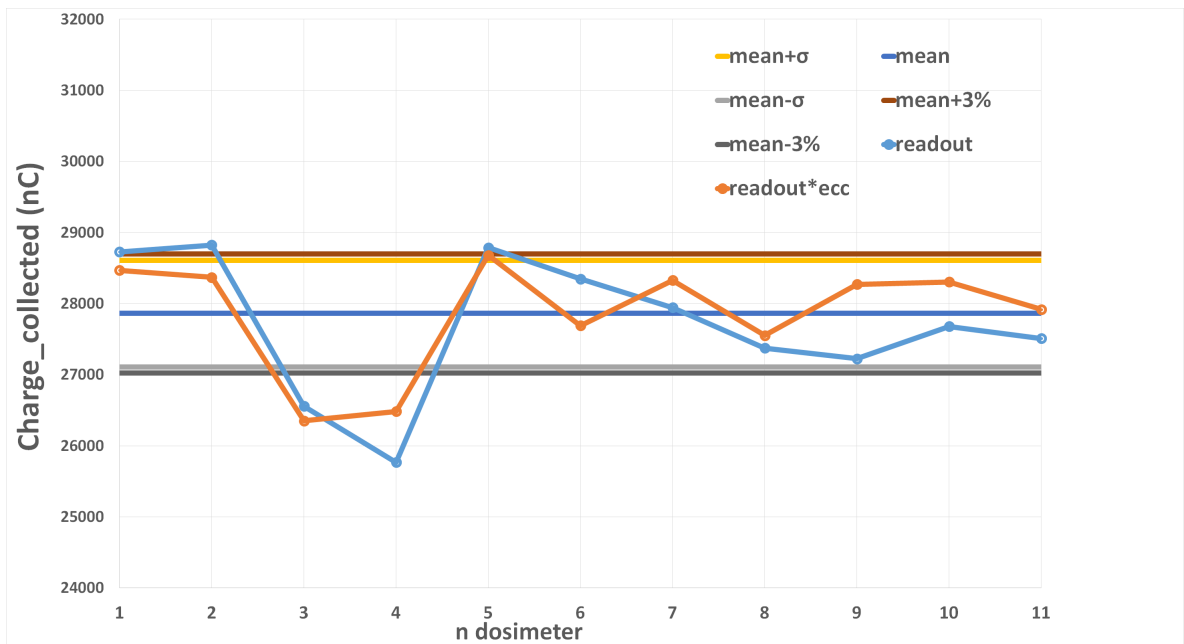


Figure 4.9: Values obtained to 11 detectors with respective corrections (Group A).

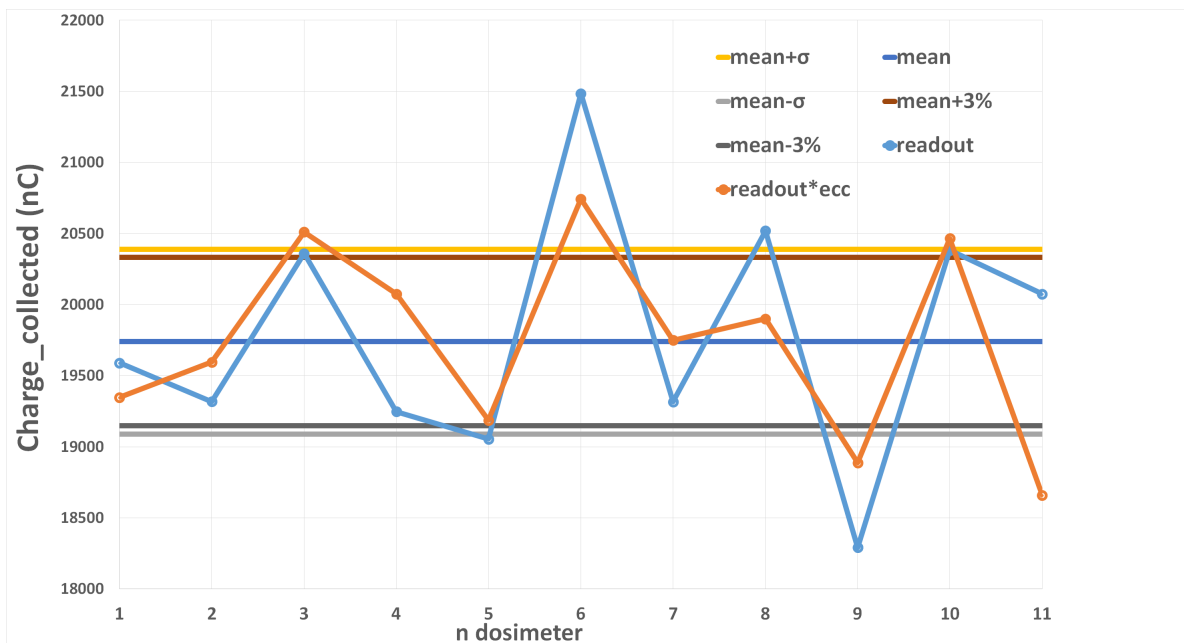


Figure 4.10: Values obtained to 11 detectors with respective corrections (Group B).

In Table 4.2, the results for MTS-100 and TLD-100 are compared.

Table 4.2: Table of results MTS-100 versus TLD-100 - Test 1.

	MTS-100	TLD-100
$\sigma_{\text{readout}}$ (%)	2.1	5.9
$\sigma_{\text{after\_ecc}}$ (%)	1.9	4.3
$\sigma_{\text{after\_ecc\_fg}}$ (%)	1.5	2.7

The standard deviation of the first set of 11 dosimeters is initially 2.1% and after application of all correction factors is reduced to 1.5% for MTS-100. The standard deviation of the first set of 11 dosimeters is initially 5.9% and after application of all correction factors is reduced to 2.7% for TLD-100.

### **Test 2 - Floor Irradiation**

In the second test, the dosimeters/slabs set-up was placed on the floor as shown in Figure 4.11 so that the field in the central zone where the dosimeters were distributed could be much more homogeneous.



Figure 4.11: Experimental set-up of the floor irradiation.

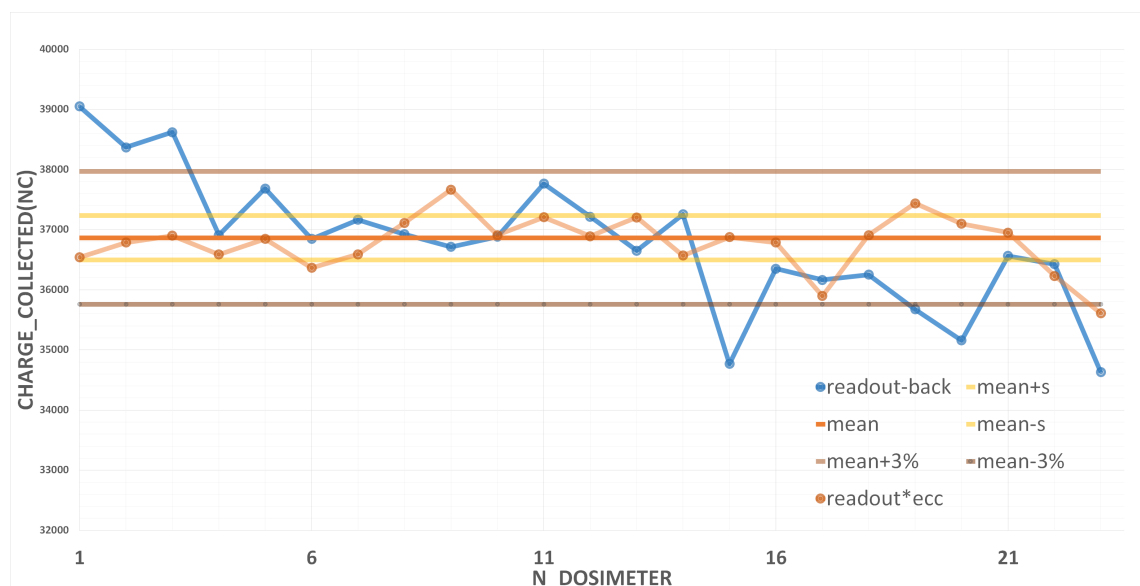


Figure 4.12: Values obtained according to the position of the detector and with respective corrections (Group A).

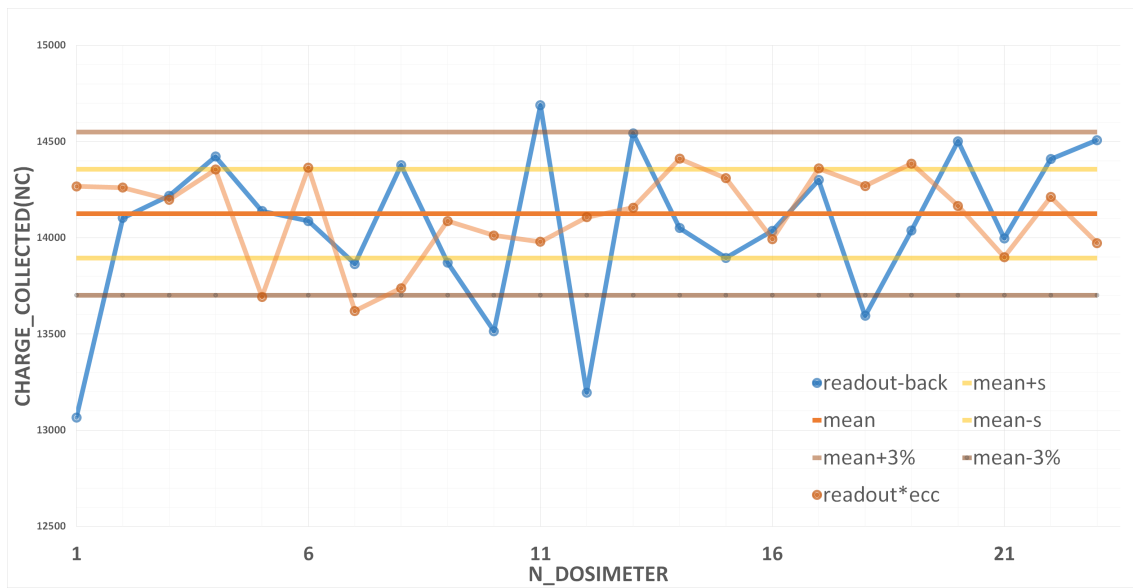


Figure 4.13: Values obtained according to the position of the detector and with respective corrections (Group B).

In Table 4.3, they are presented the results for MTS-100 versus TLD-100.

Table 4.3: Table of results MTS-100 versus TLD-100 - Test 2.

	MTS-100	TLD-100
$\sigma_{\text{readout}} (\%)$	2.9	3.7
$\sigma_{\text{after\_ecc\_fg}} (\%)$	1.2	1.6

The standard deviation of the second set of dosimeters is initially 2.9% and after application of all correction factors is reduced to 1.2% for MTS-100. The standard deviation of the second set of dosimeters is initially 3.7% and after application of all correction factors is reduced to 1.6% for TLD-100.

## 4.2.2 Background value

As mentioned in the previous sub-chapter, a subtraction of the background value after the detector has been exposed to ionizing radiation. Nevertheless, to ensure that the dosimeter is capable of being used after irradiation requires that the residual should be approximately equal to the value that the dosimeter presented before being irradiated. There are two different methods to achieve this purpose: a traditional annealing using the oven or a successive number of reading cycles.

Figures 4.14 and 4.15 show the values obtained in 20 successive reading cycles for the MTS-100 and TLD-100 detectors and in Figures 4.16 and 4.17 the same values normalized to the first reading are presented graphically. The residual value obtained after annealing in the oven is represented in orange and a zoom from the second reading to the last is also presented.



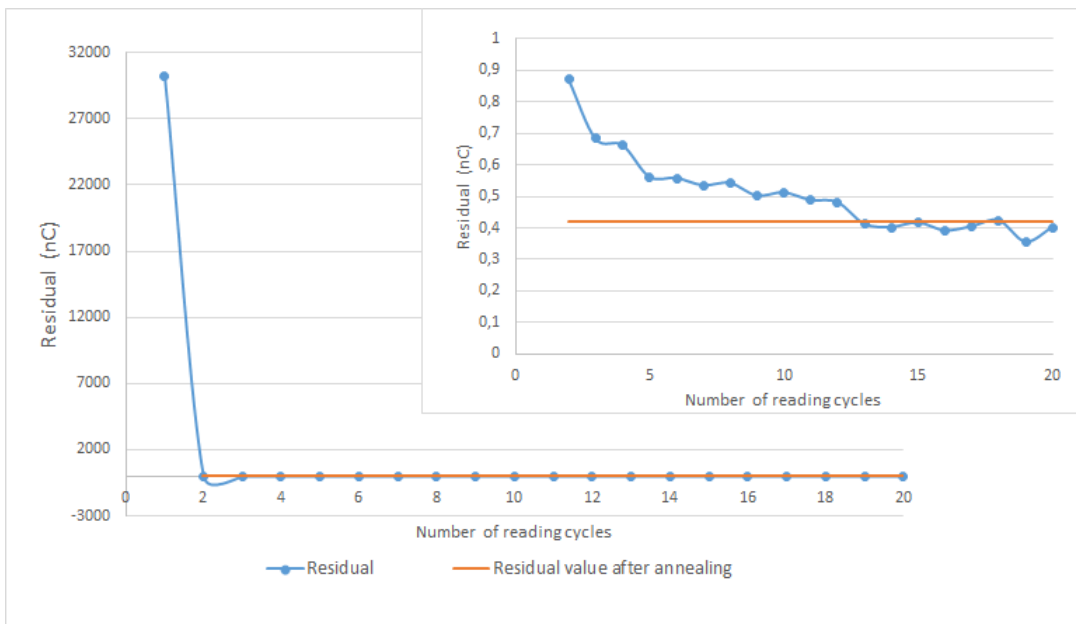


Figure 4.14: Background value for MTS-100 detectors, for irradiations of 1.36 Gy over 20 cycles of readings (Group A).

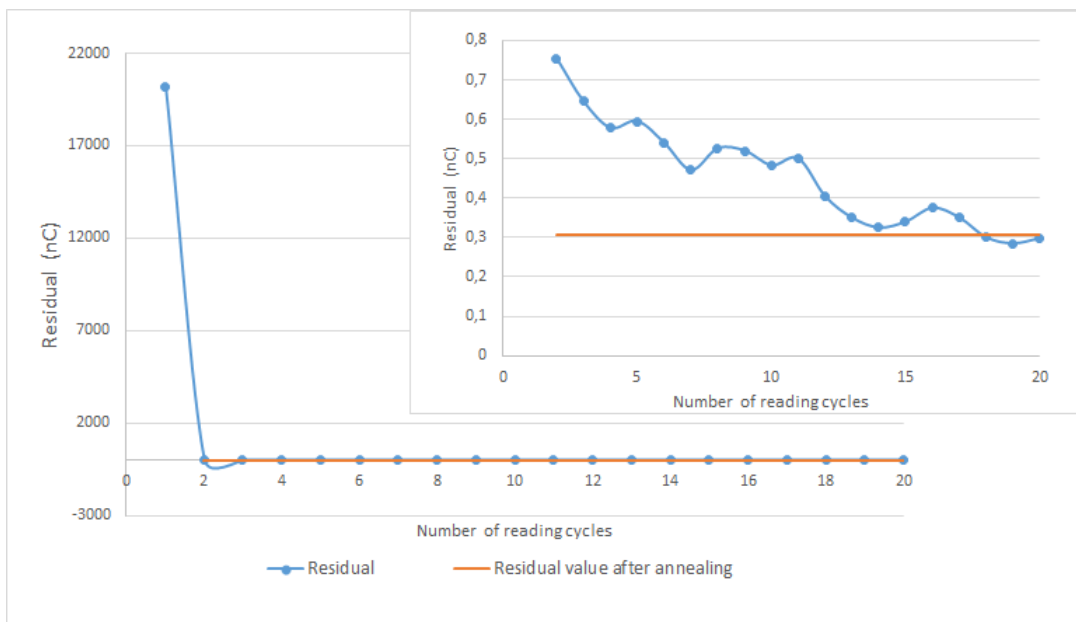


Figure 4.15: Background value, normalized to the first for TLD-100 detectors, for irradiations of 1.36 Gy over 20 cycles of readings (Group B).

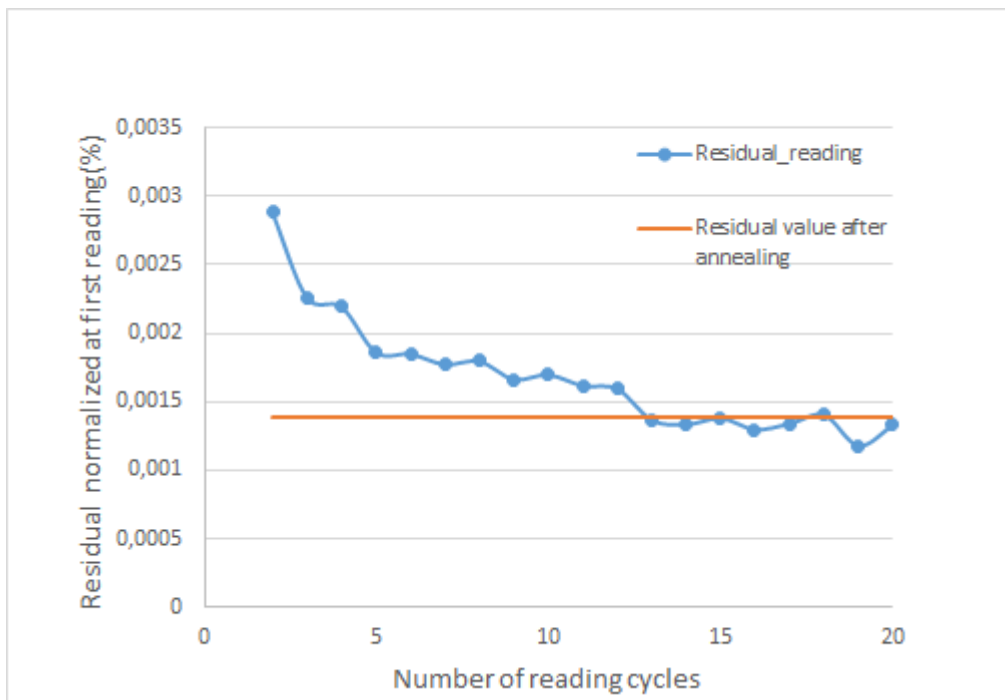


Figure 4.16: Background value, normalized to the first for MTS-100 detectors, for irradiations of 1.36 Gy over 20 cycles of readings (Group A).

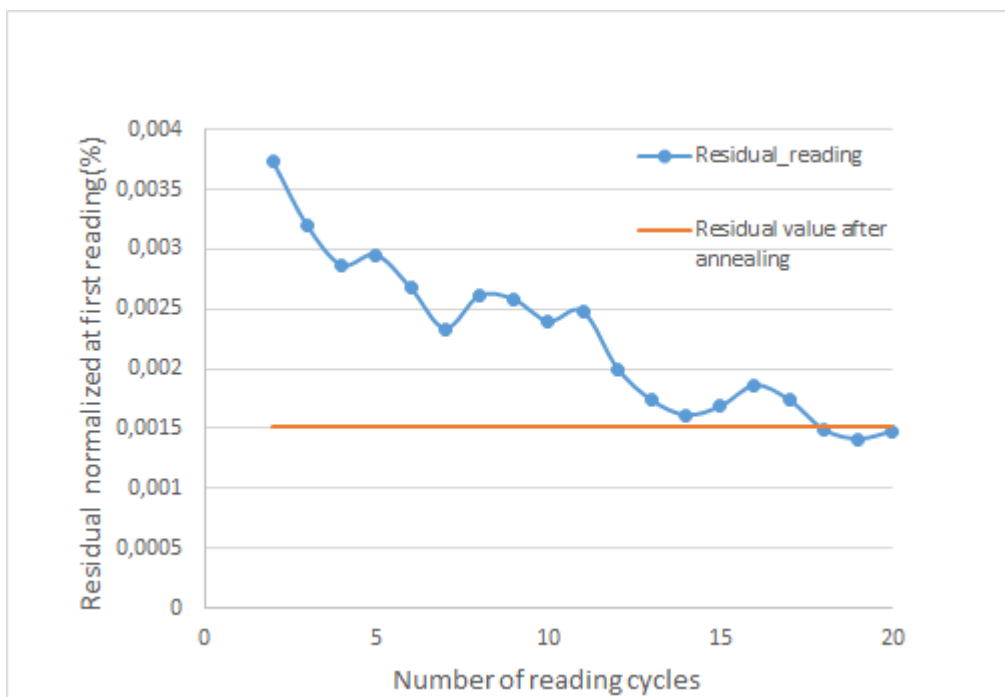


Figure 4.17: Background value, normalized to the first for TLD-100 detectors, for irradiations of 1.36 Gy over 20 cycles of readings (Group B).

In Table 4.4, are presented the results for MTS-100 versus TLD-100.

Table 4.4: Table of results MTS-100 versus TLD-100 - Background value.

		MTS-100	TLD-100
M0	nC	0.96	0.94
	%	0.003	0.005
Residual_annealing	nC	0.420	0.370
	%	0.001	0.015
Residual_20cycles	nC	0.401	0.298
	%	0.001	0.001

It is verified in these results that residual in both cases is less than 0.1% of the signal. It is visible that the measured values in consecutive cycles will be successively smaller, but with fluctuations. However, the variation between consecutive cycles becomes smaller from the twenty cycle with a standard deviation of the measurements of the order of 12% for Group A and 19% for Group B.

It was considered that the average value obtained from the last cycle constitutes the intrinsic residual of the material. This intrinsic residual verified in the twentieth reading cycle corresponds in % to 0.001 for both batches. Considering that the reader is manual and only allows the placement of one detector, the method chosen was to perform annealing in the oven.

### 4.2.3 Repeatability

In this sub-chapter it is intended to present and discuss the repeatability of values obtained for dosimeters of both types for a dose of 1.36 Gy. The test of stability of ECC and the values obtained is performed under repeatability conditions. So, by definition, repeatability is precision under exactly repeatable conditions, i.e. conditions where independent test results are obtained with the same method on identical test items in the same laboratory by the same operator using the same equipment within short intervals of time. [72]

#### 4.2.3.1 Stability of ECC

In order to have confidence in the methodology selected for obtaining the results, it is necessary to be able to guarantee that the sensitivity of the dosimeters remains constant throughout several cycles of use.

For this purpose, a set of five dosimeters was randomly selected and submitted to the same irradiation, reading and annealing sequence repeated for 10 series of measurements. 10 successive irradiation series were performed at a dose of 1.36 Gy, with the dosimeters placed solitary in the center of the PMMA plate. From the analysis of the glow curves and in each cycle of measurement, the individual correction factors were determined. Then, the mean value of ECC for each detector was determined and the deviation of each measurement to it was calculated. Thus, in the Figures 4.18 and 4.19 are represented the deviations in percentage according to the detector in question.

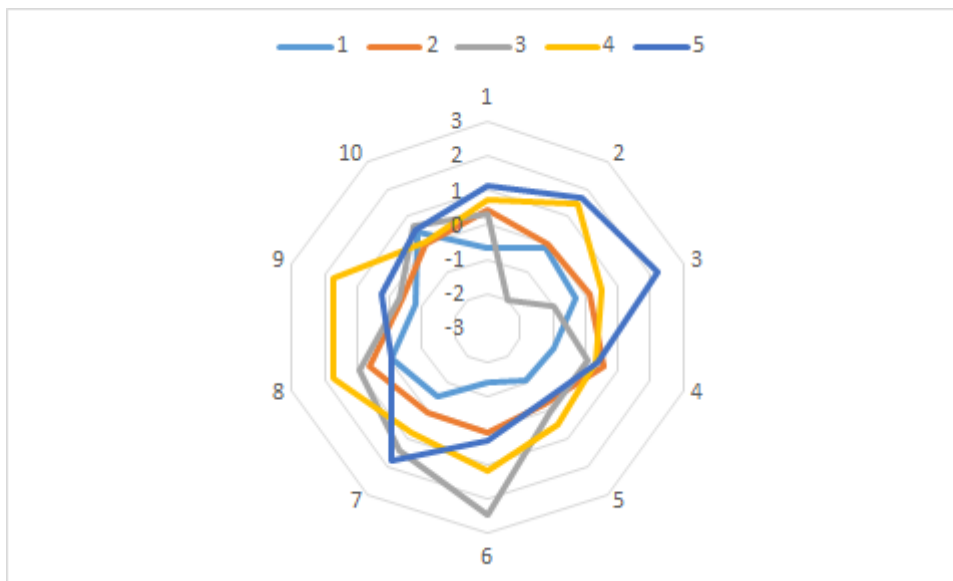


Figure 4.18: Repeatability achieved in 10 successive measurements, translated by the values of the individual correction factors obtained in each cycle - detectors irradiated at 1.36 Gy, solitary (Group A).

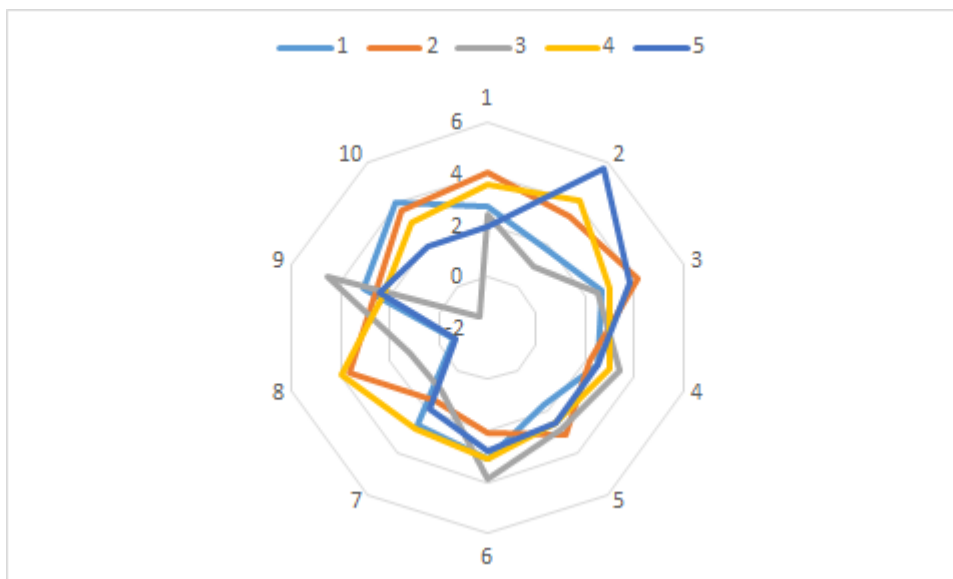


Figure 4.19: Repeatability achieved in 10 successive measurements, translated by the values of the individual correction factors obtained in each cycle - detectors irradiated at 1.36 Gy, solitary (Group B).

In Table 4.5, they are presented the results, the respective mean individual correction factors, together with their respective relative standard deviation, for 5 dosimeters MTS-100 and 5 dosimeters TLD-100.

Table 4.5: Table of results MTS-100 (Group A) versus TLD-100 (Group B).

		MTS-100	TLD-100
1	mean_ECC	0.985	0.957
	$\sigma_{\text{ECC}}$ (%)	0.5	1.2
2	mean_ECC	1.016	0.988
	$\sigma_{\text{ECC}}$ (%)	0.3	1.7
3	mean_ECC	1.016	1.016
	$\sigma_{\text{ECC}}$ (%)	1.2	0.5
4	mean_ECC	1.019	1.006
	$\sigma_{\text{ECC}}$ (%)	0.6	1.7
5	mean_ECC	1.002	0.987
	$\sigma_{\text{ECC}}$ (%)	0.8	1.5

The mean of ECC's of these five dosimeters of each manufacturers provide a measurement of the different sensitivity of the detectors composing the complete set. They are between 0.985 and 1.019 for MTS-100 and between 0.957 and 1.016 for TLD-100, with a difference of sensitivity of 3.4% and 5.9%, respectively. On the other hand, the relative standard deviations of ECC's present values between 0.5% and 0.8% for TLD-100 and between 1.2% and 1.7% for MTS-100, indicating that the individual correction factors remain stable, that is, that the sensitivity of each detector is maintained over 10 series of uses.

#### 4.2.3.2 Stability of readings

The Figures 4.20 and 4.21 illustrate the values obtained for irradiations normalized to the first reading for the MTS-100 and TLD-100 detectors, respectively. The error bars associated with the results obtained correspond to the deviation standard of the 25 measurements made for each point.

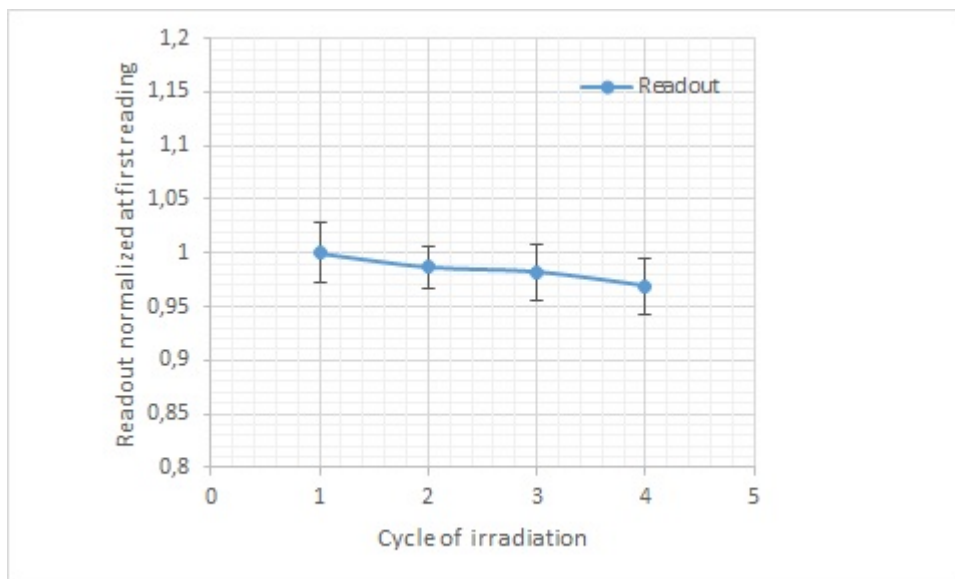


Figure 4.20: Repeatability of the MTS-100 detectors for irradiations of 1.36 Gy (Group A).

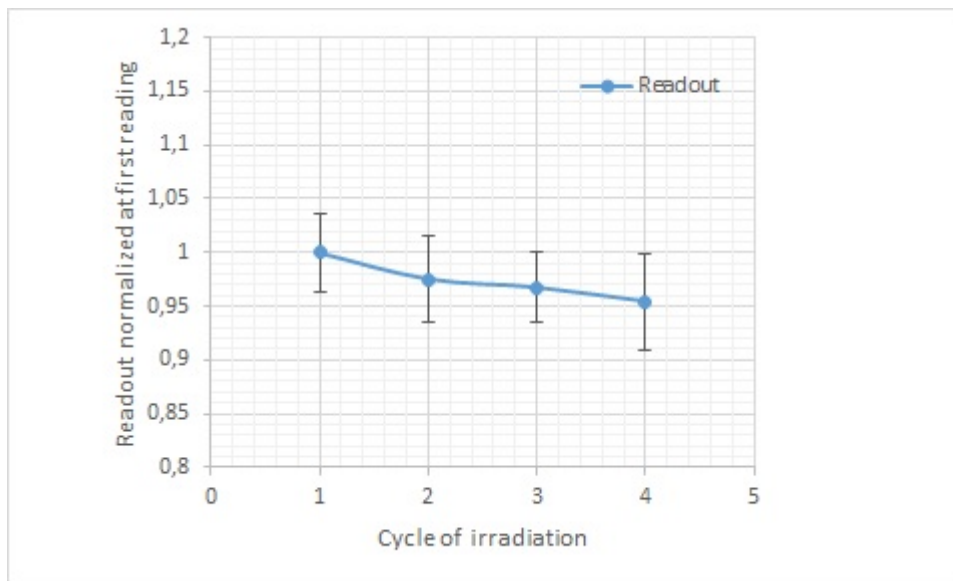


Figure 4.21: Repeatability of the TLD-100 detectors for irradiations of 1.36 Gy (Group B).

In Table 4.6, they are presented the results for MTS-100 versus TLD-100.

Table 4.6: Table of results MTS-100 versus TLD-100 - Repeatability.

	MTS-100	TLD-100
Repeatability (%)	1.1	2.8

The measurements presented in Figure 4.20 and 4.21 demonstrate that for dosimeters MTS-100 and TLD-100 a dose of 1.6 Gy does not affect the repeatability of measurements. The repeatability of MTS-100 detectors is 1.1% and of TLD-100 is 2.8%. These results demonstrate that the cycle of annealing is required so that the dosimeter is in a position to be reused and it is sufficient to ensure the integrity of the measurements taken.

So, given the fact that these sets of detectors were selected randomly, it is possible to assume that the difference in sensitivity and stability of the response observed are representative of the remaining dosimeters that constitute the batches used in the experimental work.

#### 4.2.4 Linearity

Five groups of 9 dosimeters were submitted to a cycle anneal-irradiation-readout procedure with distinct quantity of MU: 50, 100, 200, 300 and 400 MU.

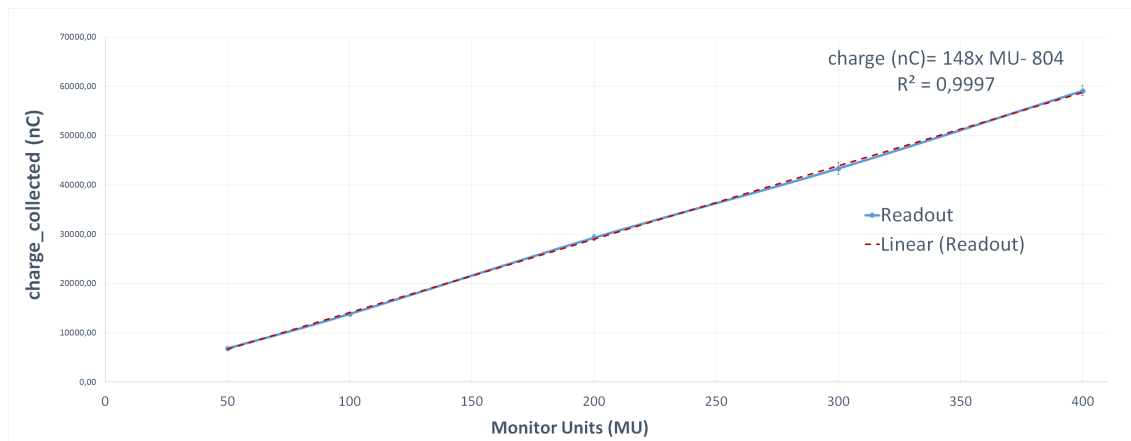


Figure 4.22: Values obtained to detectors with respective corrections and linear regression in function of quantity of MU (Group A).

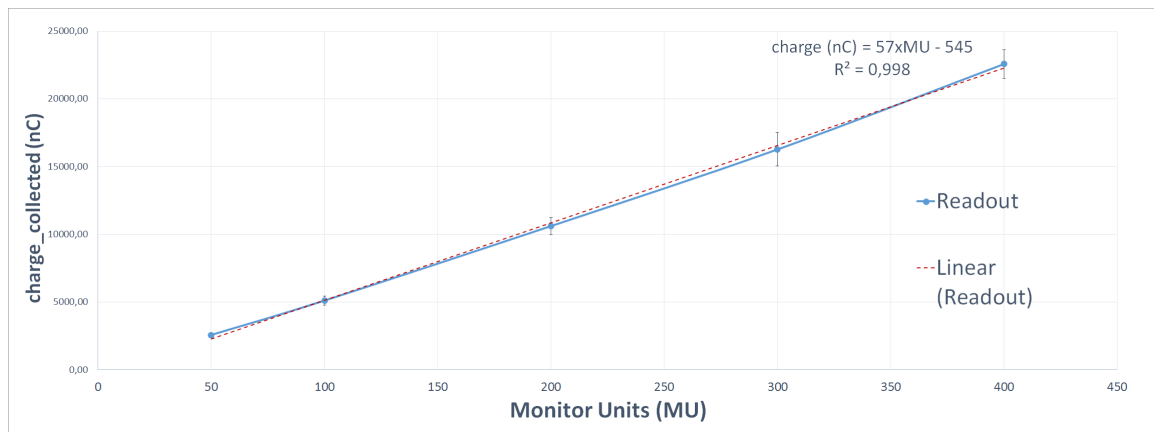


Figure 4.23: Values obtained to detectors with respective corrections and linear regression in function of quantity of MU (Group B).

The coefficient of determination, which is a statistical measurement of how well the calculated dose curve fits the measured data, obtain to group A was  $R^2 = 0.9997$  and to group B was  $R^2 = 0.998$ .

Then, leaving the linear region indicated by the manufacturer for group A, 5Gy, three other groups of 9 detectors were irradiated with 600, 800 and 1000 MU. The values obtained are presented in Figures 4.24 and 4.26.

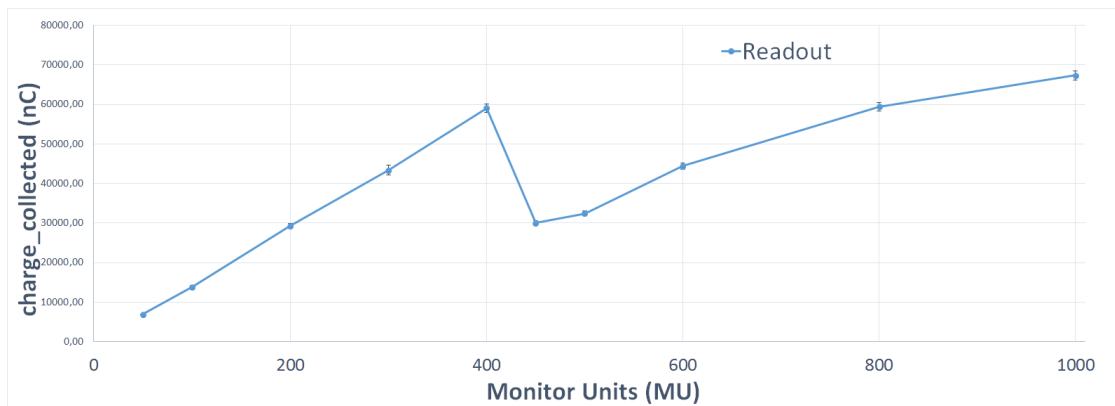


Figure 4.24: Values obtained to detectors with respective corrections and linear regression (Group A).

As can be observed, the graph of the Figure 4.24 corroborates the data provided by the manufacturer of MTS-100 until 400 MU, approximately, 2.7 Gy, but it is slightly below the expectations. After this value, the glow curve presents a completely different shape, as seen in 4.25, suggesting a permanent radiation induced damage in the crystal lattice.

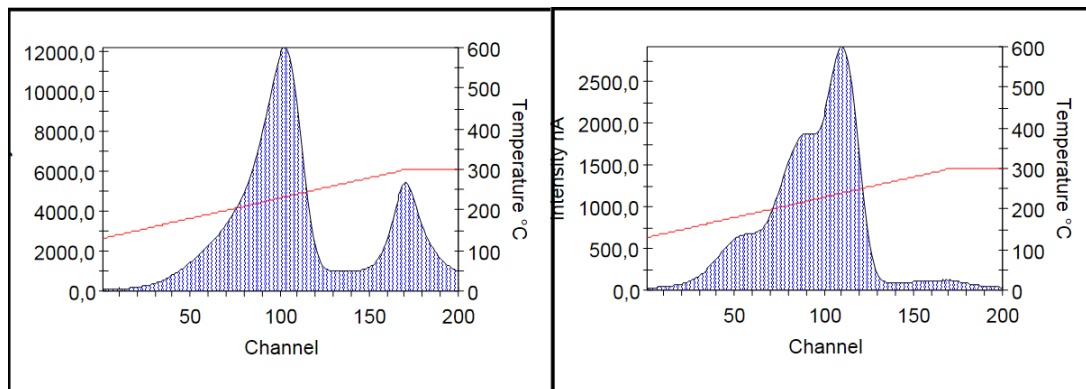


Figure 4.25: Glow curves obtain after irradiation of 800 MU versus 200 MU (Group A).

Besides the glow curve modification there was a significant sensibility decreased afterwards by approximately 50%.

On the other hand, the detectors of group B present a linear response up to 1000 MU, that is, approximately, 6.8 Gy.



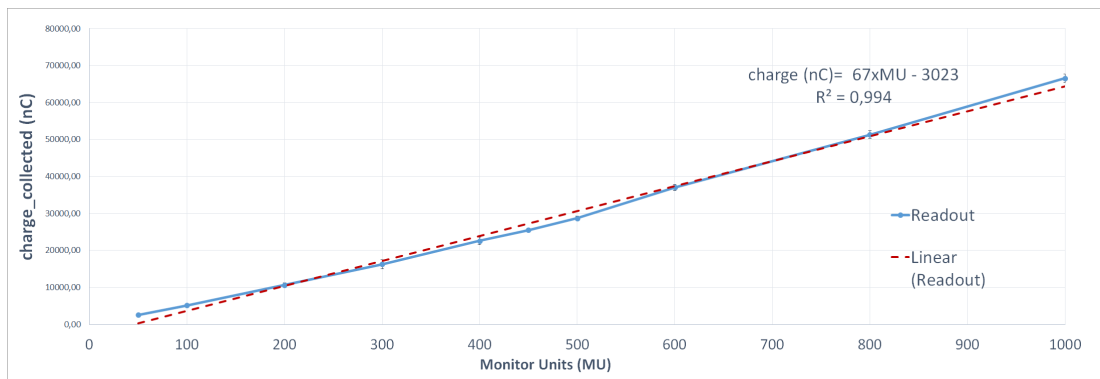


Figure 4.26: Values obtained to detectors with respective corrections and linear regression (Group B).

#### 4.2.5 Calibration curve

The interest of this work consists in using the TLD's to assess therapeutic dose distributions—e.g., in a phantom or in a real patient, then the doses of interest might be considerably higher than those of concern in routine personnel dosimetry. Indeed, the range doses might extend from less than 1 Gy to possibly beyond 10 Gy. In such instances, it must be aware of the TLDs' linearity characteristics. Many TL materials exhibit supra-linear responses beyond a few Gy, and it may be necessary to prepare a calibration curve with several measurement points that cover the dose interval of interest so that the response curve is well defined. [73]

Calibration curve determination was made by TLD's which were irradiated by different doses, between 0.34 and 2.7 Gy, for MTS-100, and between 0.34 and 6.8 Gy at the same calibration conditions. In the Figures 4.27 and 4.28 it is represented the calibration curves for both batches.

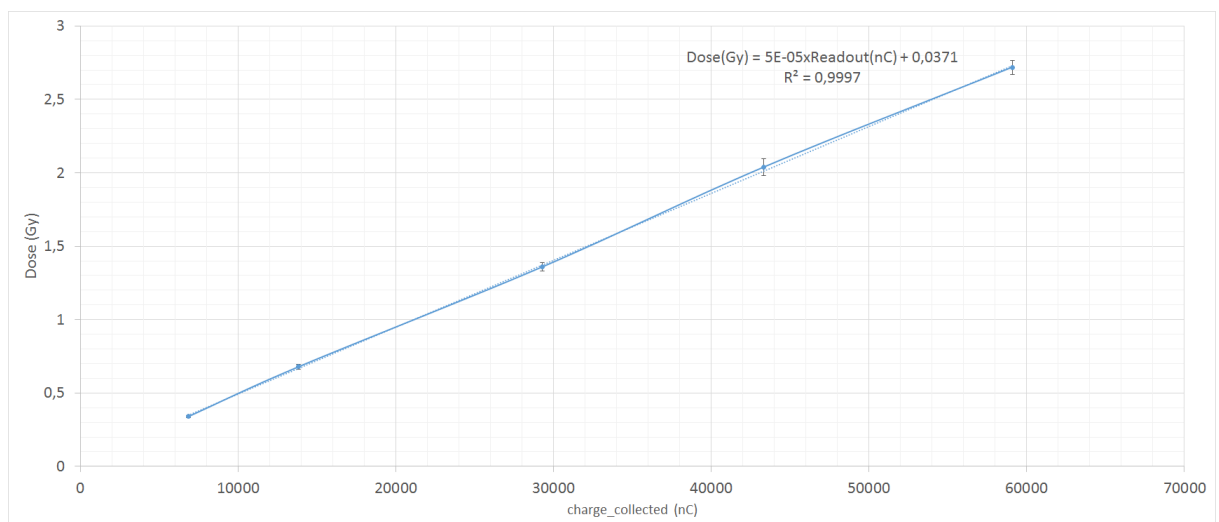


Figure 4.27: Values obtained to detectors with respective corrections and linear regression (Group A).

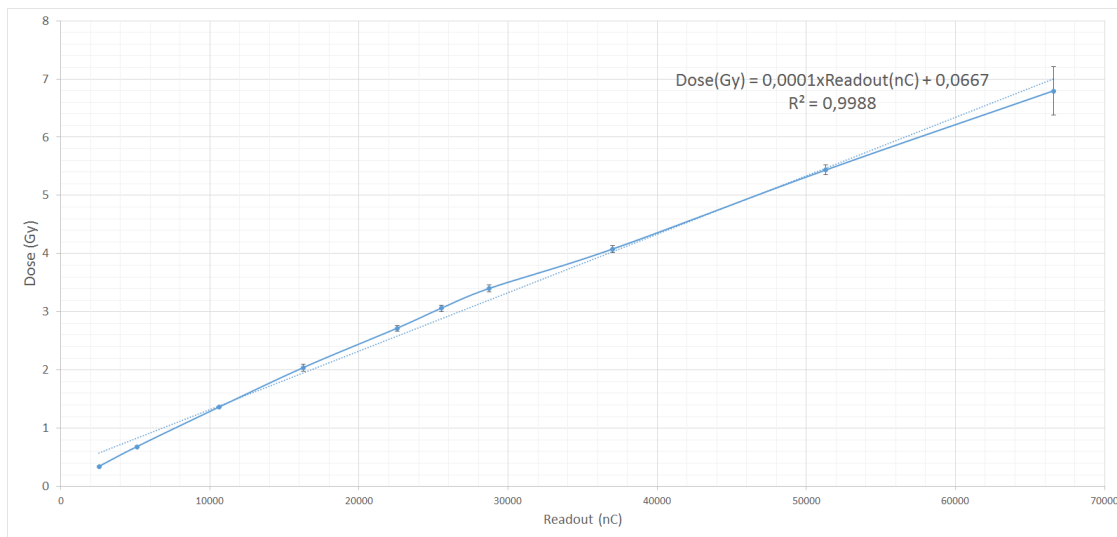


Figure 4.28: Values obtained to detectors with respective corrections and linear regression (Group B).

Therefore, each response measurement should be converted to dose by using the generated calibration curve, equation 4.7 for MTS-100 and equation 4.8 for MTS-100.

$$Dose(Gy) = 5 \times 10^{-5} \times Readout(nC) + 0.0371 \quad (4.7)$$

$$Dose(Gy) = 1 \times 10^{-5} \times Readout(nC) + 0.0667 \quad (4.8)$$

Multiple calibration curves can be used instead of using a single calibration curve over the entire dose range as a means of reducing the level of calibration uncertainty. But, since the adjustment curve obtained was the same for the two intervals more obvious to separate in batch of TLD-100 - [50;400] MU and [450;1000] MU - it is only presented an unique calibration curve.

#### 4.2.6 Energy Dependence

Considering the energies available in the linear accelerator, the values of MU to the same value the dose according with the specif paremeters is expressed in the Table 4.7.

Table 4.7: Table of specific quantity of MU for each irradiation.

Energy	Parameters	MU	Dose(Gy)	
6	PDD (%)	67.1	200	1.36
	OF	1.014		
6FFF	PDD (%)	64.2	210	1.36
	OF	1.009		
10	PDD (%)	73.9	181	1.36
	OF	1.016		
10FFF	PDD (%)	71.2	190	1.36
	OF	1.007		
15	PDD (%)	76.7	174	1.36
	OF	1.017		

Figures 4.29 and 4.30 summarizes the variation of different randomly selected groups of 9 detectors to each energy.

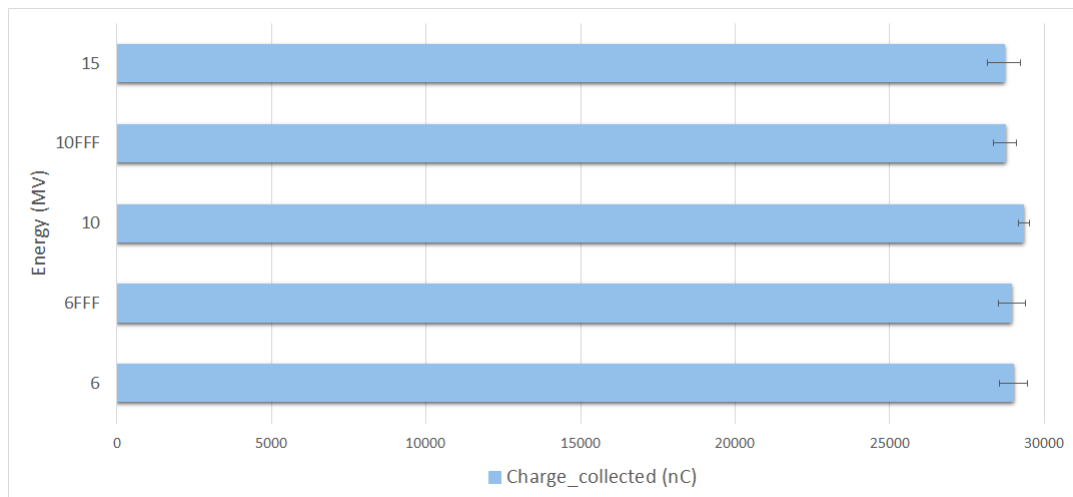


Figure 4.29: Values obtained to detectors with respective corrections (Group A).

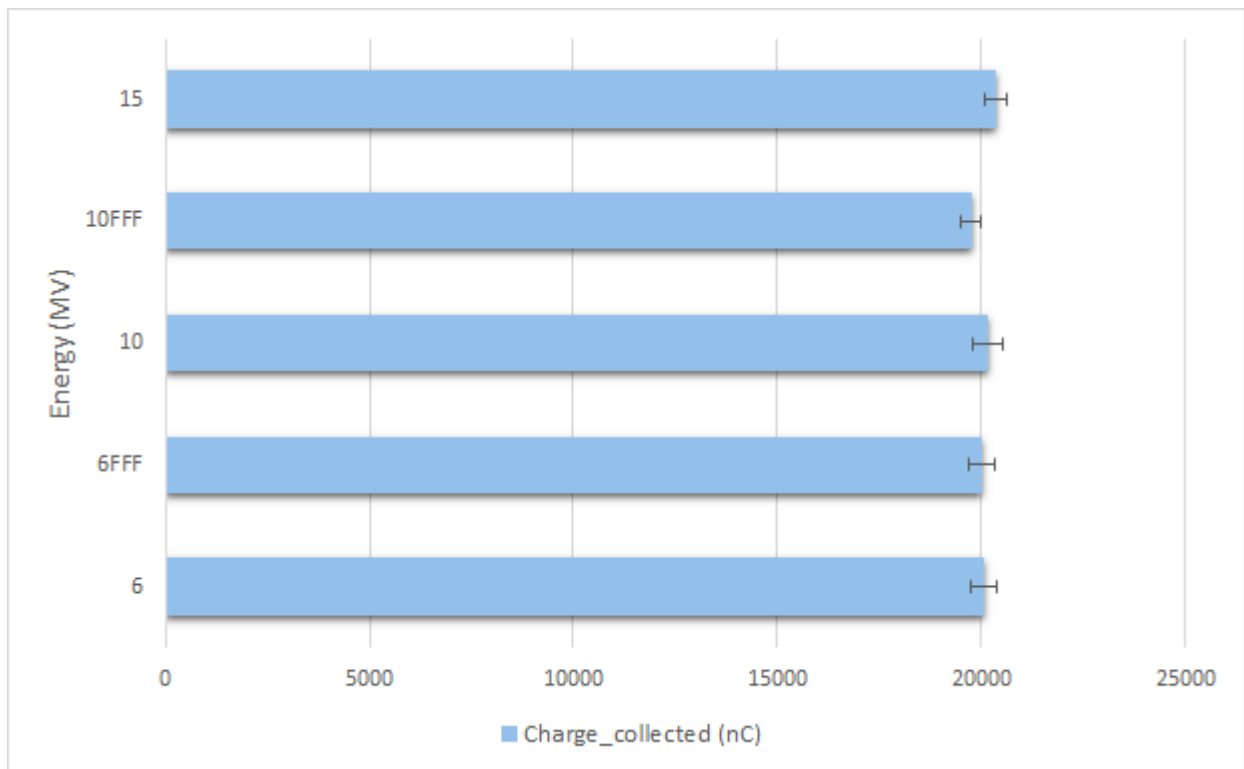


Figure 4.30: Values obtained to detectors with respective corrections (Group B).

In Table 4.8, they are presented the results for MTS-100 versus TLD-100. The reference value used for the normalization and subsequent comparison was obtained for the energy of 6 MV, one with more frequent use in EBRT, due to the increasing volume of application of special techniques such as IMRT.

Table 4.8: Table of results MTS-100 versus TLD-100.

Energy	Dose(cGy)	Deviation calculated_MU (%)	Deviation (%) Group A	Deviation (%) Group B
6	136.07	0	0	0
6FFF	136.03	-0.03	-0.2	-0.2
10	135.89	-0.13	0.9	0.4
10FFF	136.22	0.11	-0.9	-1.6
15	135.72	0.26	-1.1	1.3

Analyzing the obtained results, it is shown that all the obtained deviations are within the standard deviation obtained in the Table 4.3. Thus, it can be concluded that there is no significant energy dependence.

### 4.2.7 Estimation of Uncertainty

Uncertainty, as defined in the ISO/ASTM 51707:15 document, is the parameter obtained by measurement or calibration which, together with the measured value, marks the range of values in which the true value of the measured quantity lies. The uncertainty of measurement is the positive square root obtained from the sum of the squares of the standard uncertainties, for all uncertainty components. Besides that, the uncertainty of the result of a measurement generally consists of several components, according to [74, 75, 76], which may be grouped into two categories according to the method used to estimate their numerical values:

- (A) those which are evaluated by statistical methods;
- (B) those which are evaluated by other any means.

According to ISO/ASTM 51956:2013 a full quantitative analysis of components of uncertainty may be referred to as an uncertainty budget, and is then often presented in the form of a table. [65]

Tables 4.9 and 4.10 identify the sources of uncertainties and give estimates of their magnitudes. If a TLD system has been characterized and used in accordance with the recommended procedures, certain potential sources of uncertainty are expected to be insignificant. So, for purposes of these uncertainty analysis, where is the letter "n", the uncertainties are negligible.

Table 4.9: Budget of estimates of uncertainties for MTS-100 and TLD-100 dosimeters system utilized as individual chips.

Source of Uncertainty	MTS-100		TLD-100	
	Type A (%)	Type B (%)	Type A (%)	Type B (%)
Linac calibrated dose value	0.2	2.0	0.2	2.0
Repeatability of individual dosimeter response	0.8	2.0	1.7	2.0
Determination of calibration curve	10.0	---	11.0	---
Geometric correction - Matrix	3.0	2.0	3.0	2.0
Time between irradiation and readout: fading correction	n	n	n	n
Absorbed dose rate dependence	n	n	n	n
Directional dependence	n	n	n	n
Temperature before, during and after irradiation	n	n	n	n
Humidity dependence	n	n	n	n
Effect of size of TLD	n	n	n	n
Combined separately in quadrature	10.5	3.5	11.5	3.5
Total combined in quadrature	11.1		12.0	
Total combined X 2	22.1		24.0	

The estimation of uncertainty on Linac dose value is the standard uncertainty of the dose value obtain during daily QA on the TrueBeam STx, that are measured with a *QUICKCHECK<sup>webline</sup>* from PTW. In type B, it was considerer the maximum allowed deviation for Linac operation to occur.

Then, considering that the sets of measurements in the repeatability study were always performed under the same conditions and with the same set of dosimeters, it is reasonable to assume that the standard deviation obtained contains the uncertainties associated with the positioning of the detectors in the irradiation field and with the variations that may occur in the value obtained by the reader. In type B, it was considered the value given by manufactures.

For the determination of the uncertainty of the calibration curve, it was calculated the doses obtained by the direct calculation and then the maximum deviations were calculated.

For the geometric correction introduced, the standard deviation of the measurements obtained by the matrix, was calculated. Type B uncertainty refers to the value that is displayed in the matrix certificate provided by manufactured.

The uncertainties are assumed to be uncorrelated. They are combined in quadrature and multiplied by a coverage factor of two to provide an expanded uncertainty that corresponds approximately to a 95% level of confidence. A coverage factor is a numerical factor used as a multiplier of the combined standard uncertainty to obtain an expanded uncertainty. [68]

The total combined uncertainty for TLD-100 was 12.0% and for MTS-100 was 11.1%. The expanded uncertainty, interval about the result of a measurement that encompasses 95% of distribution of values that could reasonably be attributed to the dose, for TLD-100 was 24.0% and for MTS-100 was 22.1%.

### **4.3 Clinical Application**

The main aim of this study was to perform patient dose verification, case dose calculations were performed on phantom. TLD's were used to find out the doses and then compared with the doses calculated by TPS.

In order to test the use of the detectors in real clinical situations, avoiding prejudicial waiting and doubts to the patient, a study was made using an anthropomorphic phantom. This follows the usual procedure of patient: a planned CT was performed, a treatment plan was elaborated in TPS, it was positioned and "treated" in the LINAC in conditions similar to the real ones. It was used the anthropomorphic female phantom with breast attachment and simulated the treatment for a right breast patient. Treatment plans were used to investigate the dose distribution of the whole breast, as can be observed in Figure 4.31.



Figure 4.31: Experimental set-up of the Alderson RANDO Phantom irradiation.

The points on phantom at which the absorbed dose is measured are represented in Figure 4.32.

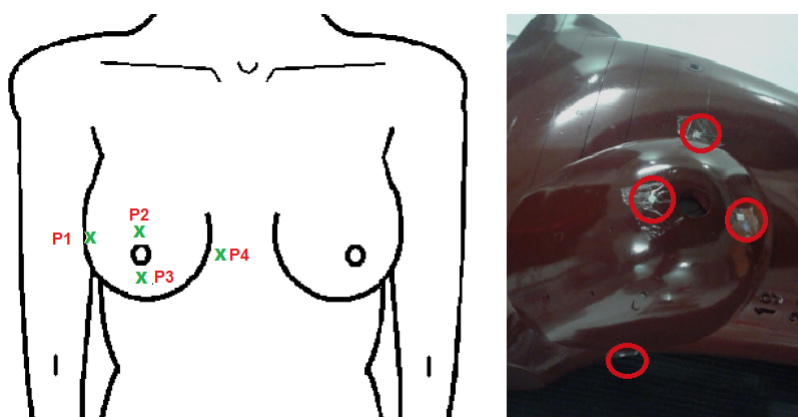


Figure 4.32: Points of measurement in Alderson RANDO Phantom irradiation a) Sketch b) Photograph.

The point dose as predicted by the TPS was compared to in vivo dose measurements at identical locations for the phantom. In Table 4.10, they are presented the results for MTS-100 versus



TLD-100, with respective deviations in % to the values calculated in TPS.

Table 4.10: Table of results MTS-100 versus TLD-100.

	MTS-100		%Deviation (TPS)	TLD-100		%Deviation (TPS)	TPS
	nC	Gy		nC	Gy		Gy
P1	8789	0.94	+2250	9880	0.53	+1228	0.04
P2	257	0.09	-70	269	0.05	-26	0.3
P3	296	0.09	-82	302	0.05	-31	0.5
P4	11686	1.2	+2900	12977	0.68	+1614	0.04

TPS algorithms are not designed nor commissioned to calculate very well dose at peripheral regions. Dose calculations from the TPS are often the only means of estimating the radiation dose reaching out-of-field locations in routine radiotherapy. However, very little data is available on the performance of these algorithms in such regions. [77]

It has been found that results don't show good agreement with the values of doses given by TPS. After some discussion with the physicist and technologist, it was verified that an error occurred in the positioning of the phantom which explains the incongruence found in the results. This means that the measurement in the phantom with TLD's allowed to notice a mistake in the positing of the fields relative to the phantom. In a real patient, this situation would be highly improbable due to other mechanisms of patient positioning that were not used in this simple demonstration.



## Chapter 5

# Conclusion and Future Work

In this chapter it will be presented the main conclusions accomplished through the realization of this work, as well as a critical analysis of the accomplishment of the goals initially established. Finally, it will be described the future work that can be still developed in this area.

### 5.1 Final considerations

The justification for *in vivo* dosimetry is mainly recommended by two important reasons: a) there is now a higher probability for treatment-related incidents due to increased complexity of planning procedures and new technologies and b) there are certain types of tumors that require a better accuracy (up to 3.5%) than 5% as recommended by ICRU Report 24 (1976). From the 4,000 near misses without adverse outcome to patients that were reported in the years from 1992 to 2007, more than 50% were related to the planning or treatment delivery stage. So, more system or equipment-related errors were reported as compared to other errors, e.g. dose prescription.

IVD is in use in EBRT to detect major errors, to assess clinically relevant differences between planned and delivered dose, to record dose received by individual patients and to fulfill legal requirements.

Then a generalized approach to dosimetry and existing dosimeters is introduced. In the final phase of the chapter, the physical processes inherent to the dosimetry systems used in the dissertation: ionization chamber and thermoluminescence detectors, are presented and a more detailed description for the TL detectors, principal object of study of this work, is explained.

After discussing briefly the essential concepts about ionizing radiation and a general theoretical framework beyond Radiotherapy, it is demonstrated the importance of quality control as well that precision and accuracy are essential in this area. Then, a novel methodology using a Octavius 1500 matrix, which allows the simultaneous irradiation of 25 TLD correcting the beam heterogeneity, was presented.

The homogeneity, repeatability, linearity, energy dependence were measured for both batches from different manufacturers and the differences in sensibility and batch heterogeneity were highlighted.

The uncertainties related to the dose assessments performed were estimated and which are around 11.1% for group A (MTS-100) and 12% for group B (TLD-100). Having in mind the overall results obtained in Chapter 4, the Radcard dosimeters would be the right choice for measuring doses below 2.5 Gy and the Harshaw dosimeters would be used for higher doses up to 6 Gy, making them a good choice for e.g. hypofractionation radiotherapy.

A Rando anthropomorphic phantom was used to compare the measured dose with the dose calculated by the treatment planning system (TPS). A positioning error was detected by this method.

In conclusion, the IVD is a technically advanced process that requires investment in special equipments, human resources and expertise. The potential benefits of IVD are a better local control rates resulting in improved disease-free survival, overall survival and quality of life. These benefits are multi-faceted and have to be viewed from several perspectives, including not only economic burden but also quality of life and disease control. So, it is desirable that, at least, all treatments with curative intent, should be verified through *in vivo* dose measurements in combination with pretreatment checks.

## 5.2 Satisfaction of Objectives

The purpose of this work was to guarantee the reliability and the accuracy indispensable in clinical *in vivo* dosimetry when applied in the patient or phantom. So, the primary objective of the work consisted in the establishment of a calibration procedure approaching the ISO 28057:2014 standard using a last generation linear accelerator and a novel beam heterogeneities correction.

The present work reached the main objective proposed, determining the feasibility of the clinical dosimetry system and establishing a protocol to achieve it. In addition, the physical characteristics of two TLD (LiF: Mg, Ti) batches from different manufactures - Radcard (MTS-100) and Thermo Scientific™ (TLD-100) were compared.

## 5.3 Future Work

Giving continuity to the theme developed in this dissertation, identified some topics that could be interesting for future work:

- Analysis of more treatment plans to confirm the validity of the method for quality control of treatments;
- Implementation of protocols of IVD in clinical practice;
- Store and analyze the dose delivered to each patient in a dose management system.

The results related to the study of the *in vivo* dose distribution in the phantom are considered preliminary results. This work represented a starting point for future work in which it is intended to obtain statistically significant results. On one hand, to optimize the determination of doses in

this type of treatment and others; on the other hand, to create a basis for recommendations of its use in clinical practice, so that the accidents can be identified, reported and minimized.



## Appendix A

# Programmable Oven

This appendix is based on the manual of Model 3204 Process Controller, Part No HA02865\_15, Date December 2015, it can be considered a condensate of the information needed for this work. [78]

The 3200 series provide precise temperature control of industrial processes and is available in three sizes. The model that is installed in laboratory of IPO-Porto is 1/16 DIN Model Number 3216.

### A.1 Front Panel

A front view of the controller is shown in figure A.1 below together with overall dimensions.

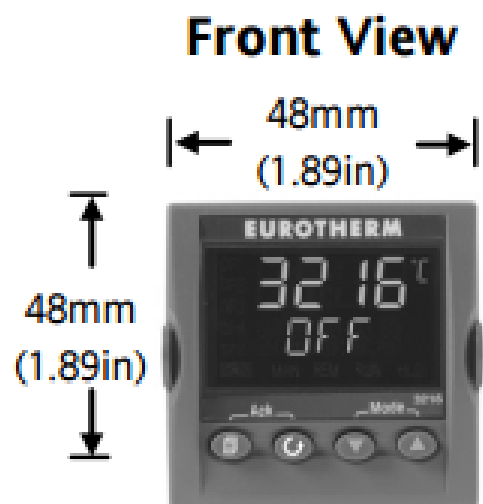






Figure A.1: Front view of the controller. [78]

Front Panel Layout is composed by beacons and operator buttons. Table A.1 summarizes them and their respective functionalities.

Table A.1: Beacons, operator buttons and their respective functionalities of the front panel.

Beacon	Functionality
ALM	Alarm active (Red)
OP1	Lit when output 1 is ON (normally heating)
OP2	Lit when output 2 is ON (normally cooling )
OP3	Lit when output 3 is ON
OP4	Lit when output 4 relay is ON (normally alarm)
Operator Buttons	Functionality
1- 	From any view - press to return to the HOME display
2- 	Press to select a new parameter. If held down it will continuously scroll through parameters
3- 	Press to decrease a value
4- 	Press to increase a value

## A.2 Commands

Initially, if the controller is not new, it can be necessary to re-enter the 'Quick Configuration' mode. This is a built-in tool which enables the user to configure the input type and range, the output functions and the display format. Two 'SETS' of five characters define a quick start code. The upper section of the display shows the set selected, the lower section shows the five digits which make up the set.



Figure A.2: The upper section of the display shows the set selected, the lower section shows the five digits which make up the set.

To chose the five characters there are two tables in the manual:

- Set 1-page 19;
- Set 2-page 20.

Definition of this sets can be done as follows:



1. Power down the controller;
2. Hold down the first button, number 1, and power up the controller again;
3. Keep the button pressed until CODE is display;
4. Enter the configuration code;
5. The quick start codes may then be set as described: a. Press any button. The characters will change to ‘-’, the first one flashing; b. Press or to change the flashing character to the required code shown in the quick code tables – see below. Note: An x indicates that the option is not fitted; c. Press to scroll to the next character.
6. When all five characters have been configured the display will go to Set 2;
7. When the last digit has been entered press again bottom 2, the display will show "**NO EXIT**";
8. Press bottom 3 or 4 to "**YES EXIT**".

The controller will then automatically go to the operator level. To enter Level 2 it is necessary to follow the next steps.

1. From any display press and hold bottom 1;
2. After a few seconds the display will show "**LEV 1 GOTO**";
3. Release bottom 1. (If no button is pressed for about 45 seconds the display returns to the HOME display);
4. Press bottom 3 or 2 to choose Lev 2 (Level 2);
5. After 2 seconds the display will show "**0 CODE**";
6. Press bottom 3 or 4 to enter the pass code. Default = ‘2’.

To select the list of parameters available in Level 2 there are a number of commands to follow by the next order:

1. Press bottom 2 to step through the list of parameters. The mnemonic of the parameter is shown in the lower display;
2. After five seconds a scrolling text description of the parameter appears;
3. The value of the parameter is shown in the upper display;
4. Press bottom 3 or 4 to adjust this value. If no key is pressed for 30 seconds the controller returns to the HOME display,

5. Back scroll is achieved when you are in this list by pressing bottom 4 while holding down bottom 2;
6. Press bottom 1 at any time to return immediately to the HOME screen at the top of the list.

To know the list of parameters available in Level 2 there are tables in the manual - page 24 to 26.

### A.2.1 Programmer - 'TM.CFG' = 'ProG'

This section describes how to operate the programmer and to set up a temperature profile. This can be done in Operator Level 2.

A programmer is generally used to control the rate of change of the process variable (PV) over several segments. The PV is generally temperature and this will be referred to in the following example in Figure A.3.

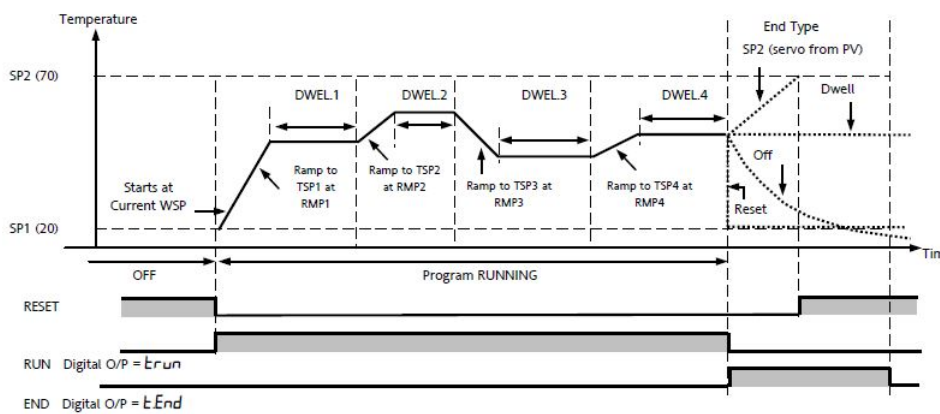


Figure A.3: An example of a program profile. Each ramp consists of a controlled rate of change of setpoint to a target level. Each ramp is followed by a dwell at that level. The ramp rate, target level and dwell time are set by the user. [78]







To set up a temperature profile repeat the steps described in Table A.2 for all segments.

Table A.2: To Set Up a Temperature Profile. [78]

Operation	Action	Indication	Notes												
Set up the Timer as a Programmer	Press  to select 'TM.CFG' Press  or  to 'PrOg'														
Set the Resolution	Press  to select 'TM.RES' Press  or  to 'Hour' or 'm n'		Resolution defines how the Dwell time is displayed. It does not set the dwell or ramp rate. Ramp Rate must be set in Level 3 or Configuration level by the 'RampUnits' parameter found in the 'SP' List, see section 10.1.												
Set the Threshold	Press  to select 'THRES' Press  or  to adjust		Threshold prevents a dwell period from starting until the process value (PV) is within the threshold value. In this example the dwell periods will not start until the PV is within 5 units of the setpoint												
Set the action to be taken at the end of the profile.	Press  to select 'END.T' Press  or  to 'OFF', 'SP2', 'dWELL' or 'rSt'		<b>OFF</b> will turn the output power off and allow the temperature to cool naturally. <b>SP2</b> the controller will continue to control at the value set by setpoint 2. <b>Reset</b> will return control to the selected setpoint. <b>Dwell</b> the controller will continue to control indefinitely at the last target setpoint.												
Set the Servo Mode	Press  to select 'SERVO' Press  or  to 'PU', 'SP', 'SPrb', or 'PURb'		In this example the program will start from the current value of the PV (temperature). See the following section for further details.												
Set the first Target Setpoint	Press  to select 'TSP.1' Press  or  to adjust		In this example the setpoint will ramp from the current value of the PV to the first target - 100												
Set the first Ramp Rate	Press  to select 'RMP.1' Press  or  to adjust		In this example the setpoint will ramp to 100 at 8.0 units per second per minute or per hour as set by the 'RampUnits' parameter in the Setpoint (SP) List, section 10.1.												
Set the first Dwell	Press  to select 'DWEL.1' Press  or  to adjust		In this example the setpoint will remain at the TSP1 value for 2 hours 11 minutes. For dwell periods greater than 1 hour, the 'Resolution' value above must be set in Hours. If it is set in minutes it cannot display more than 60 minutes. Examples of the display are shown below: <table border="1" style="width: 100%; border-collapse: collapse;"> <tr> <td style="width: 50%; padding: 2px;">Resolution set in Hour</td> <td style="width: 50%; padding: 2px;">Resolution set in m n</td> </tr> <tr> <td style="padding: 2px;">1 hour = 1:00</td> <td style="padding: 2px;">1 hour = 60:00</td> </tr> <tr> <td style="padding: 2px;">10 hours = 10:00</td> <td style="padding: 2px;">10 hours = cannot be set</td> </tr> <tr> <td style="padding: 2px;">1 min = 0:01</td> <td style="padding: 2px;">1 min = 1:00</td> </tr> <tr> <td style="padding: 2px;">1 sec = OFF</td> <td style="padding: 2px;">1 sec = 0:01</td> </tr> <tr> <td></td> <td style="padding: 2px;">1 hr:39m:59s = 99:59</td> </tr> </table>	Resolution set in Hour	Resolution set in m n	1 hour = 1:00	1 hour = 60:00	10 hours = 10:00	10 hours = cannot be set	1 min = 0:01	1 min = 1:00	1 sec = OFF	1 sec = 0:01		1 hr:39m:59s = 99:59
Resolution set in Hour	Resolution set in m n														
1 hour = 1:00	1 hour = 60:00														
10 hours = 10:00	10 hours = cannot be set														
1 min = 0:01	1 min = 1:00														
1 sec = OFF	1 sec = 0:01														
	1 hr:39m:59s = 99:59														

Finally, to operate the programmer follow the indications specified in Figure A.3 after turn on the oven and switch off the bottom Reset.

Table A.3: Operations with respective indications and actions. [78]

Operation	Action	Indication
To Run a program	Press and quickly release  + 	Beacon -- RUN = On Scrolling display - TIMER RUNNING
To Hold a program	Press and quickly release  + 	Beacon -- RUN = Flashing Scrolling display - TIMER HOLD
To Reset a program	Press and hold  +  for more than 1 second	Beacon -- RUN = Off If End Type = Off then OFF will be displayed at the end of the program
	Program ended	Beacon -- RUN = Off SPX = On if End Type = SP2 Scrolling display - TIMER END
Repeat the above to Run the programmer again (Note: it is not essential to reset it after the End state is reached)		

## **Appendix B**

# **The operational software, Thermo Scientific™ WinREMS™**

The readout system consists of two major components: the TLD Reader and the Windows Radiation Evaluation and Management System (WinREMS) software resident on a personal computer (PC), which is connected to the Reader via a serial communications port. So, this appendix is based on the manual of THERMO FISHER SCIENTIFIC ISO 9001 Quality System Certified Model 3500 Manual TLD Reader With WinREMS™ Operator's Manual Publication No. 3500-W-O-1110-006, Release Date: November 30, 2010 and it pretend to be considered a condensate of the essential information for this dissertation. [79]

### **B.1 Initial Operation**

This appendix is a guide through the initial operation of the system WinREMS™.

#### **B.1.1 Power-up**

Turn on the Reader and the PC. A WinREMS icon will appear on desktop of the computer connected to the reader, allowing direct access to the WinREMS System. Double click on the WinREMS icon.

#### **B.1.2 Initiate Workspace**

To create a new workspace, from the Main Menu click on File, New Workspace, and follow the instructions on the New Workspace Wizard show in Figures [B.1](#) to [B.5](#).

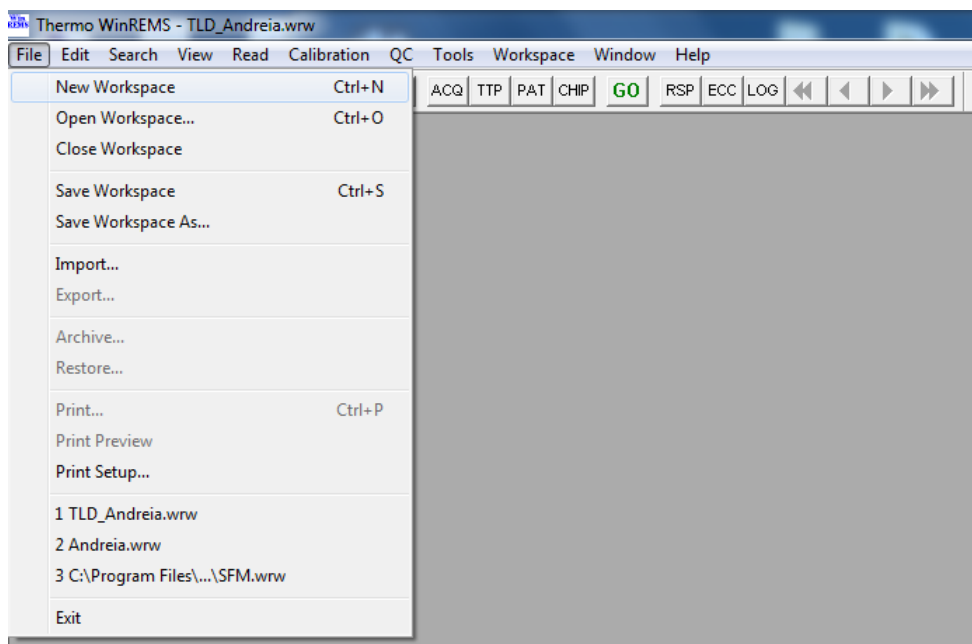


Figure B.1: Main Menu.



Figure B.2: New Workspace Wizard into view - step 1.

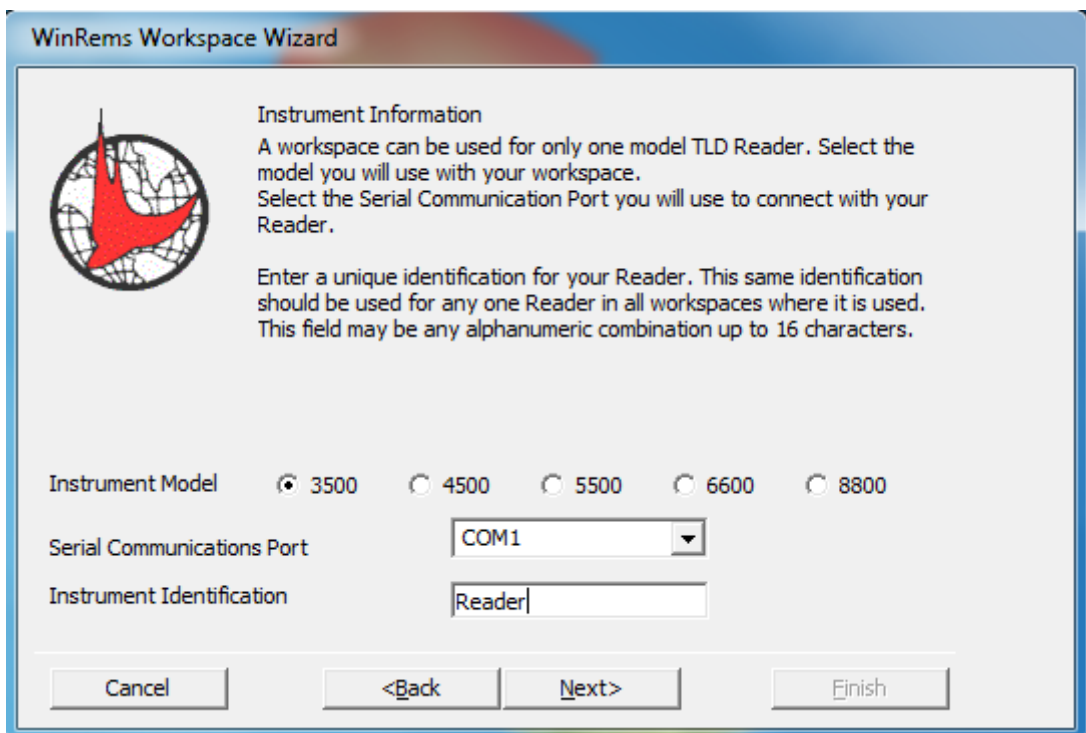


Figure B.3: New Workspace Wizard into view - step 2.

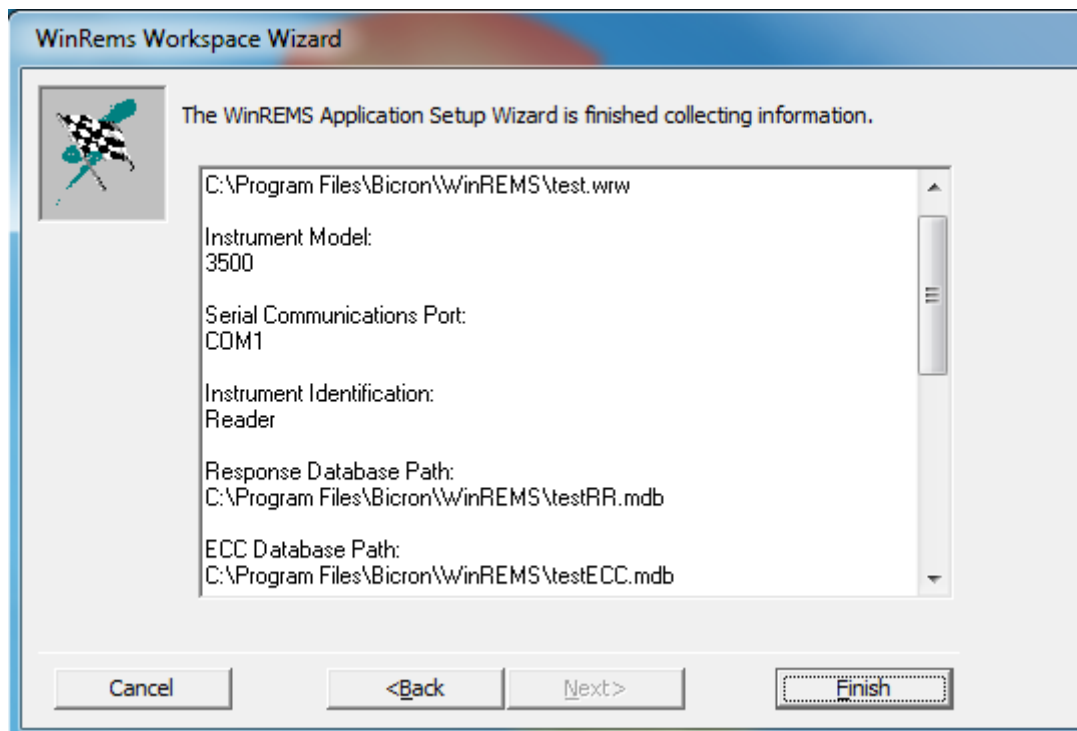


Figure B.4: New Workspace Wizard into view - step 3.

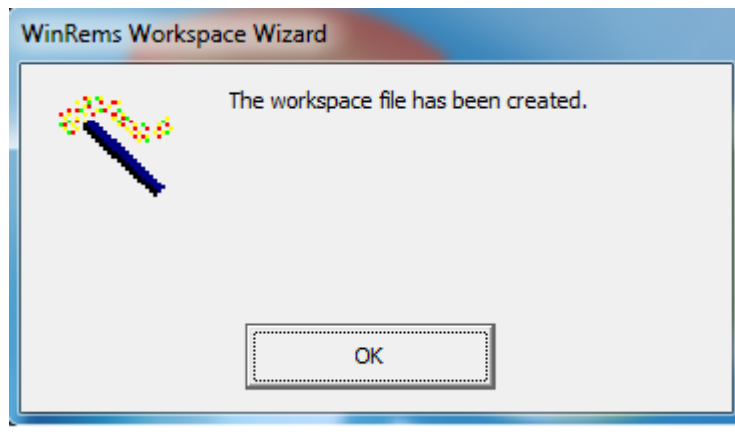


Figure B.5: New Workspace Wizard into view - step 4.

Then, to open the workspace in the Main Menu will appear with only three items on it. Click on File, Open Workspace to view the Open Workspace Dialog Box. If a file name appears with a .WRW extension, this is a workspace; click on it to open the workspace

### B.1.3 Time Temperature Profile Setup

From the WinREMS Main Menu, select Read, TTP Setup, or click on the TTP Button on the toolbar. This will bring the Enter Password Dialog Box into view (Figure B.6).

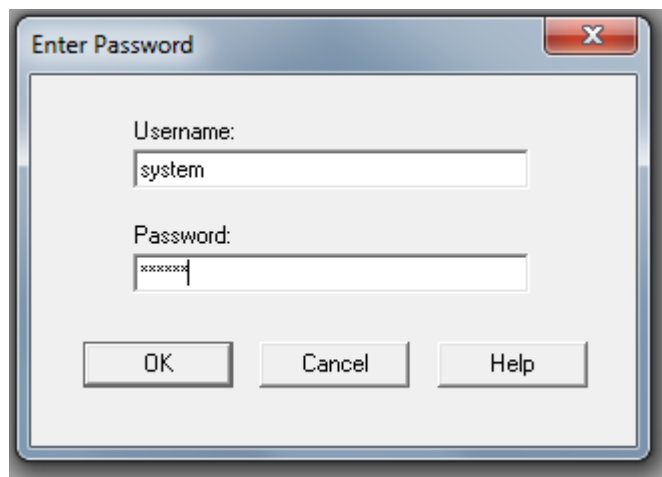


Figure B.6: Password Dialog Box into view.

Entering a valid User Name and Password will allow the access to the Time Temperature Profile Setup Dialog Box in edit mode view (Figure 3.15).

This dialog box enables the modification of the TTP parameters and the fields in this group box identify the current TTP. The TTP is the time-based profile of the temperature to which the planchet is heated during a read cycle. The settings in this box will determine how long and to what temperature the dosimeters will be heated.



The TTP has three segments: Preheat, Acquire, and Anneal. Preheat is used to eliminate the more rapidly fading low temperature peaks of the glow curve to ensure more consistent readings. Acquire is the portion of the cycle during which the PMT is actively reading the light emitted from the TLD's, collecting the 200 data points and generating the glow curve. Anneal is used to extend the time of heating without acquiring data, to ensure that the entire TL signal is removed from the material.

### B.1.4 Acquisition Setup

From the WinREMS Main Menu, select Read, Acquisition Setup, or click on the ACQ Button on the tool bar. This will bring the Enter Password Dialog Box into view. Entering a valid User Name and Password will allow you access to the Acquisition Setup Dialog Box in edit mode (Figure B.7).

The screenshot shows the 'Acquisition Setup' dialog box with the following fields and options:

- Setup Info:** Title: adquirir, Mode: Read Dosimeters, Date Edited: 25-05-2017, Edited by: system.
- Apply Factors:** RCF, ECC, Background, Quality (all unchecked).
- Export:** Format: Text File, File Path: C:\Users\sinf\Desktop.
- Print:** Format: Glow Curves.
- PMT Noise:** Interval: 10, Range: [ 1 , 400 ] pC.
- Reference Light:** Interval: 10, Range: [ 1 , 1500 ] nC.
- Limits:** If reading (in response units) exceeds:
  - 999999 . halt instrument
  - 999999 . reread dosimeter
  - 999999 . mark with warning flag
- Current Setup:** New, Delete, Copy, Paste buttons.
- Buttons:** OK, Cancel, Help.

Figure B.7: Acquisition Setup Dialog Box in edit mode view.

The fields in the box "Export" enable the exportation of a data file in ASCII format as data is being acquired. It is possible to print the results data as it is generated, clicking on the arrow to view the selections, which are: 'None', 'Glow Curves', 'Regions of Interest' and 'Computed Exposure.'

PMT Noise and Reference Light are two groups of Fields for the purpose of checking the consistency and accuracy of the readings. Each type of reading has an Interval and a Range. The Interval Field sets the number of dosimeters that will be read between a successive PMT or Reference Light readings. The system will also take a PMT Noise and a Reference Light Reading at the beginning and end of each group of dosimeters, as defined by the Group ID. The Range Field sets the range of acceptable values for the reading. If a reading falls outside of this range, the reader sends a warning message to the screen. The PMT Noise, or Dark Current, is a reading taken with no dosimeter or any other light source under the PMT Assembly. Its purpose is to measure electronic noise in the system and determine if there are any light leaks in the system. The Ref Light reading is taken with the Reference Light directly in view of the PMTs. This light provides a consistent light source to detect any drift in the system or accumulation of dirt on the PMT Lenses. A setting of '0' in either the PMT Noise or Ref Light Interval Field will result in the system not taking any readings of that type. For following the tutorial of the Manual, it should be enter 10 in both Interval Fields.

The parameters in the group box Reading "Limits" define three actions that can be taken at unusually high reading levels. How the set of these is chosen will depend on the level of readings anticipated.

Finally, to record the information it is necessary to click on the OK Button.

## **B.2 Reading TL Materials**

The following is the procedure used to read a TL element.

### **B.2.1 Start Reader**

First, the Reader has to be turned on with nitrogen flowing for 30 minutes to bring the PMT temperature down to its operating level. Second, the Read Dosimeters Dialog Box has to be edit from the Main Menu, then the next step is the selection of Read, Start, or click on the GO Button on the tool bar. This will bring up the Read Dosimeters Dialog Box (Figure B.8) with the Response Screen in the background.

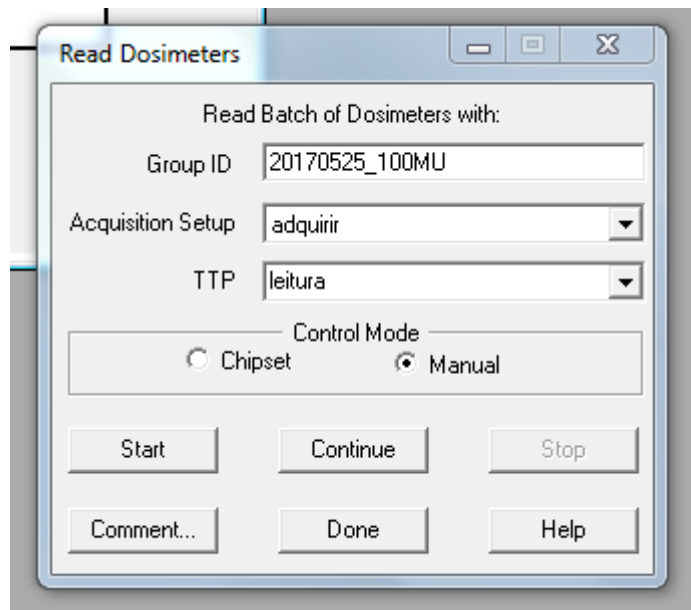


Figure B.8: Read Dosimeters Dialog Box.

Enter a Group ID. This may be up to sixteen characters (ASCII letters, numbers, or the underscore character) that will be a name that will uniquely identify the group of readings that will be produced. In this work, the identification chosen was the date of irradiation and the quantity of MU delivered to the group of dosimeters. Select the Acquisition Setup created in Sub-chapter B.1.4 by clicking on the arrow to view the list of available setup profiles.

The Control Mode box offers two choices for how to control the Reader. In Chipset Mode, the dosimeter ID and the TTP are determined from the Chipset File. In the Manual Mode, no Chipset File is used, and it is necessary to enter the Dosimeter ID and TTP manually as observed in Figure B.9 .

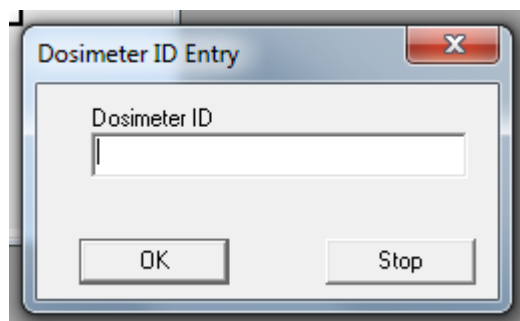


Figure B.9: Read Dosimeters Dialog Box - Dosimeter ID Entry.

During this work, the Dosimeter ID was the number attributed to each detector.

## B.2.2 Start Reader Process

The initialization of the Read process happens before the click on the Start Button, the plot area of the computer screen will clear and the Read Dosimeters Dialog Box will automatically minimize.

### B.2.2.1 Take PMT and Reference Light Readings

A message box will appear with the message “Perform PMT noise reading” (Figure B.10). To take a PMT Noise Reading, the Drawer has to be pulled and opened until the Drawer Field on the screen (near the bottom left corner) displays ‘between’. Note that this message will remain until the Drawer is almost all the way out; however, for good PMT Noise readings, the Drawer should be in far enough that the Planchet is not visible. The next step is to press the READ Button on the Reader.

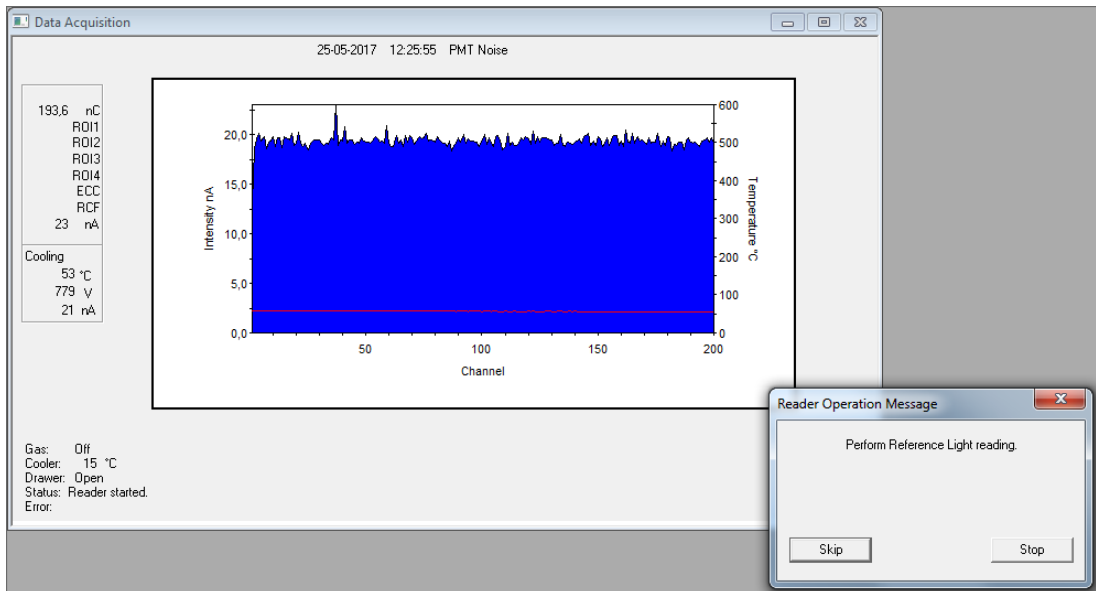


Figure B.10: Data Acquisition Dialog Box - PMT Noise Reading.

After the PMT Noise Reading is complete, a message box will appear reminding the user to take a Reference Light Reading. The Drawer was to be pulled all the way out so the Drawer Field reads 'Open'. This is the position for the Reference Light Reading. Lastly, the final step is to press the READ Button on the front of the Reader.

### B.2.2.2 Read a Dosimeter

Place a TL detector in the recess in the planchet and close the Sample Drawer. Press the READ Button to start the TL data acquisition. The glow curve will be plotted on the screen as it is acquired. When the cycle has been completed, the curve on the computer screen will be re plotted to full scale, and the numeric results will appear on the left side of the screen. The screen will look similar to that shown in Figure B.11.

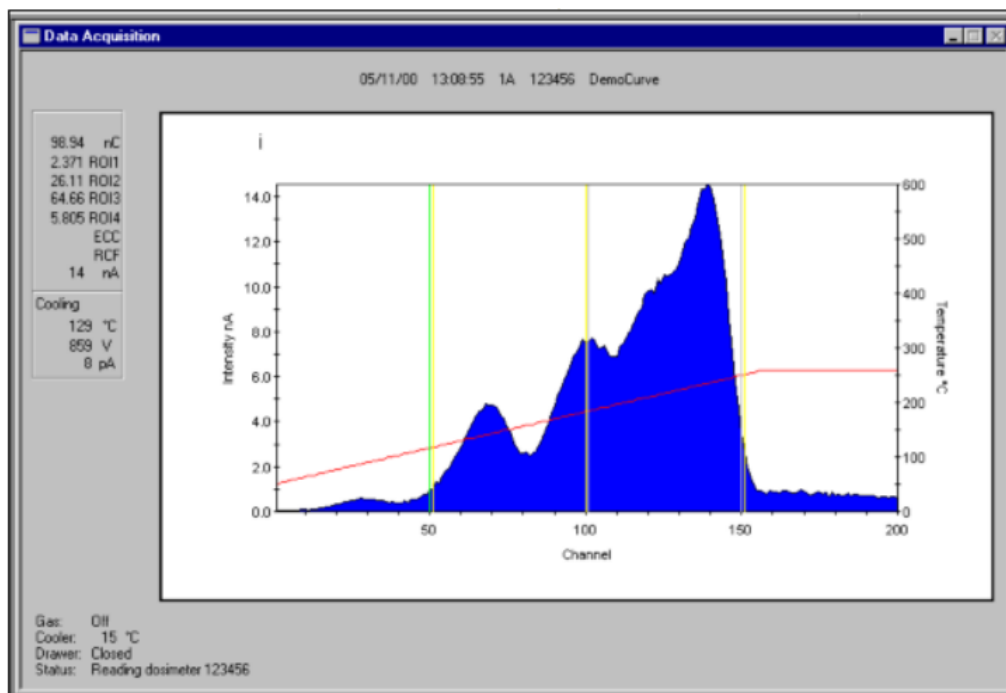


Figure B.11: Results Screen Dialog Box - Glow Curve.

The results screen displays the results of the TLD Reading as it is being generated. The center portion of the screen displays the full glow curve in solid blue, with a red line to indicate the temperature of each point. If Regions of Interest have been defined, they are identified by color-coded vertical lines. Above the glow curve area is a line of information about the dosimeter record (examples from Figure 3-1): Date and time of the reading (05/11/00 13:08:55); TTP Number (1); Acquisition Mode (A); Dosimeter ID (123456); and Group ID (DemoCurve). In a box to the left of the curve, the dosimetric information is displayed. The first value is the total integral (98.94) expressed in the units generated by the RCF, if applied. If no RCF was applied, the integral is expressed in nanoCoulombs (nC). If the ECC, Quality Factor, or Background were applied in the Reading, they will also be incorporated in the total integral. Immediately below the total integral are the integrals for as many Regions of Interest (ROI) as were selected (2.371, etc), expressed in the same units as the total integral. Immediately below the ROIs are the ECC and RCF values if they were applied. The next line shows the Intensity of the peak channel in nanoAmperes (14).

The last four lines in the lower box show the status of four reading parameters: TTP Phase (Cooling), Gas Temperature (129), High Voltage (85), and Current in the last channel read (8).

Instrument status information is displayed in the bottom left corner: Gas flow status (Off), Cooler Temperature (15° C), Drawer position (closed), Status (Reading Dosimeter 123456).

### B.2.2.3 Continue Readings

After a reading is completed, a message box will appear with the message “Instrument is cooling.” When the planchet temperature drops to the higher of 50 °C or to the preheat temperature, the

message box will disappear.

**NOTE:** It is important to wait until the message box disappears for the following reasons:

1. To avoid burning/injuring the operator;
2. To prevent putting the next chip on a hot planchet, which would remove a portion of the glow curve;
3. Pressing the READ button before the temperature is below the required level will result in an error condition and a warning message.

You may then pull the Drawer out and remove the to continue reading TL samples, repeat steps described in Subsub-chapters [B.2.2.2](#) and [B.2.2.3](#). If the message "Please read PMT noise and Test Light now" appears, return to steps described in Subsub-chapter [B.2.2.1](#).

### **B.2.3 Complete Read Process**

After taking these readings, it is necessary to bring up the Read Dosimeters Dialog Box and Click on the Done Button to complete the read process.

# References

- [1] ISO/TC 85/SC 2 Radiological Protection. ISO 28057:2014 - Dosimetry with solid thermoluminescence detectors for photon and electron radiations in radiotherapy. Technical report, 2014.
- [2] J. Alves. *Estudo do LiF:Mg, Cu, P (GR-200) e do LiF:Mg, Ti (TLD- E, 100) no Domínio das Baixas Doses de Radiação Gama: Estabilidade Térmica Limites de Detecção*. PhD thesis, Universidade Nova de Lisboa, 1999.
- [3] The American Cancer Society medical and editorial content team. Glossary: Definitions & Phonetic Pronunciations, 2015. URL: <https://www.cancer.org/cancer/glossary.html>.
- [4] F. Ferlay J, Soerjomataram I, Ervik M, Dikshit R, Eser S, Mathers C, Rebelo M, Parkin DM, Forman D, Bray. GLOBOCAN 2012 v1.0,Cancer Incidence and Mortality Worldwide: IARC CancerBase No. 11, 2013. URL: <http://globocan.iarc.fr/Default.aspx>.
- [5] WHO. Global status report on noncommunicable diseases 2014. Technical report, 2014. URL: [www.who.int/nmh/publications/ncd-status-report-2014/en/](http://www.who.int/nmh/publications/ncd-status-report-2014/en/), arXiv:9789241564854, doi:ISBN9789241564854.
- [6] IAEA. Radiation Protection and Safety of Radiation Sources: International Basic Safety Standards (GSR Part 3). *International Atomic Energy Agency Vienna*, 3:471, 2014. URL: [http://www-pub.iaea.org/MTCD/Publications/PDF/Pub1578\\_{\\_}web-57265295.pdf](http://www-pub.iaea.org/MTCD/Publications/PDF/Pub1578_{_}web-57265295.pdf){%}0Ahttp://www-pub.iaea.org/MTCD/publications/PDF/Pub1578\_{\_}web-57265295.pdf, doi:STI/PUB/1578.
- [7] Dr. Howard Markel. Science Diction: How 'X-Ray' Got Its 'X'. URL: <http://www.npr.org/templates/story/story.php?storyId=127932774>.
- [8] ICRP 30. Prevention of Accidents to Patients Undergoing Radiation Therapy - ICRP Publication 86. Technical report, 2000.
- [9] Ben Mijnheer, Sam Beddar, Joanna Izewska, Chester Reft, Sam Beddar, and Joanna Izewska. In vivo dosimetry in external beam radiotherapy In vivo dosimetry in external beam radiotherapy. 070903:1–19, 2013. URL: <https://www.ncbi.nlm.nih.gov/pubmed/23822404>, doi:10.1118/1.4811216.
- [10] J. NOVOTNY. Accidents in radiotherapy: lack of quality assurance? URL: [http://www.iaea.org/inis/collection/NCLCollectionStore/{\\_}Public/29/029/29029219.pdf](http://www.iaea.org/inis/collection/NCLCollectionStore/{_}Public/29/029/29029219.pdf).
- [11] Alireza Shirazi Mahdi Sadeghi, Milad Enferadi. External and internal radiation therapy: Past and future directions. *Journal of Cancer Research and Therapeutics*, 6(3):239–248, 2010.

- [12] World Health Organization: WHO. Media centre - Cancer, 2017. URL: <https://www.iarc.fr/en/about/index.php>.
- [13] World Health Organization. Chapter 1: Burden : mortality , morbidity and risk factors. Technical report, 2011. doi:ISBN9789240686458.
- [14] R Baskar, K A Lee, R Yeo, and K W Yeoh. Cancer and radiation therapy: current advances and future directions. *Int J Med Sci*, 9(3):193–199, 2012. URL: <https://www.ncbi.nlm.nih.gov/pubmed/22408567>, doi:10.7150/ijms.3635.
- [15] Juliette Thariat, Jean-Michel Hannoun-Levi, Arthur Sun Myint, Te Vuong, and Jean-Pierre Gerard. Past, present, and future of radiotherapy for the benefit of patients. *Nat Rev Clin Oncol*, 10(1):52–60, 2013. doi:10.1038/nrclinonc.2012.203.
- [16] ICRU. ICRU - Prescribing, Recording and Reporting Photon Beam Therapy - Report 50. Technical report, 1993. URL: <https://icru.org/link-index>.
- [17] Cristiane Barsanelli. *Métodos para implementação da dosimetria in vivo (dose de entrada) com dosímetros termoluminescentes na radioterapia externa com feixe de fóton*. PhD thesis, Universidade de São Paulo, 2006. URL: <http://www.teses.usp.br/teses/disponiveis/85/85131/tde-03052012-103720/pt-br.php>, doi:10.11606/D.85.2006.tde-03052012-103720.
- [18] Søren M Bentzen. Preventing or reducing late side effects of radiation therapy : radiobiology meets molecular pathology. 6(September):702–713, 2006. URL: <https://www.ncbi.nlm.nih.gov/pubmed/16929324>, doi:10.1038/nrc1950.
- [19] Rajamanickam Baskar, Jiawen Dai, Nei Wenlong, Richard Yeo, and Kheng-Wei Yeoh. Biological response of cancer cells to radiation treatment. *Frontiers in molecular biosciences*, 1(November):4, 2014. URL: <https://www.ncbi.nlm.nih.gov/pmc/articles/PMC4429645/>, doi:10.3389/fmolb.2014.00024.
- [20] Omar Desouky, Nan Ding, and Guangming Zhou. Targeted and non-targeted effects of ionizing radiation. *Journal of Radiation Research and Applied Sciences*, 8(2):247–254, 2015. URL: <http://www.sciencedirect.com/science/article/pii/S1687850715000333>, doi:10.1016/j.jrras.2015.03.003.
- [21] Y Asumasa N Ishimura, A Kihiro N Akai, T Akayuki Y Oshimasu, Y Ukinobu Y Agyu, K Iyoshi N Akamatsu, H Iroshi S Hindo, and O Samu I Shida. Long-term results of fractionated strontium-90 radiation therapy for pterygia. 46(1):137–141, 2000. URL: <https://www.ncbi.nlm.nih.gov/pubmed/10656385>.
- [22] Bengt Karlsson, D Ph, L O N G Term, R Esults After, F Ractionated R Adiation, D Ph, Ingmar Lax, D Ph, and Julian Bailes. Long-term results after fractionated radiation therapy for large brain arteriovenous malformations. 57(1):42–49, 2005. URL: <https://www.ncbi.nlm.nih.gov/pubmed/15987539>, doi:10.1227/01.NEU.0000163095.56638.26.
- [23] Semi B Harrabi, Sebastian Adeberg, Thomas Welzel, Stefan Rieken, Daniel Habermehl, Jürgen Debus, and Stephanie E Combs. Long term results after fractionated stereotactic radiotherapy ( FSRT ) in patients with craniopharyngioma : maximal tumor control with minimal side effects. *Radiation Oncology*, pages 1–7, 2014. URL: <https://www.ncbi.nlm.nih.gov/pubmed/25227427>.



- [24] Mark Kelley and Fishel Melissa. *DNA Repair in Cancer Therapy*. Academic Press, 2016.
- [25] INTERNATIONAL ATOMIC ENERGY AGENCY. *Radiation Oncology Physics: A Handbook for Teachers and Students*, volume 98. 2005. [arXiv:S0031-9155\(02\)36442-X](https://arxiv.org/abs/S0031-9155(02)36442-X), [doi:10.1038/sj.bjc.6604224](https://doi.org/10.1038/sj.bjc.6604224).
- [26] Frank Attix. *Introduction to radiological physics and radiation dosimetry*. New York, 1986. [doi:10.1002/9783527617135](https://doi.org/10.1002/9783527617135).
- [27] Lawrence RC Camphausen KA. *Principles of Radiation Therapy*. Cancer Management: A Multidisciplinary Approach, 11 ed edition, 2008.
- [28] Dr Tim Wood. Image quality, scatter and contrast agents. URL: <http://slideplayer.com/slide/2395464/>.
- [29] F.M. KHAN. *The Physics of Radiation Therapy*, 2003.
- [30] International Atomic Energy Agency. *Quality Assurance in Radiation Dosimetry: Achievements and Trends*, 2009. URL: [https://www.iaea.org/About/Policy/GC/.../gc53inf-3-att2{\\_\)en.pdf](https://www.iaea.org/About/Policy/GC/.../gc53inf-3-att2{_)en.pdf).
- [31] Narayan CA Gupta T. Image-guided radiation therapy: Physician's perspectives. *Journal of Medical Physics / Association of Medical Physicists of India*, 37(4):174–182, 2012. URL: <https://www.ncbi.nlm.nih.gov/pmc/articles/PMC3532745/>, [doi:10.4103/0971-6203.103602](https://doi.org/10.4103/0971-6203.103602).
- [32] ICRU. ICRU – Determination of Absorbed Dose in a Patient Irradiated by Beams of X or Gamma Rays in Radiotherapy Procedures – Report 24. Technical report, 1976. URL: <https://icru.org/link-index>.
- [33] D.P Huyskens, R Bogaerts, J Verstraete, M Loof, H Nystrom, C Fiorino, S Broggi, N Jornet, M Ribas, and D.I. Thwaites. Practical guidelines for the implementation of in vivo dosimetry with diodes in external radiotherapy with photon beams (entrance dose), 2001. URL: <https://goo.gl/WXyWUB>, [doi:10.1016/S0167-8140\(01\)80842-2](https://doi.org/10.1016/S0167-8140(01)80842-2).
- [34] Iaea Human and Health Series. *Development of Procedures for In Vivo Dosimetry in Radiotherapy*. *IAEA Reports Series*, pages 1 –195, 2013. URL: [http://www-pub.iaea.org/MTCD/Publications/PDF/Pub1606{\\_\)web.pdf](http://www-pub.iaea.org/MTCD/Publications/PDF/Pub1606{_)web.pdf), [doi:10.1016/0167-8140\(90\)90102-3](https://doi.org/10.1016/0167-8140(90)90102-3).
- [35] Pam Cherry; Angela Duxbury, editor. *Practical Radiotherapy: Physics and Equipment*. Wiley-Blackwell, 2nd editio edition, 2009. URL: <http://eu.wiley.com/WileyCDA/WileyTitle/productCd-1444316184.html>.
- [36] Chen Pagonis, Vasilis, Reuven. *Thermally and Optically Stimulated Luminescence: A Simulation Approach*. John Wiley & Sons, Ltd, 2011. [doi:10.1002/9781119993766](https://doi.org/10.1002/9781119993766).
- [37] Aftab Ahmed Khuhro. What is difference between valence shell and valence band?, 2014. URL: <https://socratic.org/questions/what-is-difference-between-valence-shell-and-valence-band>.
- [38] G. Bemski. *Physics Review* 111. pages 1515–1518, 1958.

- [39] A.J.J. Bos. High sensitivity thermoluminescence. *Nucl. Instr. and Meth. in Phys. Res. B* 184 3, 2001. URL: [https://www.researchgate.net/publication/222281182\\_{\\_}High\\_{\\_}sensitivity\\_{\\_}thermoluminescence](https://www.researchgate.net/publication/222281182_{_}High_{_}sensitivity_{_}thermoluminescence).
- [40] Dr. Arnold S. Marfunin. *Spectroscopy, Luminescence and Radiation Centers in Minerals*. Russian Academy of Sciences, Moscow, Russian Federation, 1979. doi:10.1007/978-3-642-67112-8.
- [41] S.W.S McKeever. Defect Complexes and Thermoluminescence in LiF. *Radiation Protection Dosimetry*, 6:49–51, 1984.
- [42] Horowitz Yigal. *Microdosimetric Response of Physical and Biological Systems to Low- and High-LET Radiations: Theory and Applications to Dosimetry*. Elsevier, 2006.
- [43] Y. S. Horowitz and M. Moscovitch. Highlights and pitfalls of 20 years of application of computerised glow curve analysis to thermoluminescence research and dosimetry. *Radiation Protection Dosimetry, Volume 153, Issue 1*, pages 1–22, 2013. URL: <https://doi.org/10.1093/rpd/ncs242>.
- [44] M. OBERHOFER AND A. SCHARMANN. Applied Thermoluminescence Dosimetry Lectures of a course held at the Joint Research Centre, 1979.
- [45] J. Daniel Bourland. *Radiation Oncology Physics*. 2016. URL: <https://doi.org/10.1016/B978-0-323-24098-7.00006-X>.
- [46] Paul R Steinmeyer. Magazine, Ion chambers - RSO. Vol.8 No.5. URL: <http://www.fisicaonline.it/pdf/gasdetector/betafactorwow.pdf>.
- [47] Juan R. Física e Instrumentacion Medicas, 1992.
- [48] Michael GOITEN. *Radiation Oncology: A Physicist's Eye View*. New York : Springer, 2007.
- [49] Glenn F Knoll. *Radiation detection and measurement*. New York: Wiley, 3rd ed edition, 1999.
- [50] Radcard s. c. LiF:Mg,Ti Thermoluminescent phosphor & pellets. URL: <http://www.radcard.pl/det/mtsn.html>.
- [51] Thermo Scientific™. TLD-100™ Thermoluminescent Dosimetry Material. URL: <https://www.thermofisher.com/order/catalog/product/SN010106>.
- [52] Thermofisher. Thermofisher- 3500TLDDS3. URL: <https://www.stage.thermofisher.com/order/catalog/product/3500TLDDS3{#}/legacy=thermoscientific.com>.
- [53] Syed Ahmed. *Physics and Engineering of Radiation Detection*. Elsevier Ltd, 2014.
- [54] Indra J Das. Accelerator beam data commissioning equipment and procedures: Report of the TG-106 of the Therapy Physics Committee of the AAPM. *Med. Phys.* 35 (9), 2009. URL: <https://www.ncbi.nlm.nih.gov/pubmed/18841871>.
- [55] AAPM. AAPM's TG-51 protocol for clinical reference dosimetry of high-energy photon and electron beams. *Med. Phys.* 26 (9), 1999.

- [56] International Atomic Energy Agency. Absorbed Dose Determination in External Beam Radiotherapy: An International Code of Practice for Dosimetry Based on Standards of Absorbed Dose to Water. Technical Reports Series No. 398. Technical report, Vienna, 2000. URL: [www-pub.iaea.org/MTCD/publications/PDF/TRS398{ }scr.pdf](http://www-pub.iaea.org/MTCD/publications/PDF/TRS398{ }scr.pdf).
- [57] PTW Headquarters. Smarter Moves in IMRT QA. OCTAVIUS® 1500. URL: <http://www.ptw.de/3090.html>.
- [58] Rui P RODRIGUES. Radiações Aplicadas às Tecnologias da Saúde. URL: [url:http://pt.slideshare.net/yuri61/mestrado-em-radioterapia](http://pt.slideshare.net/yuri61/mestrado-em-radioterapia).
- [59] Varian. TrueBeamArchitecture, 2010. URL: <https://www.varian.com/sites/default/files/resource{ }attachments/TrueBeamArchitecture{ }RAD10152{ }Oct2010.pdf>.
- [60] Edward C. Halperin, Carlos A. Perez, and Luther W. Brady. *Perez and Brady's principles and practice of radiation oncology*. Philadelphia: Lippincott Williams & Wilkins, 5th ed. edition, 2008.
- [61] Philip Mayles, Alan Nahum, and Jean-Claude Rosenwald. *Handbook of Radiotherapy Physics - Theory and Practice*. 2007.
- [62] Radiology Support Devices. Alderson Radiation Therapy phantom (ART). URL: <http://www.rsdphantoms.com/rt{ }art.htm>.
- [63] PTW Headquarters. Acrylic and RW3 Slab Phantoms. URL: <http://www.ptw.de/acrylic{ }and{ }rw3{ }slab{ }phantoms0.html>.
- [64] Dostmann-electronic. Manual OPUS 10 -Version V5 (3/2002), 2002. URL: <http://www.dostmann-electronic.de>.
- [65] ISO/TC 85 Nuclear Energy Nuclear Technologies Protection and Radiological. ISO/ASTM 51956:2013. Practice for use of a thermoluminescence-dosimetry system (TLD system) for radiation processing. Technical report, 2013.
- [66] IAEA. Assessment of occupational exposure due to external radiation sources and intakes of radionuclides personal dosimeters. URL: <http://slideplayer.com/slide/6626518/>.
- [67] George Chabot. Health Physics Society- Instrumentation and Measurements — Personnel Monitoring (PM), 2012. URL: <https://hps.org/publicinformation/ate/q10100.html>.
- [68] ISO/TC 85 Nuclear Energy Nuclear Technologies Protection and Radiological. ISO/ASTM 52628:2013. Preview Standard practice for dosimetry in radiation processing. Technical report, 2013.
- [69] Chien Yi, Kuo Chi, Hsin Hsiung, and Lung Kwang. Optimizing the TLD-100 readout system for various radiotherapy beam doses using the Taguchi methodology. *Applied Radiation and Isotopes*, 68(3):481–488, 2010. URL: <http://dx.doi.org/10.1016/j.apradiso.2009.12.001>, doi:10.1016/j.apradiso.2009.12.001.